

THE IMPACT OF FLOW CONNECTIVITY ON THE INTERPRETATION OF
PUMPING TEST DATA

by

Buse Yetiști

B.Sc. in Civil Engineering, Boğaziçi University, 2017

Submitted to the Institute of Environmental Sciences
in partial fulfillment of the requirements for the degree of
Master of Science
in
Environmental Technology

Boğaziçi University

2020

ACKNOWLEDGEMENTS

I would like to express my gratitude to my thesis advisor, Prof. Dr. Nadim Coptu, for his guidance, support, and patience. It is an honor to work with him.

I would also like to acknowledge my jury members; Assoc. Prof. Dr. Abdurrahman Ufuk Şahin and Assist. Prof. Dr. İrem Dalođlu Çetinkaya for spending their valuable time on evaluating this study.

I would like to express special thanks to my partner, Ođuz Bařkaya, for his constant support and encouragement.

Lastly, I am thankful for my parents, Nur Őlker and Şafak Yetiřti, and for my little sister, Zeynep Yetiřti. Having you around makes me a better person.

ABSTRACT

THE IMPACT OF FLOW CONNECTIVITY ON THE INTERPRETATION OF PUMPING TEST DATA

The spatial variability of subsurface flow parameters, such as the transmissivity or storativity, is a common feature of all geologic systems. Traditional geostatistical techniques expressed this heterogeneity in terms of two-point correlations. Recent research suggests that such characterization technique may not be adequate to fully represent the complex patterns of flow and transport in heterogeneous subsurface systems. The concept of flow connectivity has been introduced to describe how different regions of the aquifer relate to each other. In this study, the impact of point-to-point flow connectivity on radially convergent flow towards a well is investigated numerically. A Monte Carlo approach is adopted whereby a large number of heterogeneous aquifer systems with different levels of connectivity are synthetically generated and then used to simulate pumping tests. Two pumping test methods, the Cooper-Jacob Method and the Continuous Derivation Method, are used to estimate the flow parameters from the time-drawdown curves, and examine how the estimated parameters relate to the underlying heterogeneous aquifer systems. Results indicate that the estimated transmissivity value approaches to the geometric mean of the full transmissivity field as the time-drawdown derivative dataset is included in the interpretation. On the other hand, the estimated storativity is strongly influenced by the spatial distribution of the transmissivity, the aquifer point-to-point flow connectivity and the relative locations of the observation and pumping wells. The relations between the estimated storage coefficient and a static measure of connectivity are also examined.

ÖZET

AKIŞ BAĞLANTISALLIĞININ POMPAJ DENEYİ VERİLERİNİN YORUMLANMASINA ETKİSİ

Hidrolik iletkenlik ya da transmisivite gibi yeraltı akış parametrelerinin mekana bağlı olarak değişim göstermesi tüm jeolojik sistemlerin ortak bir özelliğidir. Geleneksel jeostatistiksel teknikler bu heterojenliği iki nokta korelasyonları olarak ele almaktadır. Buna göre, iki noktadaki akış parametrelerinin kovaryansı yalnızca mesafenin bir fonksiyonu olarak ifade edilmiştir. Son araştırmalar, bu karakterizasyon tekniğinin, heterojen yeraltı sistemlerindeki karmaşık akış ve taşınım modellerini temsil etmek için yeterli olmayabileceğini göstermektedir. Bu sorunu ele almak ve akiferin farklı bölgelerinin birbiriyle nasıl ilişki kurduğunu tanımlamak adına akış bağlantısallığı kavramı üzerine yoğunlaşmaktadır. Bu çalışmada, akış bağlantısının yanıl yeraltı suyu akışına ve pompaj testi verilerine olan etkisi sayısal olarak incelenmiştir. Pompaj testleri uygulamada yeraltı akış parametrelerinin belirlenmesinde sıklıkla kullanıldığı için bu çalışmanın da temelini oluşturmaktadır. Farklı akış bağlantı seviyelerine sahip çok sayıda heterojen akifer sistemi sentetik olarak üretilmiş ve bu akiferlerde pompaj deneylerinin simüle edildiği bir Monte Carlo yaklaşımı benimsenmiştir. İki farklı pompalama deneyi çözümüleme yöntemi, Cooper-Jacob Yöntemi ve Sürekli Türevleme Yöntemi, zaman-alçalma eğrilerinden faydalanarak akış parametrelerini belirlemek ve bu parametrelerin heterojen akifer sistemleri ile ilişkisini incelemek için kullanılmıştır. Sonuçlar, hesaplanan transmisivite değerlerinin sentetik olarak oluşturulan alanların transmisivite değerlerinin geometrik ortalamasına yakınsadığını göstermektedir. Öte yandan, yeraltı suyu seviyesi alçalma verilerinden hesaplanan depolama katsayısı transmisivitenin mekansal dağılımına, akifer noktadan noktaya akış bağlantısına ve gözlem ve pompalama kuyularının konumuna göre değişim göstermektedir. Son olarak, bu iki yöntemle hesaplanan depolama katsayıları ile statik bir bağlanabilirlik ölçüsü arasındaki ilişki incelenmektedir.

TABLE OF CONTENTS

ACKNOWLEDGEMENTS	ii
ABSTRACT	iii
ÖZET	iv
TABLE OF CONTENTS	v
LIST OF FIGURES	vi
LIST OF TABLES	ix
LIST OF LIST OF SYMBOLS/ABBREVIATIONS.....	x
1. INTRODUCTION.....	1
2. LITERATURE REVIEW.....	5
2.1. Aquifer Characteristics and Their Stochastic Analysis.....	5
2.2. Interpretation of Groundwater Flow and Contaminant Transport Parameters Based on Pumping Test Analysis.....	9
2.3. Connectivity as a Novel Geostatistical Parameter	12
3. RESEARCH OBJECTIVE.....	16
4. METHODOLOGY	17
4.1. Generation of Transmissivity Fields	17
4.2. Simulation of Pumping Tests	19
4.3. Estimation of Groundwater Flow and Solute Transport Parameters.....	21
4.3.1. Cooper-Jacob Method	21
4.3.2. Continuous Derivation Method.....	22
4.4. Calculation of Integral Connectivity Scales of Generated Fields	24
5. RESULTS.....	26
5.1. Generation of Transmissivity Fields	26
5.2. Pumping Test Simulations	29
5.3. Static Measure of Connectivity	31
5.4. Application of Cooper-Jacob Method	34
5.5. Application of Continuous Derivation Method.....	44
6. CONCLUSIONS AND FUTURE RESEARCH.....	78
REFERENCES.....	83

LIST OF FIGURES

Figure 1.1. Distribution of Earth's water	1
Figure 1.2. Distribution of freshwater based on its source.....	2
Figure 5.1. Graphical representation of a randomly selected (a) Gaussian field, (b) low-T connected field, and (c) high-T connected field	29
Figure 5.2. MODFLOW simulation outputs for a randomly selected Gaussian, low-T connected and high-T connected fields. (a) shows drawdown vs. time at $r/I=0.1$. (b) shows drawdown derivative vs. time with the observation well is located at $r/I=0.1$. (c) shows drawdown vs. time at $r/I=0.5$. (d) shows drawdown derivative vs. time with the observation well is located at $r/I=0.5$	31
Figure 5.3. Connectivity function as a function of separation distance for a randomly selected unconditional Gaussian field (field 10), and its variations different levels of connectivity as low-T connected and high-T connected.....	32
Figure 5.4. Integral connectivity scales of (a) unconditional and (b) conditional realizations	34
Figure 5.5. Histogram of T/T_g of unconditional realizations where $r/I=0.1$	35
Figure 5.6. Histogram of S/S_0 of unconditional realizations where $r/I=0.1$	36
Figure 5.7. Transmissivity vs integral connectivity scale for (a) high-T connected fields, (b) low-T connected fields, (c) Gaussian fields and (d) all fields combined together for unconditional realizations where the observation well is located at $r/I=0.1$	38
Figure 5.8. Estimated storativity vs integral connectivity scale of combined field sets. (a) and (b) correspond to unconditional realizations with the observation well located at $r/I=0.1$ and $r/I=0.5$, respectively. (c) and (d) show conditional realizations with the observation well located at $r/I=0.1$ and $r/I=0.5$, respectively.	42
Figure 5.9. Histograms of S/S_0 estimated for unconditional fields where (a) $r/I=0.1$ and (b) $r/I=0.5$ and conditional fields where (c) $r/I=0.1$ and (d) $r/I=0.5$	44

- Figure 5.10. Estimated transmissivity as a function of time for randomly selected Gaussian fields. (a) and (b) correspond to unconditional realizations with the observation well located at $r/I=0.1$ and $r/I=0.5$, respectively. (c) and (d) show conditional realizations with the observation well located at $r/I=0.1$ and $r/I=0.5$, respectively47
- Figure 5.11. Estimated transmissivity as a function of time for randomly selected high-T connected fields. (a) and (b) correspond to unconditional realizations with the observation well located at $r/I=0.1$ and $r/I=0.5$, respectively. (c) and (d) show conditional realizations with the observation well located at $r/I=0.1$ and $r/I=0.5$, respectively49
- Figure 5.12. Estimated transmissivity as a function of time for randomly selected low-T connected fields. (a) and (b) correspond to unconditional realizations with the observation well located at $r/I=0.1$ and $r/I=0.5$, respectively. (c) and (d) show conditional realizations with the observation well located at $r/I=0.1$ and $r/I=0.5$, respectively51
- Figure 5.13. Estimated transmissivity as a function of radial distance for randomly selected Gaussian fields. (a) and (b) correspond to unconditional realizations with the observation well located at $r/I=0.1$ and $r/I=0.5$, respectively. (c) and (d) show conditional realizations with the observation well located at $r/I=0.1$ and $r/I=0.5$, respectively54
- Figure 5.14. Geometric mean of transmissivity as a function of radial distance for randomly selected Gaussian fields of (a) unconditional realizations and (b) conditional realizations56
- Figure 5.15. Comparison of T_{geomean} (thin lines) and T_{est} (bold lines) as a function of r/I for randomly selected (a) Gaussian, (b) low-T connected, and (c) high-T connected unconditional selected fields. Black lines show field B and red lines show field E realizations. Observation well is located at $r/I=0.1$58
- Figure 5.16. T_{geomean} vs. T_{est} at distance (a) $r/I=0.5$, (b) $r/I=1$, (c) $r/I=5$, and (d) $r/I=10$ for all unconditional realizations60
- Figure 5.17. Estimated storativity as a function of time for randomly selected Gaussian fields. (a) and (b) shows unconditional realizations where the observation well is located at $r/I=0.1$ and $r/I=0.5$, respectively. (c) and (d) shows conditional realizations where the observation well is located at $r/I=0.1$ and $r/I=0.5$, respectively65

- Figure 5.18. Estimated storativity as a function of time for randomly selected high-T connected fields. (a) and (b) shows unconditional realizations where the observation well is located at $r/I=0.1$ and $r/I=0.5$, respectively. (c) and (d) shows conditional realizations where the observation well is located at $r/I=0.1$ and $r/I=0.5$, respectively68
- Figure 5.19. Estimated storativity as a function of time for randomly selected low-T connected fields. (a) and (b) shows unconditional realizations where the observation well is located at $r/I=0.1$ and $r/I=0.5$, respectively. (c) and (d) shows conditional realizations where the observation well is located at $r/I=0.1$ and $r/I=0.5$, respectively.71
- Figure 5.20. Estimated storativity as a function of radial distance from the extraction well for randomly selected Gaussian fields. (a) and (b) shows unconditional realizations where the observation well is located at $r/I=0.1$ and $r/I=0.5$, respectively. (c) and (d) shows conditional realizations where the observation well is located at $r/I=0.1$ and $r/I=0.5$, respectively74
- Figure 5.21. Estimated storativity at $t=1$ vs integral connectivity scale of combined field sets. (a) and (b) correspond to unconditional realizations with the observation well located at $r/I=0.1$ and $r/I=0.5$, respectively. (c) and (d) show conditional realizations with the observation well located at $r/I=0.1$ and $r/I=0.5$, respectively76

LIST OF TABLES

Table 4.1. Parameter values used in Gaussian transmissivity field generation.....	18
Table 4.2. Summary information of the transmissivity fields used in the study.....	19
Table 4.3. Required parameters for the pumping test simulations.....	20
Table 5.1. Average and standard deviation of integral connectivity scales over the field sets, Gaussian, low-T connected, and high-T connected.....	33
Table 5.2. Average and standard deviation of transmissivities estimated for different types of realizations and fields	38
Table 5.3. Average and standard deviation of normalized storativities estimated for different types of realizations and fields	44
Table 5.4. Integral connectivity scales of selected fields	45
Table 5.5. Coefficient of determination for different field types at various distances.....	61
Table 5.6. Average and standard deviation of normalized storativities estimated at t=1 time units for different types of realizations and fields.....	77

LIST OF LIST OF SYMBOLS/ABBREVIATIONS

Symbol	Explanation	Unit
A	Cross Sectional Area	[L ²]
b	Aquifer Thickness	[L]
h	Separation Distance	[L]
h _d	Hydraulic Head	[L]
I	Integral Scale	[L]
I _{con}	Integral Connectivity Scale	[L]
K	Hydraulic Conductivity	[L/T]
Q	Flow Rate	[L ³ /T]
r	Radial Distance From The Well	[L]
S	Storativity	[-]
S ₀	Initial Storativity	[-]
S _s	Specific Storage	[1/L]
s	Drawdown	[L]
T	Transmissivity	[L ² /T]
T'	Transformed Transmissivity	[L ² /T]
T _{est}	Estimated Transmissivity	[L ² /T]
T _{geomean}	Geometric Mean of Transmissivity	[L ² /T]
U	Theis Equation Well Parameter	[-]
σ^2	Variance	[-]
Abbreviation	Explanation	
Avg	Average	
CD	Continuous Derivation Method	
CP	Number of Connected Pairs	
High-T	High-Transmissivity	
Low-T	Low-Transmissivity	
St Dev	Standard Deviation	
TP	Number of Total	Pair

1. INTRODUCTION

Water is one of the essential resources for the survival of humans and living organisms on Earth. Although 80% of the Earth surface area is covered with water, the freshwater that can be utilized for personal, domestic, agricultural and industrial purposes accounts for only 3% of the total amount (Figure 1.1). Moreover, 69% of freshwater is in the form of glaciers and not available for use. Groundwater, which is the water stored under the surface of Earth, in the pores of rocks and soil, accounts for 97% of unfrozen freshwater (Kresic, 2007). As shown in Figure 1.2, the volume of groundwater accounts for most of the total amount of freshwater that is available to use.

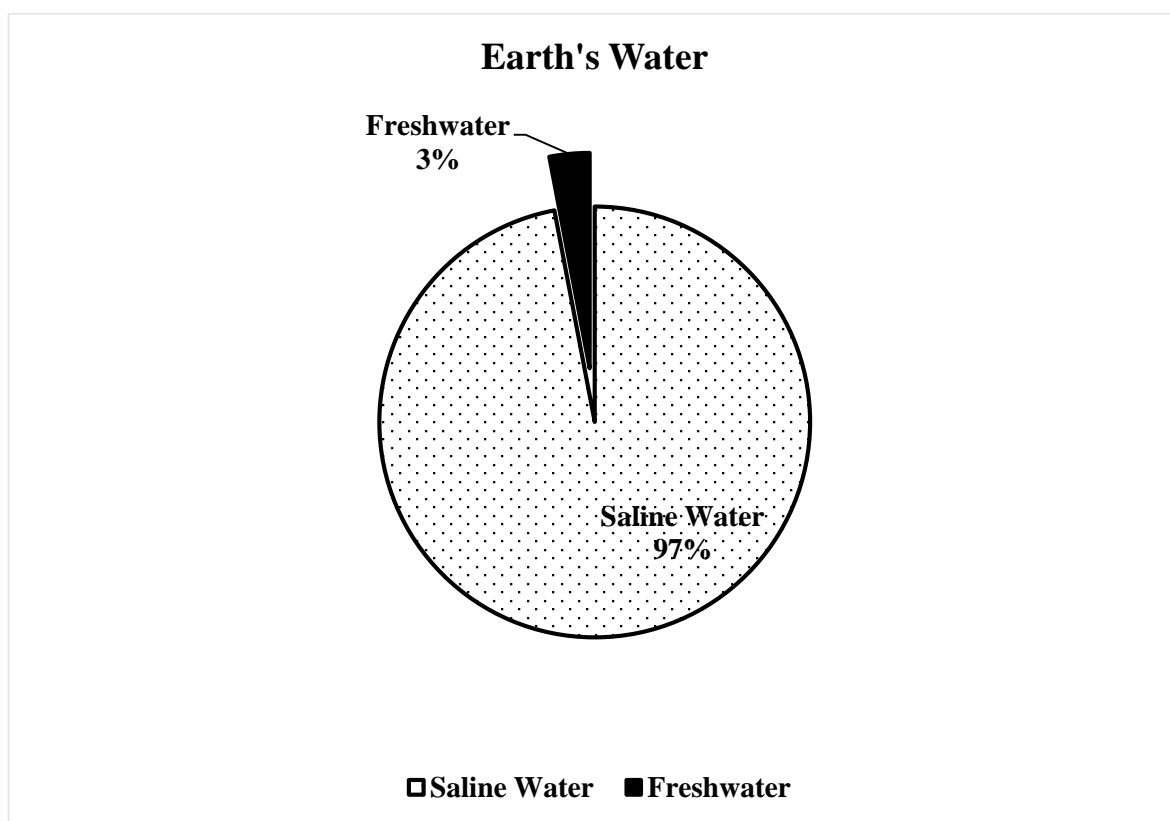


Figure 1.1. Distribution of Earth's water

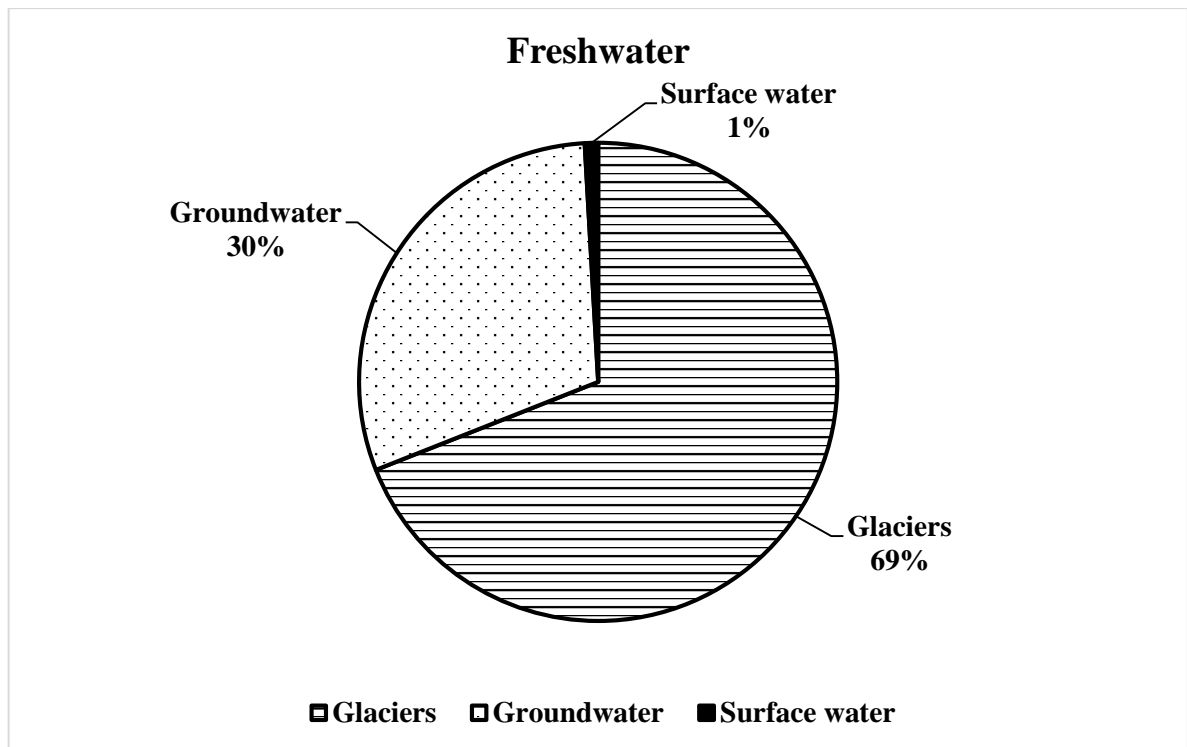


Figure 1.2. Distribution of freshwater based on its source

Groundwater is the most precious resource of fresh water not only because it is the most abundant but also because of its resilience to the impacts of seasonal changes and temperature variations compared to surface waters. Moreover, it is generally less polluted than surface water bodies. It is a critical buffer resource, especially where surface waters are not sufficient such as in arid and semi-arid regions. In other words, groundwater is almost readily available to use, reliable in drought years and, under normal conditions, it requires minimal treatment (Foster and Chilton, 2003). It should be noted that although groundwater bodies are less sensitive to human-based pollution than surface water bodies, when groundwater is polluted it is much more challenging to remove the contaminants due to difficulties in determining the source and location of contamination, physical inaccessibility, and the need to remediate large volumes of groundwater. Moreover, it may take tens or even hundreds of years to experience the adverse impacts of pollution which makes control of pollution more problematic.

The modeling of groundwater flow and contaminant fate and transport has become an effective tool for evaluating the availability of groundwater resources, assessing the impact of pollution if there is any, and in support of remedial activities. Accurate modeling of subsurface flow and pollutant transport requires accurate estimates of aquifer parameters to represent the essential features of the subsurface system. All aquifers have two major characteristics: the capacity of water flow and the capacity for water storage. Hydraulic conductivity and transmissivity are the

parameters used to define the capacity of water flow, and specific storage or storativity are the parameters that determines the capacity of water storage. In order to model groundwater flow and contaminant transport behavior of an aquifer realistically, transmissivity and storativity should be estimated properly over the entire domain of interest.

It is widely acknowledged in the literature that these parameters vary significantly in space and that variability has a large influence on the behavior of groundwater flow and contaminant transport (Dagan and Neuman, 1997). Therefore, developing accurate representations of aquifers systems for modeling purposes requires the use of data acquisition and interpretation techniques that can provide quantitative detailed information about the spatial variability of the flow parameters.

Pumping tests have been used for the estimation of subsurface flow parameters for many decades. Pumping tests involve the extraction of water and monitoring the change in water levels at one or more observation wells. From the water level response, the aquifer parameters are estimated. Traditionally, pumping test interpretation techniques are based on the assumption of soil homogeneity (Sanchez-Vila et al., 1999). However, extensive field data have shown that subsurface flow parameters are almost always heterogeneous with complex patterns of spatial variability (Seyfried and Wilcox, 1995; Fogg et al., 1998; Kresic, 2007). Moreover, the use of average values of flow parameters in modeling efforts can lead to inaccurate predictions of flow and transport.

The complexity in the spatial variability of subsurface formations has led researchers to develop the field of geostatistics (Gelhar, 1993). Geostatistics is the application of statistical techniques to Earth sciences that was developed to account for the heterogeneity of the subsurface and the uncertainty in the definition of Earth properties. In geostatistics, soil parameters are defined in a stochastic framework, meaning that they do not have a single unique value but can have a range of possible values. This range of possible values reflects the level of uncertainty in the definition of these parameters. As a result, the dependent variables, such as groundwater flow and transport parameters, are also considered as random spatial variables. In recent years, these geostatistical methods have been widely used to account for soil heterogeneity relating to groundwater flow problems.

A fundamental feature of geostatistics is that parameters are correlated in space, meaning that parameters, such as hydraulic conductivity, at two locations are correlated. This correlation is expressed in terms of a covariance function that is a function of separation distance of these two points. The covariance function defines statistically the spatial heterogeneity of the parameters.

However, it has been reported in the literature that this two-point statistical approach is often not sufficient to fully represent complex patterns of flow and transport in heterogeneous subsurface systems (Sanchez-Vila et al., 1996; Gomez-Hernandez and Wen, 1998; Western et al., 2001). Two aquifers may have the same two-point statistical parameters, variance, and integral scale, but may end up showing very different water flow or solute transport behaviors.

To address this issue, the concept of flow connectivity has been introduced to describe how different regions of the aquifer relate to each other. Flow connectivity refers to the presence of preferential flow channels where the groundwater flow and contaminant transport can occur faster than the other regions of the aquifer. Although the concept of flow connectivity is simple to understand and has been often reported in field studies, there is no single quantitative measure of connectivity that is accepted universally (Renard and Allard, 2011). Moreover, the impact of connectivity on pumping tests is still not well understood. Thus, the main focus of this study is to examine the impact of the flow connectivity on radially converging flow to a well in the heterogeneous confined aquifers and on the interpretation of pumping tests. This way, the interpreted flow parameters using pumping test analysis may be estimated more accurately by taking the spatial subsurface structure and flow connectivity into consideration. Ultimately, the performances of the groundwater flow and transport models that use these estimated parameters as input are improved since the real aquifers are represented more realistically.

2. LITERATURE REVIEW

2.1. Aquifer Characteristics and Their Stochastic Analysis

A natural geological formation that allows a significant amount of water to flow under the surface is called an aquifer (Kresic, 2007). There are 3 general types of aquifers, namely confined, unconfined, and semi-confined or leaky. A confined aquifer can be defined as an aquifer that is located between two impermeable layers and totally saturated with water. An unconfined aquifer, on the other hand, has no confining layer at the top, but still sits upon an impermeable bed. Leaky aquifers occur when the underlying and/or overlying layers allow some inflow into the aquifer.

Groundwater flows from locations of high hydraulic head to low hydraulic head. The first quantitative analysis of water flow through porous media was performed by Henry Darcy in 1856 in the city of Dijon, France to describe water flow through sand beds. He designed an experiment that allows water to flow through a homogeneous sand bed and derived the rate of flow equation empirically as given below:

$$Q = -KA \frac{\Delta h_d}{\Delta l} \quad (2.1)$$

Where

Q	rate of flow [L^3/T]
K	hydraulic conductivity [L/T]
A	cross sectional area [L^2]
Δh_d	hydraulic head difference [L]
Δl	length of flow [L]

Darcy Law (1856) that is shown by equation (2.1) states that the rate of flow through porous media is directly proportional to the cross-sectional area of flow (A) and the hydraulic head difference between the initial and final points (Δh), and is inversely proportional to the length of flow (Δl). The proportionality constant K is referred to as the hydraulic conductivity, which is a measure of how easily a fluid can pass through the soil. It depends on both soil type and fluid properties and has units of [L/T]. When the fluid flowing through the porous media is water, the hydraulic conductivity range is from about 10^{-2} m/s in gravel to 10^{-17} m/s in clay (Heath, 1983).

Hydraulic conductivity is an essential parameter to understand the behavior of subsurface water flow. However, the wide range of values observed in real soils means that the accurate definition of the hydraulic conductivity is difficult in practice.

In many cases, it is more convenient to work with the transmissivity parameter (T) which is the integral of hydraulic conductivity as a function of aquifer thickness and has a dimension of $[L^2/T]$. The mathematical equation of transmissivity is given in equation (2.2) below:

$$T = \int Kdz \quad (2.2)$$

The second fundamental parameter for the characterization of groundwater flow behavior is the specific storage (S_s), which is defined by Freeze and Cherry (1979) as “the volume of water than an aquifer releases from storage, per unit aquifer volume per unit decline in the hydraulic head”. It has units of $[1/L]$ and it is a function of aquifer and water compressibility, water density, soil porosity (the volume of voids over the total volume of soil) and gravitational acceleration.

A parameter directly related to the specific storage is the storativity (S) which is the volume of water released from unit surface area of the aquifer for a unit decline in the hydraulic head (Delleur, 1999). For confined aquifers, storativity equals to specific storage times the saturated thickness of the aquifer:

$$S = S_s b \quad (2.3)$$

Where

S	storativity [-]
S_s	specific storage $[1/L]$
b	aquifer thickness $[L]$

These parameters are often determined from pumping test analysis, which includes examining the change in water levels at various locations due to water extraction from a pumping well. The change in water level due to pumping is referred to as drawdown (s). Generally, the drawdown vs. time graphs observed at the pumping well or nearby monitoring wells due to constant pumping are analyzed to determine flow and storage parameters (Delleur, 1999). However, commonly used

pumping test analysis methods are based on aquifer homogeneity and isotropy, which are almost never the case in real life. Numerous studies have shown that flow parameters vary significantly in space in a complex pattern (Gelhar, 1984; Kuang et al., 2020). Thus, one single estimate of flow parameters would not be adequate to provide a good representation of the whole subsurface structure.

Spatial variability of flow and transport parameters can be defined at various characteristic length scales ranging from the pore scale (in the order of millimeters), to the local scale (in the order of up to several tens of meters) and regional scale (in the order of up to several kilometers) (Dagan, 1986). Characteristic length is defined by Dagan (1986) as “the average distance over which properties are correlated”. Because of that, identifying the length scale of concern is an essential step before starting the analysis. The emphasis in this study is on the intermediate (local scale heterogeneity) which is relevant to many contamination fate and transport problems.

The spatial variability and high uncertainty in flow parameters have led to the development of stochastic analysis in hydrogeology. In a stochastic approach, the flow parameters are treated as spatial random variables and it is assumed that they can be represented by statistical models. As a result, dependent parameters such as hydraulic head, velocity and concentration are also random spatial functions. (Gomez-Hernandez, 1998).

It has been observed at numerous field experiments that the hydraulic conductivity and transmissivity are often log-normally distributed (Freeze, 1975; Gelhar, 1993). In other words, the natural logarithm of transmissivity has normal Gaussian distribution which is the distribution of many other parameters in nature. In order to work with a normal distribution, a new variable Y , where $Y = \ln T$ or $Y = \ln K$ is defined and used for calculations. Because Y is normally distributed, its histogram can be represented by two statistical measures: its mean and variance, where mean is the arithmetic average of natural logarithms of measured data, or the geometric mean of the untransformed hydraulic conductivity or transmissivity data, and variance is the spread of measured data around the mean (Kitanidis, 1997). Based on these observations, the multivariate Gaussian spatial random function model is often used for the representation of spatial variability of flow parameters such as the hydraulic conductivity or transmissivity. This fundamental continuous model assumes that the flow parameters have a Gaussian distribution and are correlated in space. The model enables the statistical representation of flow parameters in terms of the mean and semivariogram, or a covariance function which is typically expressed in terms of the variance and correlation scale. The correlation scale indicates the distances over which a parameter is correlated

in space. Larger values of the correlation scale means that the correlation persists over longer distances.

While the mean and variance combine all available data without considering their location, the semi-variogram (also the covariance) describes the spatial variability and the continuity of the parameters within the field. The semi-variogram is calculated as the difference of all measured data pairs separated at a fixed distance from each other. Deciding on the most accurate semi-variogram function is critical for the development of the geostatistical model. The most commonly used semi-variogram in hydrogeology is the exponential model since it provides an effective representation of the spatial distribution of soil parameters (Kitanidis, 1997; Dagan and Neuman, 1997). The exponential semi-variogram function is shown in equation (2.4) below:

$$\gamma(h) = \sigma^2 \left(1 - \exp\left(-\frac{h}{I}\right) \right) \quad (2.4)$$

Where

$\gamma(h)$ semi-variogram function

h separation distance,

σ^2 variance of the log-transmissivity distribution,

I integral scale which describes the distance over which the parameter of concern shows correlation in scale. For distances greater than $3I$, data are assumed to be completely independent from each other.

As such the log-transmissivity field can be represented using three statistical parameters, namely, the log-transmissivity mean, variance and semi-variogram integral scale (Rubin, 2003; Copty and Findikakis, 2004a). The main problem with this classical stochastic approach, which relies on two-point statistics, is that it only considers the flow parameters separated by a certain distance and ignores the values between the two points. Because of that, it is not always sufficient to grasp the heterogeneity of flow parameters. In the recent literature, a new statistical parameter, referred to as connectivity is introduced in an attempt to represent the spatial variability of parameters and how they are connected in space (Westen et al., 2001; Zinn and Harvey, 2003; Renard and Allan, 2011). Flow and transport connectivity is reviewed in detail in Section 2.3.

2.2. Interpretation of Groundwater Flow and Contaminant Transport Parameters Based on Pumping Test Analysis

A pumping test is the most commonly used field experiment for the estimation of subsurface flow parameters. It includes extraction of water, generally at a constant rate, and recording of the drawdown curve at the pumping well and several observation wells. The time-dependent drawdown curve is then analyzed with either analytical or numerical methods. The first analytical estimation method of flow and transport parameters using the drawdown curve was proposed by Theis (1935). This method requires graphical curve matching for estimation, and it is derived for pumping tests in confined aquifers. The Theis equation is can be written as:

$$s(r,t) = \frac{Q}{4\pi T} W(u) \quad (2.5)$$

$$u = \frac{r^2 S}{4Tt} \quad (2.6)$$

Where

- r radial distance from the pumping well [L],
- t pumping time [T],
- Q constant well discharge [L^3/T],
- T transmissivity of the aquifer [L^2/T],
- S storativity of the aquifer, [-],
- $s(r,t)$ drawdown as a function of time and radial distance from the well, [L],
- $W(u)$ Theis well function, [-]

The well function is defined as:

$$W(u) = \int_u^{\infty} \frac{e^{-u}}{u} du \quad (2.7)$$

It can also be written in a series form as follows:

$$W(u) = -0.5772 - \ln(u) + u - \frac{u^2}{2*2!} + \frac{u^3}{3*3!} - \frac{u^4}{4*4!} + \dots \quad (2.8)$$

As mentioned above, the Theis method is a graphical application that gives estimates of the transmissivity and storativity if the other parameters, flow rate, distance and time, are known. It requires the graphical matching of $W(u)$ vs. $1/u$ curve with the drawdown vs. time curve. Then, drawdown, time, parameter u , and $W(u)$ are determined from the point of match. When multiple pumping tests are performed, each test is typically analyzed separately.

It is important to note that this method is built on many assumptions. The fundamental assumptions are as follows:

- The aquifer is considered as infinite in size, homogeneous, isotropic, confined and uniform in thickness.
- Well storage is ignored; all discharge is received from the aquifer.
- Fully penetrating, 100% efficient well is assumed.

If the conditions are not met, which happens frequently in real life, then this method cannot be used and other estimation methods should be considered (Kresic, 2007).

Cooper-Jacob (1946) proposed a modified version of the Theis equation that does not require graphically matching and thus, it simplifies the estimation of flow and transport parameters. It involves the semi-log plot of drawdown data and the method is only applicable for the late times of the drawdown curve where the parameter u is equal to or less than 0.1 (Kresic, 2007). Briefly, late time drawdown data are averaged to estimate flow and transport parameters. After estimation of the transmissivity (T) and storativity (S), the u parameter should be recalculated to make sure that its condition is still met. As the Cooper-Jacob method starts from the Theis solution, it relies on the same assumptions as Theis method. The heterogeneity of soil, for example, cannot be investigated with these methods. Due to the oversimplification of subsurface system, the estimated parameters may not be adequate to represent real field conditions.

In recent years, many studies have been conducted to examine the effects of subsurface heterogeneity and spatial variability of the flow and transport parameters on the estimates of flow parameters derived from pumping tests. Butler (1990) demonstrated that the estimated transmissivities using the Theis Method gets affected by the transmissivity around the well. Feitosa et al. (1994) used an inverse method to estimate flow parameters as a function of radial distance from the extraction well by positioning the transmissivity field as consequent homogeneous rings.

Meier et al. (1998) numerically investigated the impact of aquifer heterogeneity on the estimated parameters from the analysis of pumping tests. They found that the estimated transmissivity of the heterogeneous field was close to the geometric mean of the transmissivity calculated by the Cooper-Jacob Method. Moreover, it was shown that the observation location does not affect the estimated transmissivity significantly. Estimated storativity, on the other hand, varied significantly with the location of observation.

Because pumping tests are cost intensive, generally only one or a few pumping tests are present for a given field and it is difficult to infer information about the statistical parameters of local scale heterogeneity from limited data using the classical interpretation techniques. Lately, a number of new techniques have been developed in an attempt to estimate the statistical parameters that describe the hydraulic conductivity field from pumping tests. The rationale of these methods is to try and maximize the information that can be inferred from pumping test data.

Coptý and Findikakis (2004b) attempted to estimate the statistical parameters of the transmissivity field using time-drawdown data derived from pumping tests. For this purpose, synthetic transmissivity fields with different log-transmissivity variance and integral scale values were generated and the time-drawdown graph of each field is computed under constant well discharge. The transient drawdown of an equivalent homogeneous field was also computed for comparison and normalization. Then, a Bayesian parameter estimation method was applied to get the probability distribution functions of log-transmissivity variance and integral scale. They concluded that the semi-variogram can be estimated from pumping test data, and the accuracy of the estimated semi-variogram increases as the number of pumping tests increase.

Neuman et al. (2004) developed a graphical type-curve method for the estimation of the variance and integral scale of local log-transmissivity fields from quasi steady state distance-drawdown data due to constant well discharge. They also concluded that the reliability of the estimates increases as the number of available pumping test data increases. Neuman et al. (2007) applied the type-curve method for an aquifer in Tübingen, Germany. They performed pumping tests in four wells and estimated the log transmissivity mean, variance and integral scale. They compared their estimations with estimates produced from large number of field measurements of hydraulic conductivity. They found that distance-drawdown data obtained from the four pumping tests is sufficient to infer the spatial structure of transmissivity for this site. However, they were unable to compare their estimations for the integral scale since the measurements were obtained from a limited number of boreholes. Riva et al (2009) also applied that methodology to interpret the

pumping test data of an aquifer in Poitiers, France. They used the results of 32 hydraulic tests that were performed in 2004 and 2005 and applied the type-curve estimation method. Then, they compared their results with deterministic approach results and geostatistic analysis of previous geophysical data of the site. They concluded that their results were consistent with geophysical information and the general trend in published worldwide data. An overarching review of pumping test interpretation techniques for the estimation of hydraulic conductivity can be found in Sanchez-Vila et al. (2006).

Coptý et al. (2011) used the drawdown data and its time derivative for the estimation of flow parameters at the pumping test evolves in time using a variation of Theis (1935) equation. In this method, it is assumed that the heterogeneous system can be defined with a homogeneous system where the estimated parameters change and evolve throughout the test. After the flow parameters are estimated, the time-dependent function was converted to distance-dependent. This way, the change in flow parameters in time and space can be analyzed and heterogeneity can be taken into consideration. Avci et al. (2011) developed a novel graphical method, based on the Theis method, called incremental area method (IAM) that facilitated the estimation of flow and transport parameters. This method also enabled the determination of the type of the aquifer system, such as confined, unconfined, or leaky (Avci et al., 2013).

Demir et al. (2017) investigated the possibility of estimating the integral scale and variance from pumping tests. They used the methodology derived by Coptý et al. (2011), referred to as continuous derivation (CD) to first estimate the transmissivity as a function of radial distance, and then applied a Bayesian parameter estimation method on the estimated transmissivities to obtain the probability distribution functions of transmissivity variance and integral scale. Their results showed that the data obtained from as little as 5 pumping tests were enough to estimate the statistical parameters of the transmissivity field.

2.3. Connectivity as a Novel Geostatistical Parameter

It has been observed that even though different fields share the same log-transmissivity mean, variance, and integral scale values, they may not exhibit the same water flow and solute transport behavior (Zinn and Harvey, 2003). In other words, those three fundamental statistical parameters may not be sufficient to accurately simulate groundwater flow and contaminant transport. A new additional parameter was introduced by the authors which is referred to as the connectivity between the points. Connectivity refers to how two points in the aquifer are related to each other. It can be

simply defined as the presence of preferential channels in the aquifer that allows faster water flow than the other parts of the aquifer (Garcia et al., 2010). Connectivity cannot be represented by the standard geostatistical approach, because the semi-variogram only considers the difference of the values between two points that are separated at a fixed distance and does not take into account the values located between and connecting these two points (Western et al., 2001). Although it can be easily understood intuitively that different aquifers may have different levels of connectivity structures, it is not that trivial to find a parameter to express connectivity numerically. It is more widely investigated in oil industry and petroleum engineering, since it is essential to understand the geological system between the extraction well and the oil reservoir. In Karst aquifer systems, connectivity is a dominant feature as cracks in the rock volume generates preferential flow paths. In soils, on the other hand, the attempts to conceptualize connectivity and its impact on groundwater flow and contaminant transport is relatively new and still requires additional work (deMarsily, 2005; Renard and Allan, 2011).

Renard and Allan (2011) provide a summary of connectivity measures used in hydrogeology and petroleum engineering. They group the measures as static and dynamic connectivity, based on whether they are affected by physical processes such as subsurface water flow, contaminant transport, or the boundary conditions of the aquifer. The static connectivity scale is a function of the spatial distribution of the property (such as hydraulic conductivity) and it is independent of the physical processes. In other words, static connectivity scales do not change based on flow or transport. The dynamic connectivity on the other hand is dependent on the flow or solute transport response.

A number of static connectivity measures with different levels of complexity have been proposed in recent years. Many of these measures have been adopted from the field of integral geometry in mathematics (Renard and Allan 2011). For domains defined as either permeable/non-permeable based on some threshold, the number of clusters can be considered as a simple measure of the connectivity (Allard, 1993). The Euler characteristic, which is a parameter that can be computed from the number of vertices, edges areas and volumes of an object, is also a measure of static connectivity (Serra, 1984). From the theory of percolation, Havedik et al. (2007) proposed the use of the ratio of the volume (or area in 2D domains) to the total volume (or area) of the domain as a measure of static connectivity. Another metric of connected is the ratio of the number of connected grids to the total number of permeable grids. For continuous fields such as the hydraulic conductivity of the transmissivity which vary continuously in space, Renard and Alard (2011)

propose the application of the above connectivity metrics with different thresholds between permeable and non-permeable grids to get a more complete image of the domain connectivity.

Another metric of the static connectivity is the integral connectivity scale proposed by Western et al (2001). This scale is only based on the spatial distribution of the transmissivity field, and it does not change based on physical processes such as pumping or boundary conditions.

Many researchers have argued that the hydraulic conductivity or transmissivity in the field is not well described with the broadly used multi-Gaussian assumption. The multi-Gaussian model assumes that areas of average hydraulic conductivity tend to be connected in space with isolated pockets of high or low permeability. Zinn and Harvey (2003) developed a method that allows the definition of non-Gaussian fields where high transmissivity areas or low transmissivity areas are spatially connected. Although all three types of fields have the same two-point statistics- i.e., the same log-transmissivity mean, variance and integral scale, their connectivity structures are very different. It is found that the connected high-conductivity field had greater effective conductivity than the geometric mean. Significant solute transfer between the mobile-immobile domain is also observed. The connected low-conductivity field, on the other hand, had smaller effective conductivity than the geometric mean, and no significant solute transfer was observed between the domains. The traditional multi-Gaussian field was the only one that was consistent with the existing stochastic theory.

Dynamic measures of connectivity, on the other hand, are affected by the imposed boundary conditions and by changes in flow and transport conditions. For example, in the unsaturated zone, the value of hydraulic conductivity and its connectivity with other regions is affected by the distribution of the water saturation in the soil. Some of the dynamic metrics can be calculated in field experiments more easily than static connectivity metrics. If the existence of some level of correlation between dynamic and static connectivity measures can be shown by further studies, then it would be possible to quantify the level of connectivity of an aquifer by static measures combined with dynamic measures that are derived from the field tests (Renard and Allan, 2011).

Knudby and Carrera (2005) evaluated several dynamic conductivity indicators and tested them on well-connected and multigaussian fields. They used steady-state flow simulations to test dynamic flow connectivity indicators, and advective transport for transport connectivity indicators. They concluded that some of the tested indicators, especially the indicator that is defined as the ratio of effective conductivity to the geometric mean of the conductivity, responded well to changes

in connectivity features. They found a weak connection between flow and transport indicators and argued that flow connectivity is strongly affected by the low-K barriers in the path, whereas transport connectivity is controlled by the width of the high-K path. In a subsequent study, Knudby and Carrera (2006) analyzed the use of apparent diffusivity as a dynamic connectivity measure, which is the estimated transmissivity over the estimated storativity calculated based on Cooper-Jacob Method (1946), as a flow and transport indicator. They found that the apparent diffusivity provides a good correlation between flow and transport connectivity indicators for most aquifers.

Trincherro et al. (2008) analyzed the relationship between flow and transport connectivity indicators. They proposed the use of the estimated storativity as a dynamic flow connectivity indicator and estimated porosity as a transport connectivity indicator. The flow connectivity indicator was calculated based on the Cooper-Jacob method (1946). They used perturbation theory to analyze the relationship between the flow and transport connectivity indicators. It was concluded that the estimated porosity is a function of point transmissivity values, the distance between the injection and observation points, and estimated storativity.

Dato et al, (2019) examined numerically the impact of the hydraulic conductivity connectivity on the breakthrough curves of a pollutant due to pumping from a well. The results of this study show that the hydraulic conductivity structure is not significant for mildly heterogeneous aquifers but can be more important for highly heterogeneous systems. The authors argue that the imposed pumping rate forces flow and solute transport to flow through high conductivity zones even if they are disconnected.

3. RESEARCH OBJECTIVE

This study focuses on the assessing the impact of flow connectivity on the interpretation of pumping tests. The analysis considers two-dimensional radially convergent flow towards a fully penetrating well in a heterogeneous confined aquifer with different levels of connectivity. The first objective of this study is to numerically investigate the effect of flow connectivity on the estimated groundwater flow parameters, transmissivity and storativity. The parameters are numerically calculated using two different estimation techniques, namely the Cooper-Jacob method and the continuous derivation method. The aim here is to explore the correlation between flow parameters and flow connectivity.

The second objective is to broaden the understanding of flow connectivity by examining the relationship between estimated parameters and the underlying level of flow connectivity. The main purpose here is to investigate whether estimated flow parameters could give some information about the level of field connectivity. It is done by comparing and investigating the estimated parameters obtained from synthetically-generated fields with different levels of static connectivities. In the end, results from different interpretation techniques are compared and the ability to estimate quantitative measures of connectivity from pumping tests is evaluated.

The overarching aim of this research is to advance the understanding of water flow and contaminant transport parameters in order to increase the accuracy of groundwater flow and contaminant transport modeling in porous media.

4. METHODOLOGY

Numerical modeling is used to assess the impact of connectivity on pumping tests and to examine whether connectivity indicators can be estimated from pumping test data. First, the synthetic transmissivity fields are generated, and the fields are conditioned using the method proposed by Zinn and Harvey (2003). Then, a well is placed at the center of each field and a pumping test simulation is performed using MODFLOW computer program (Harbough et al., 2000). The change in the groundwater level as a function of time is recorded as the output of the simulation. After that, the groundwater flow and contaminant transport parameters transmissivity and storativity are estimated using two different interpretation techniques, namely the Cooper-Jacob Method (1946) and the Continuous Derivation Method (Copty et al. 2011). Independent of the pumping tests and parameter estimations, the connectivity scale of each generated field is calculated using a static connectivity measure derived by Western et al. (2001). In the end, the relationship between the connectivity scale and estimated parameters is analyzed. The correlation between the transmissivity estimate and the geometric mean of transmissivity field is also examined.

4.1. Generation of Transmissivity Fields

Transmissivity fields are generated using a sequential Gaussian simulation program (sgsim) which is a module of a public-domain geostatistical library called GSLIB (Deutsch and Journel, 1998). The natural logarithm distribution of transmissivity is a multivariate Gaussian distribution. For simplicity, these fields that have multivariate Gaussian distribution for natural logarithm of transmissivities will be referred to as Gaussian transmissivity fields, or Gaussian fields.

Generated fields have a general size of 999 by 999 arbitrary length units (lu) and uniform grid size of 1 by 1. The mean and the variance of the generated $\ln(T)$ fields are taken as 0 and 1, respectively. Thus, the standard normal distribution is assumed for the probability distribution functions of the log-transmissivity fields. Since the focus of this study is on the local scale heterogeneity, the integral scale is taken as 10 to provide the intermediate correlation length scale (Dagan, 1986; Zheng and Silliman, 2000). The semivariogram function is assumed to be exponential which is often used in hydrological models (Kitanidis, 1997).

In this study, the pumping well is located at the center of each field. Butler (1990) showed that the transmissivity at the location of pumping can have a big influence on the estimation of flow and transport parameters. In order to analyze this impact, the first set of the Gaussian fields are assumed

to have a variable transmissivity at the location of extraction and referred to as unconditional fields, and the second set of the Gaussian fields are assumed to have a constant transmissivity at the location of pumping and referred to as conditional fields. In total, 200 Gaussian transmissivity fields, 100 of which are unconditional and 100 of which are conditional, are generated. The conditional fields are also produced by sgsim module of GSLIB, where the natural logarithm of transmissivity at the center is assumed 0.2. The statistical variables for unconditional and conditional realizations are given in Table 4.1 below.

Table 4.1. Parameter values used in Gaussian transmissivity field generation

Parameters	Gaussian Transmissivity Fields	
	Unconditional	Conditional
Type of Field	Unconditional	Conditional
Number of Realizations	100	100
Semivariogram Type	Exponential	Exponential
Mean	0	0
Variance	1	1
Integral Scale	10	10
Transmissivity at the Extraction Location	Variable	Constant, $\ln(T)=0.2$

The connected high transmissivity and connected low transmissivity fields are generated using the method proposed by Zinn and Harvey (2003). The non-Gaussian fields are generated by transforming the synthetically developed Gaussian fields. This conceptual idea of field transformation takes its foundation from an explanation given by Journel and Deutch (1993), which says that, in reality, the extreme transmissivities, high or low, tend to cluster as isolated groups, whereas transmissivities closer to the mean usually form channels within the field. In order to use this characteristic, first, the absolute value of each transmissivity value of the field is taken. This way, all extreme high/low values are converted to extreme high values. In other words, this new field is expected to have isolated clusters of high transmissivities and channels of low transmissivity. Then, the cumulative distribution function (CDF) of this new field is normalized in order to convert its distribution to the normal distribution. This way, the mean and variance became 0 and 1, respectively. These fields with channels of low transmissivities are referred to as low transmissivity connected fields, or low-T connected fields. The mapping is performed using the following equation:

$$\ln(T') = \sqrt{2} \operatorname{erf}^{-1} \left(2 \operatorname{erf} \left(\frac{|\ln(T)|}{\sqrt{2}} \right) - 1 \right) \quad (4.1)$$

Where

T' transformed transmissivity

T transmissivity of the original Gaussian field

Then, the last group of the fields, high transmissivity connected fields or high-T connected fields are generated by mirroring the values of the low transmissivity connected field around the mean. Examples of the generated Gaussian, low-T connected, and high-T connected fields are given in Section 5.1.

As mentioned above, natural logarithm of transmissivity at the location of pumping well is assumed 0.2 for the conditional Gaussian fields. This condition, together with equation (4.1), results in having constant transmissivity values at the location of pumping for conditional non-Gaussian fields. The corresponding natural logarithm of transmissivity at the location of extraction is calculated as -1 for low-T connected fields (Equation 4.1), and as 1 for high-T connected fields. The realizations used for this study are summarized in Table 2.

Table 4.2. Summary information of the transmissivity fields used in the study

Field Types	Field Sets	Number of realizations	T at the pumping well location
Unconditional	Gaussian	100	Variable
	Low-T Connected	100	Variable
	High-T Connected	100	Variable
Conditional	Gaussian	100	Constant, $\ln(T)=0.2$
	Low-T Connected	100	Constant, $\ln(T)=-1$
	High-T Connected	100	Constant, $\ln(T)=1$

4.2. Simulation of Pumping Tests

Pumping tests are simulated using the computer program MODFLOW, a widely used public-domain groundwater simulator (Harbough et al., 2000). MODFLOW uses the finite-difference numerical approach to simulate the hydraulic head distribution under various boundary conditions. In this study, the pumping well is located at the center of the field, and two monitoring wells are located at distances $r/I=0.1$ and $r/I=0.5$, with distances normalized by the integral scale, I . This way, two transient drawdown curves are analyzed for each field. A total of 600 transmissivity fields that

were generated in Section 4.2 were used for the pumping test simulations. Other important parameters used for the simulations are shown in Table 4.3 below. After the necessary parameters are defined, pumping simulations are performed for each aquifer transmissivity field individually. In order to obtain these individual simulations, a script was written to automatically change the transmissivity input file of MODFLOW while keeping all other parameters the same. This way, the pumping tests are performed for each of the 600 generated aquifer transmissivity field. The storativity was assumed to be uniform equal to 10^{-4} which is a typical value for confined aquifers (Freeze and Cherry, 1979).

Table 4.3. Required parameters for the pumping test simulations

Parameter description	Value
the time unit of the simulation	time units
the length units of the simulation	lu
aquifer type	confined
flow condition	transient
flow rate (positive:injection, negative:extraction)	-2
duration of the simulation	2
number of layers in the model grid	1
number of rows	999
number of columns	999
column spacing in the row direction	1 lu
row spacing in the column direction	1 lu
initial head	20 lu
storativity	1.00E-04
transmissivity	spatially variable, generated using the GSLIB geostatistics software

In this study, the aquifer is assumed to be confined and fully saturated with water. Constant head conditions are imposed at the outer boundaries. Pumping tests are performed on generated synthetically generated transmissivity fields and it is assumed that the pumping tests are terminated before the prescribed head at the boundaries influenced the simulated drawdown. It means that it is expected that the drawdown curve is not affected by the change in boundary conditions. In order to test the validation of this assumption, several pumping tests are continued until the drawdown curves obtained with different boundary conditions start to differ and the tests are terminated before the curves start to diverge.

4.3. Estimation of Groundwater Flow and Solute Transport Parameters

4.3.1. Cooper-Jacob Method

The late time data of the drawdown curve is used for the flow and transport parameter estimation with the Cooper-Jacob method (1946). Assuming that the parameter u is equal to or less than 0.1, the Theis well function can be simplified as:

$$W(u) = -0.5772 + \ln(u) \quad (4.2)$$

or

$$W(u) = \ln \frac{2.25Tt}{r^2S} \quad (4.3)$$

Then, the Cooper-Jacob equation becomes:

$$s(r,t) = \frac{Q}{4\pi T} \ln \frac{2.25Tt}{r^2S} \quad (4.4)$$

In order to make the equation more workable, the natural logarithm is changed to logarithm base 10. The fraction inside the logarithm is also separated and written in two parts. This way, the drawdown curve can be plotted to $\log(t)$ semilogarithmic sheets. The last form of the equation becomes:

$$s(r,t) = \frac{2.303Q}{4\pi T} (\log_{10}(t) + \log_{10}(\frac{2.25T}{r^2S})) \quad (4.5)$$

If drawdown vs. log time graph is drawn, the slope of this line is $\frac{2.303Q}{4\pi T}$, and the intercept of the line with drawdown axis is $\frac{2.303Q}{4\pi T} \log_{10}(\frac{2.25T}{r^2S})$. Using the line equation, the parameters S and T are calculated.

The estimation of flow parameters is done by linear regression. The general representation of a linear equation is given below:

$$y = ax + b \quad (4.6)$$

The parameters a and b are formulated as follows:

$$a = \frac{n \sum xy - \sum x \sum y}{n(\sum x^2) - (\sum x)^2} \quad (4.7)$$

$$b = \frac{\sum y \sum x^2 - \sum x \sum xy}{(\sum x^2) - (\sum x)^2} \quad (4.8)$$

The linear regression formulation and Cooper-Jacob equation is combined, and the final equations are given as below:

$$\frac{2.303Q}{4\pi T} = \frac{n \sum \log(t)s(r,t) - \sum \log(t) \sum s(r,t)}{n \sum (\log(t))^2 - (\sum \log(t))^2} \quad (4.9)$$

$$\frac{2.303Q}{4\pi T} \log\left(\frac{2.25T}{r^2 S}\right) = \frac{\sum s(r,t) \sum (\log(t))^2 - \sum \log(t) \sum \log(t)s(r,t)}{\sum (\log(t))^2 - (\sum \log(t))^2} \quad (4.10)$$

Where

n number of data points

Based on Equations (4.9) and (4.10), transmissivity and storativity parameters are determined when other variables are known and predefined. For each realization, the estimations are made at two different locations using the drawdown curves obtained from two observation wells. The method is applied for all realizations. In order to facilitate the interpretation of final estimations, both transmissivity and storativity are normalized based on the geometric mean of T and constant S_0 respectively used in the pumping test simulations.

4.3.2. Continuous Derivation Method

In this method, the drawdown data and its time derivative are used for the determination of flow parameters at a specific point in time (Copty et al., 2011). The analysis is then repeated for all pumping times. Data from different times are not jointly used in this method because different part

of the aquifer influence the pumping well at different times. This allows for better identification of the flow parameters in heterogeneous aquifers.

The drawdown function was used as it is defined in Theis method. The well function $W(u)$ was written as its integral form. Recall from Section 2.2:

$$\text{Equation (2.5):} \quad s(r,t) = \frac{Q}{4\pi T} W(u)$$

$$\text{Equation (2.6):} \quad u = \frac{r^2 S}{4Tt}$$

The log time derivative of the drawdown is given in the following:

$$s' = \frac{\partial s}{\partial \log_{10} t} = \frac{2.3Q}{4\pi T} e^{-u} \quad (4.11)$$

The ratio of drawdown to its derivative is shown below equation:

$$\gamma = \frac{2.3s}{s'} = W(u) * e^u \quad (4.12)$$

The unique parameter u that is necessary to generate that specific ratio is calculate and this u value is denoted as u^* . Then, the flow parameters transmissivity and storativity are calculated for a given time as given below:

$$T = \frac{Q}{4\pi s(t)} W(u^*) \quad (4.13)$$

$$S = \frac{4Ttu^*}{r^2} \quad (4.14)$$

After the flow parameters are estimated, the time-dependent function can be converted to distance-dependent using the following equation:

$$r^* = \sqrt{\frac{4Tt}{1.65S}} \quad (4.15)$$

In order to smoothen the small fluctuations in the data, a moving average is used on estimated parameters. First, the flow and transport parameters are calculated as a function of pumping time. Then, the time-dependent parameter curves are converted to radial distance-dependent curves in order to fully understand the effect of the expansion of the effective area on the values of the estimated parameters. To facilitate the interpretation of final estimations, both transmissivity and storativity are normalized based on the values used for the pumping simulations, as it was done for the parameters estimated by the Cooper-Jacob Method.

Moreover, the geometric mean of generated transmissivity field as a function of radial distance around the well is also calculated and compared with estimated transmissivity curve to investigate the relationship between the two. The geometric mean of transmissivity fields are calculated using the generated transmissivity fields. Starting from the location of the extraction well, the radial distance around the well is gradually increased and the geometric mean of the transmissivity values that are located closer to the well than the radial distance is calculated.

4.4. Calculation of Integral Connectivity Scales of Generated Fields

The integral connectivity scale of each generated field is calculated using the method proposed by Western et al. (2001). First, a binary indicator variable is defined at each grid. If the cell is having a high transmissivity value, then the indicator takes the value 1, and 0 otherwise. The status of the cell as high-transmissivity or low-transmissivity is decided based on a predetermined threshold transmissivity value. The integral connectivity, $\tau(h)$ is defined as the probability that two points separated a distance of h fall within the same cluster. In this study, the threshold transmissivity value is chosen as 1. The generated binary matrix shows the size of high/low transmissivity clusters and each cluster is labeled with a unique value. In order to label each cluster, a loop goes through all points in the binary matrix. When an unlabeled high-T point is encountered, it is labeled with a unique cluster number. Then, the four neighbor cells to that point are checked to see whether they too are high-T. Any adjacent high T points are also labeled with the same cluster number and the procedure is repeated for every point in the matrix.

After the clusters are determined, the connectivity function is calculated as follows. Starting from the first point (1,1) of the cluster matrix and looping through all points, whenever a high-T

point is detected, a second loop starts and calculates the separation distances between that high-T point and all the points in the matrix. The number of total pairs for each separation distance bin are incremented accordingly. When the second loop encounters another high-T point which has the same cluster number as the initial high-T point, the number of connected pairs for that separation distance is also incremented by one. When both of the loops are executed, the connectivity of every bin is computed as the ratio of the number connected pairs (equivalent to probability) to the number of total pairs in that bin. The connectivity function is shown in Equation 4.16. The integral connectivity scale is then computed as the integral of the connectivity function as shown in Equation 4.17. This connectivity function provides a measure of static flow connectivity that is independent of the pumping test and the ensuing flow field.

$$\tau(h) = \frac{CP}{TP} \quad (4.16)$$

Where

$\tau(h)$	Connectivity function
h	Separation distance
CP	Number of connected pairs
TP	Number of total pairs

$$I_{con} = \int_0^{\infty} \tau(h) dh \quad (4.17)$$

Where

I_{con}	Integral connectivity scale
-----------	-----------------------------

After the integral connectivity scale of each simulation is calculated, the estimated flow parameters and the calculated integral connectivity scales are analyzed together for possible correlation.

5. RESULTS

This chapter presents the results of the numerical investigation of the impact of connectivity on groundwater flow parameters estimated from pumping tests. Section 5.1 presents the synthetically generated transmissivity fields used in the numerical simulations. As noted in Chapter 4, a total of 600 fields are generated: 200 Gaussian, 200 low-T connected and 200 high-T connected fields. Section 5.2 examines the pumping test simulations and shows the transient drawdown and drawdown derivative for randomly selected realizations to better understand the impact of connectivity on the drawdown behavior that can be obtained from the pumping tests. Section 5.3 presents the integral connectivity scale, a static measure of connectivity. Example connectivity functions and the integral connectivity scales of each field used in the study are also presented. Section 5.4 presents the interpreted pumping test analysis using the Cooper-Jacob method and shows the estimated groundwater flow parameters, transmissivity and storativity. The correlation of the estimated parameters to the connectivity measures calculated in the previous section are examined. Lastly, Section 5.5 presents the application of the Continuous Derivation method on pumping test data for the estimation of the flow parameters. The estimated parameters as a function of both time and radial distance are shown for five randomly selected high-T connected, Gaussian, and low-T connected fields. In addition, the geometric mean of transmissivity fields as a function of radial distance are also calculated and compared with the transmissivity estimated with the Continuous Derivation to examine the relation of the estimated transmissivity to the underlying aquifer heterogeneity.

5.1. Generation of Transmissivity Fields

In this section the generated transmissivity fields, which are grouped as Gaussian, high-T connected and low-T connected fields, are presented. As described in Section 4.1, the Gaussian fields are generated using the sequential Gaussian simulation program, *sgsim*, of the geostatistical library *GSLIB* (Deutsch and Journel, 1998).

The main statistical parameters used to generate the Gaussian transmissivity fields are the mean $m_Y=0$, variance $\sigma^2_Y=1$, and the integral scale $I=10$ length units (lu) where $Y=\ln(T)$ is the natural log transform of T . Defining the main random variable as Y instead of T guarantees that negative t values are not generated. The storativity is assumed to be uniform. This is justified as numerous field studies have shown that the variation of S is much smaller than that of T . In order to

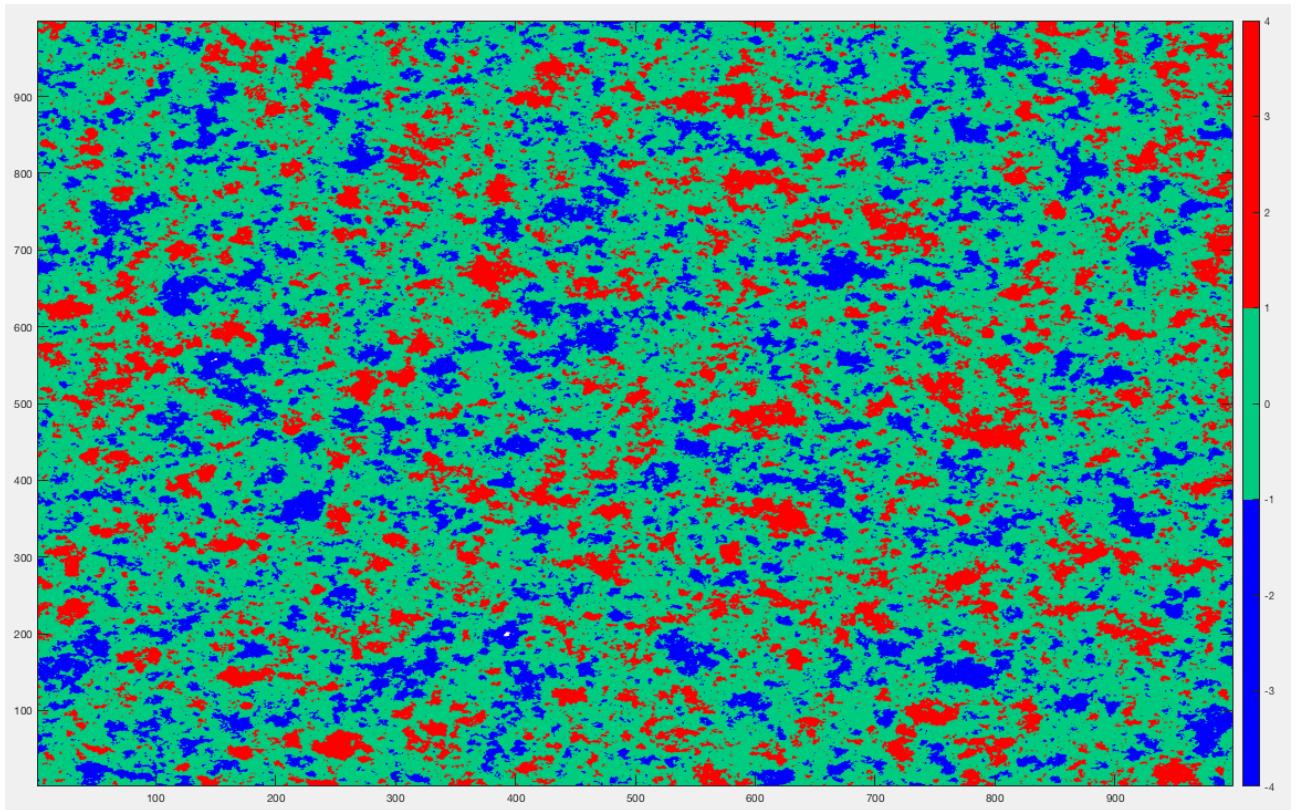
observe the effect of transmissivity at the location of pumping, one half of the Gaussian realizations are assumed to have a variable transmissivity at the pumping location, the other half, referred to as conditional transmissivity fields, are assumed to have a constant transmissivity taken as $\ln(T)=0.2$ (Table 4.1).

The non-Gaussian low-T connected and high-T connected fields are generated according to the method of Zinn and Harvey (2003). In total 200 fields are generated for each type of field (Table 4.2).

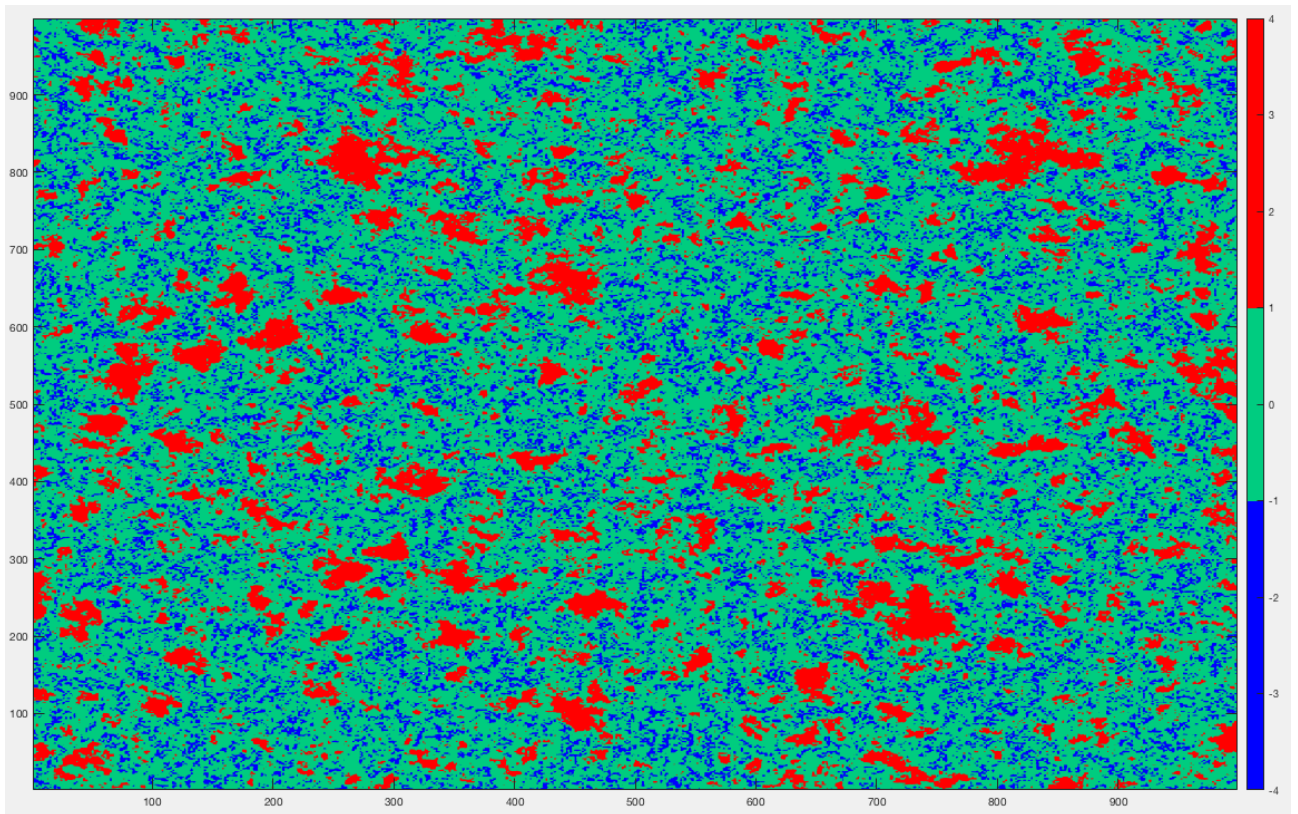
Figure 5.1a, b, and c show a randomly selected generated Gaussian field along with the corresponding low-T connected and high-T connected fields, respectively. As mentioned before, these generated fields represent the distribution of the natural logarithm of transmissivity values $Y=\ln(T)$.

The natural logarithm of transmissivities that are larger than 1 are shown in red, the values between 1 and -1 are shown in green, and the values smaller than -1 are shown in blue. In Figure 5.1a, it can be observed that the middle range transmissivity values (green color) are well connected with discontinuous clusters of high and low transmissivity values. This type of field with discontinuous high and low transmissivity clusters is a feature of Gaussian fields that has been reported in the literature (e.g., Trinchero et al., 2008; Renard and Allard, 2011). In Figure 5.1b, low transmissivity values generated channels in blue, and high transmissivity values remained as discontinuous clusters. Hence, this type of field is called low-T connected fields. Figure 5.1c is the mirror of Figure 5.1b around the mean. Because of that mirroring effect, now high transmissivity channels and low transmissivity clusters can be observed. This last type of field is referred to as high-T connected fields. Similar features are observed in the other generated transmissivity fields and are therefore not shown here.

(a)



(b)



(c)

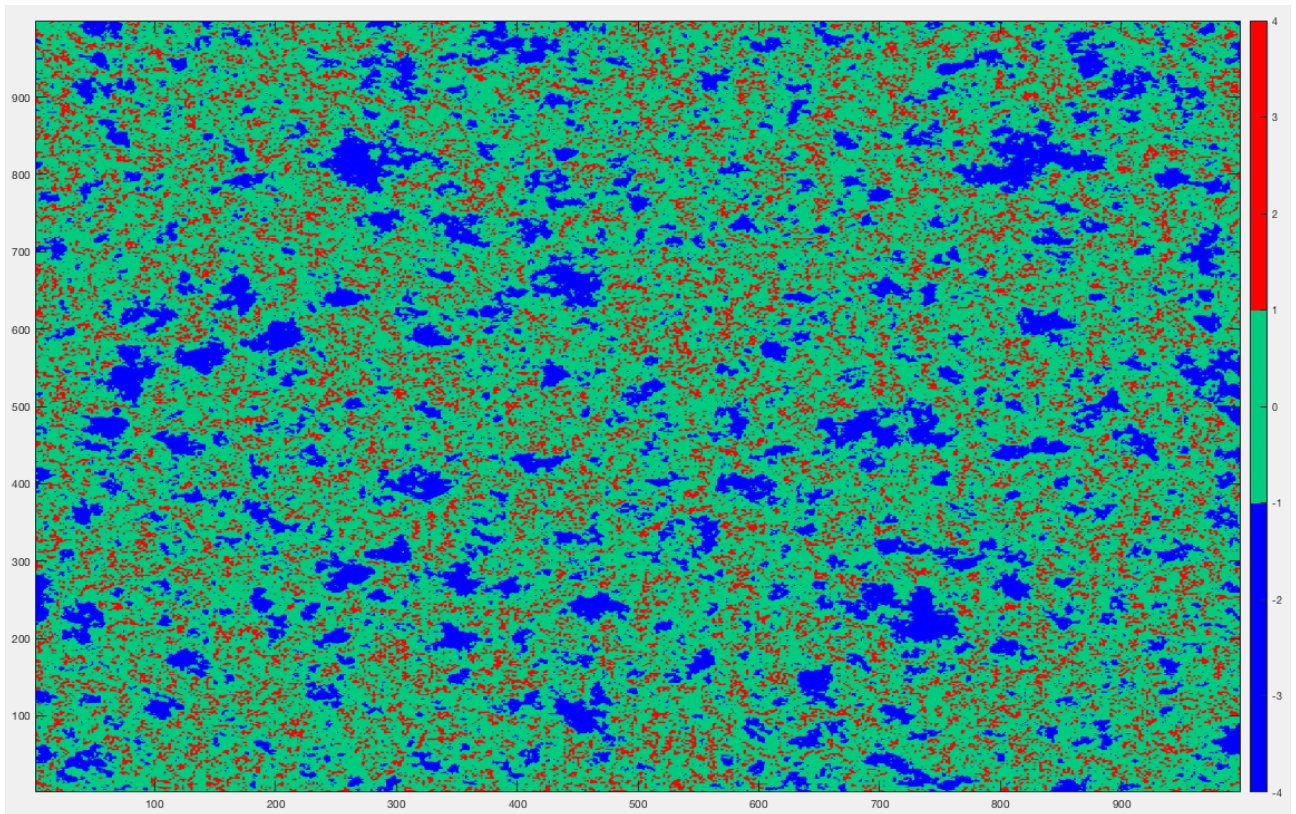


Figure 5.1. Graphical representation of a randomly selected (a) Gaussian field, (b) low-T connected field, and (c) high-T connected field

5.2. Pumping Test Simulations

This section describes the pumping test simulations that were performed using MODFLOW groundwater flow simulation model (Harbough et al., 2000). Each transmissivity fields (600 in total) presented in the previous section were used for the simulations. In order to explore the effect of observation location on parameter estimation, two observation wells are located at two different locations $r/I=0.1$ and $r/I=0.5$, where r represents the radial distance from the pumping location, and I represents the integral scale, which is assumed as 10 lu. The necessary variables used in the simulation are listed in Table 4.3. The outputs of the pumping tests are the transient drawdown curves obtained at two different locations for all generated fields. The drawdown derivative with respect to the log of the time, $ds/d\log(t)$ are also calculated since they will be used for the parameter estimation using the Continuous Derivation method.

Figure 5.2 shows the results obtained from the pumping test for a randomly selected field set. Figure 5.2 a and b demonstrate the transient drawdown curve and time derivative of the drawdown

curve, respectively. The observation well is located near the pumping well, where $r/I=0.1$. Figure 5.2 c and d show the transient drawdown and drawdown derivative curves, where $r/I=0.5$.

Comparison of the transient drawdown curves obtained at two different locations show that the drawdown increases with distance for all types of fields. Water extraction starts from the pumping well location and expands radially in time. Because of that, the drawdown is expected to be smaller as the radial distance from the pumping well increases. Moreover, it can be seen that when the pumping is terminated, low-T connected field has the largest drawdown, and the high-T connected field has the smallest. But this is not necessarily the case for all other realizations.

The shape of the drawdown and drawdown derivative curves depend on the actual transmissivity distribution around the pumping well. It is seen that the derivative curves exhibit more variability than the drawdown. For that reason, it has been reported in the literature that the derivative may be a better parameter to reveal information about the aquifer heterogeneity.

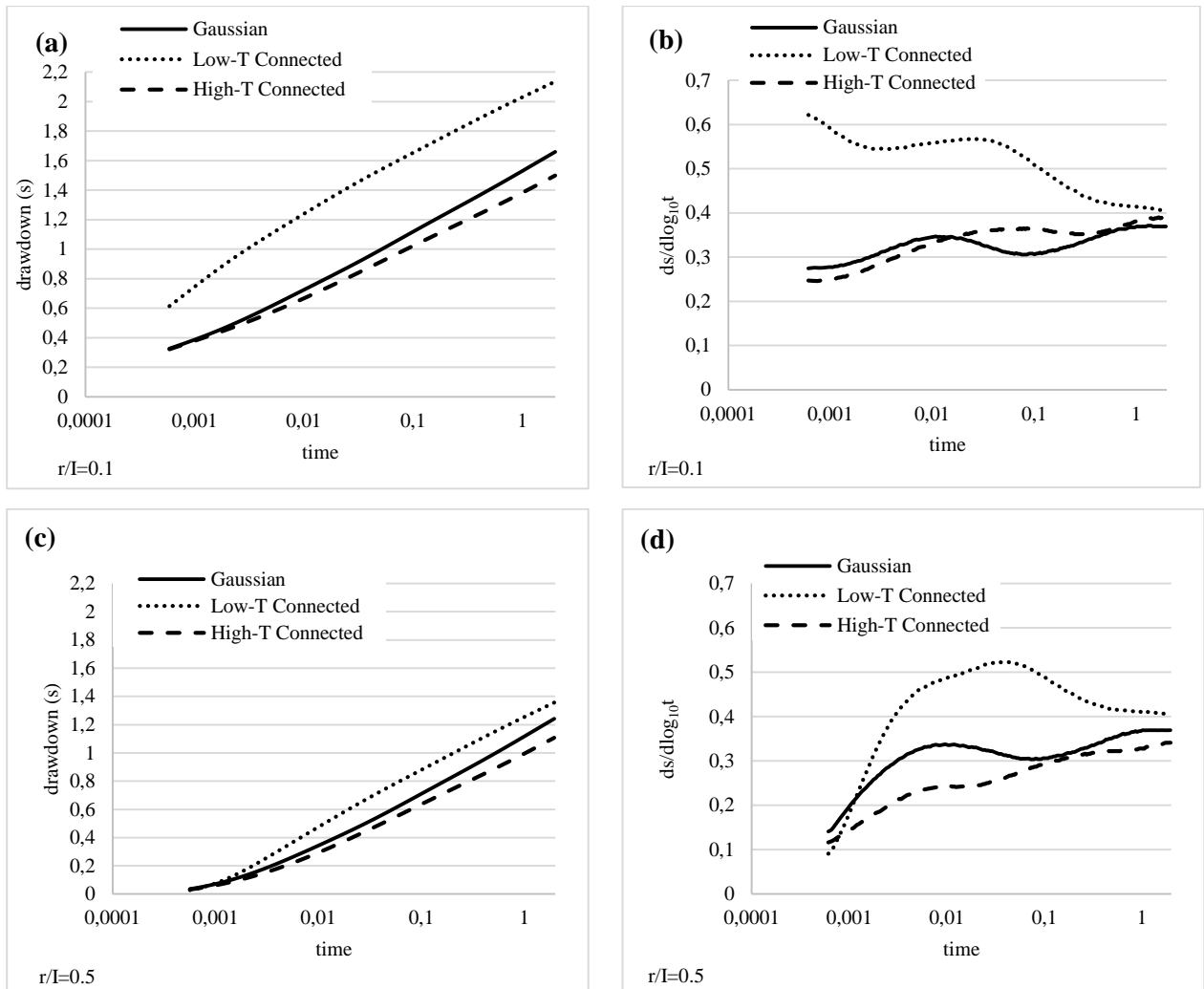


Figure 5.2. MODFLOW simulation outputs for a randomly selected Gaussian, low-T connected and high-T connected fields. (a) shows drawdown vs. time at $r/I=0.1$. (b) shows drawdown derivative vs. time with the observation well is located at $r/I=0.1$. (c) shows drawdown vs. time at $r/I=0.5$. (d) shows drawdown derivative vs. time with the observation well is located at $r/I=0.5$.

5.3. Static Measure of Connectivity

In this section, the connectivity function and its integral, which is referred to as the integral connectivity scale, are calculated based on the method proposed by Western et al. (2001). This methodology provides a static measure of connectivity meaning that it is independent of the flow (pumping rate, boundary conditions, etc.). The calculation procedure is explained in Section 4.4. Transmissivity fields described in Section 5.1 are used for the calculation of the connectivity measure. The calculation of the integral connectivity is applied to all generated transmissivity fields.

Figure 5.3 shows the connectivity function of a randomly selected Gaussian field and its non-Gaussian variations, high-T connected and low-T connected fields. These three fields only vary in their levels of connectivity. The integral connectivity scale, which is the measure of connectivity, is the integral of the connectivity function; it can be determined by numerically calculating the area under the connectivity curve. Here, for this randomly selected example field set, it can be seen that the high-T connected field has the largest integral connectivity scale, followed by the Gaussian field. Low-T connected field has the smallest integral connectivity scale, as expected. This confirms the initial expectation that fields with high transmissivity channels throughout the field should have a larger integral connectivity scales, whereas the fields with low transmissivity barriers should have smaller integral connectivity scales. Figure 5.3 shows that the connectivity function generally decreases with distance, however, because of the irregular shape of structures some fluctuations occur.

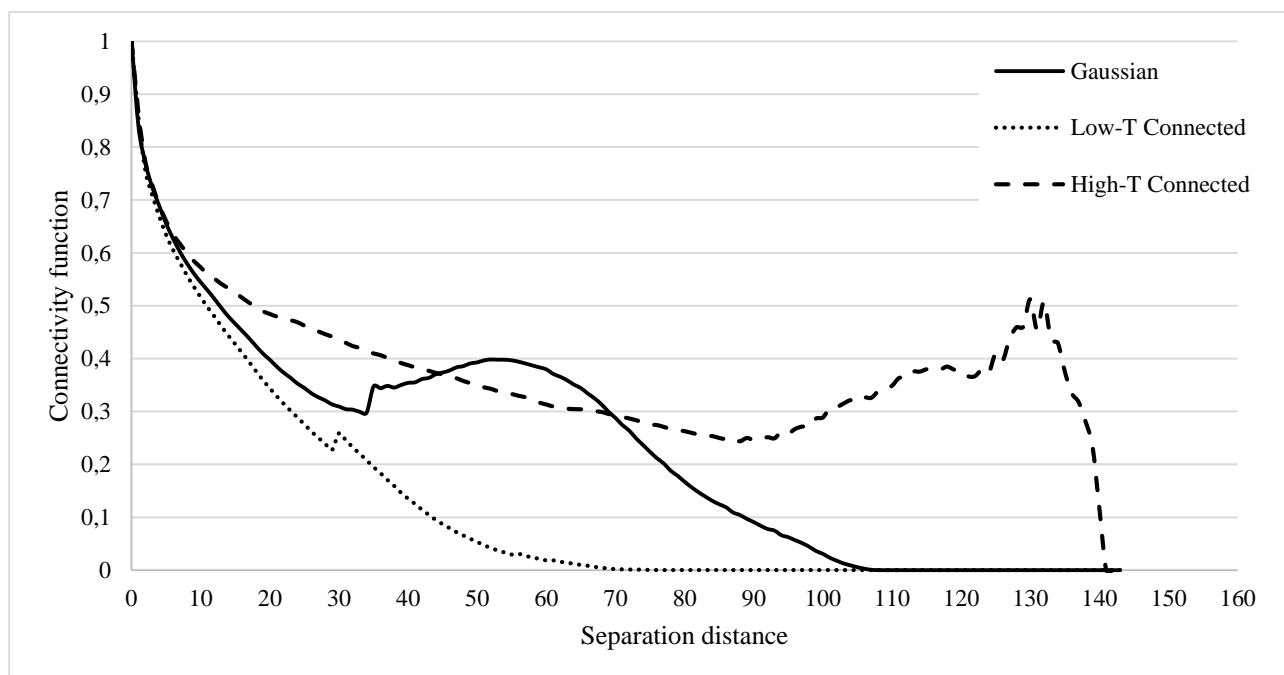


Figure 5.3. Connectivity function as a function of separation distance for a randomly selected unconditional Gaussian field (field 10), and its variations different levels of connectivity as low-T connected and high-T connected

Table 5.1 represents the average and the standard deviation of integral connectivity function that are calculated over the different types of fields and generation conditions. On average, high-T connected fields have larger integral connectivity scales, followed by Gaussian fields and low-T connected fields, respectively. This ranking is valid for both unconditional and conditional fields. This result is also consistent with the initial expectation. The standard deviations, on the other hand,

are generally large for all types and this indicates that the integral connectivity scale of individual fields varies widely. Low-T connected fields have lower standard deviations for both conditions. When the unconditional and unconditional realizations are evaluated together, the conditional realizations have relatively smaller standard deviations for all field types because of the additional constraint on them (transmissivity at the well is $Y=\ln(T)=0.2$).

Figure 5.4 shows the integral connectivity scale of each transmissivity field used in this study. Although many low-T connected fields have smaller integral connectivity scales compared to their Gaussian and high-T connected versions, some exceptions can be also observed. Moreover, high-T connected fields do not always have the largest integral connectivity scales and many exceptions with Gaussian fields having the largest integral connectivity scale can be observed both for unconditional and conditional realizations. Thus, although the average integral connectivity scales follow the expected trend, this is not always the case for individual field sets. Because of that, it can be said that the method of integral connectivity scale proposed by Western et al. (2001) may not be enough to differentiate the fields with different levels of connectivity generated by the method proposed by Zinn and Harley (2003). On the other hand, one can say that the fields generated by using the Zinn and Harvey method may not always comply with the integral connectivity scales.

Table 5.1. Average and standard deviation of integral connectivity scales over the field sets, Gaussian, low-T connected, and high-T connected

	Gaussian		Low-T Connected		High-T Connected	
	Average (lu)	standard deviation (lu)	Average (lu)	standard deviation (lu)	Average (lu)	standard deviation (lu)
Unconditional realizations	33.48	19.88	19.88	13.68	43.93	19.43
Conditional realizations	33.03	18.15	17.98	9.15	46.22	18.14

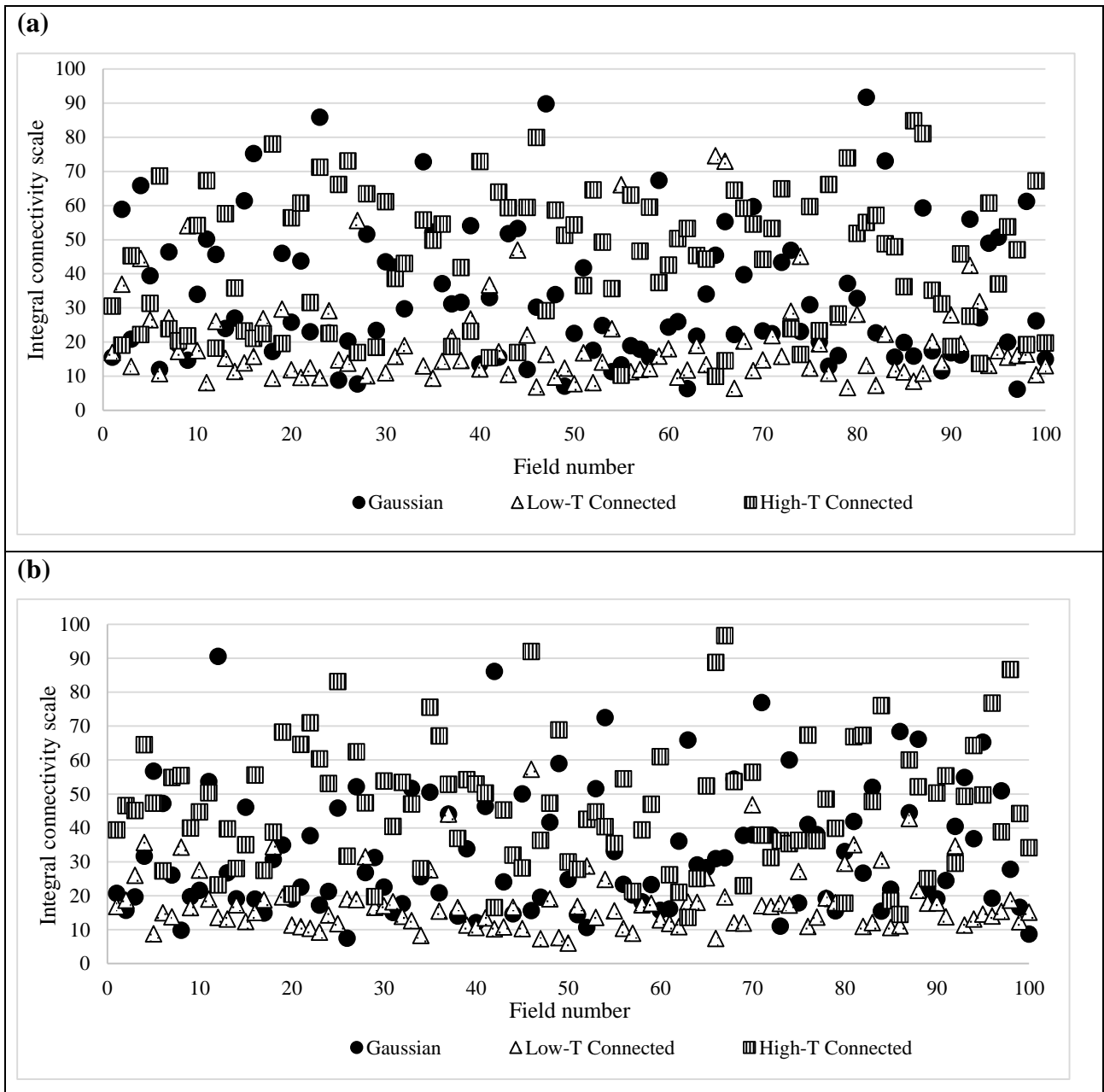


Figure 5.4. Integral connectivity scales of (a) unconditional and (b) conditional realizations

5.4. Application of Cooper-Jacob Method

This section describes the pumping test analysis and estimation of groundwater flow parameters using the Cooper-Jacob linear estimation method. As mentioned in Section 4.3.1, this method uses the late time data of the drawdown curves obtained from pumping tests to estimate a single representative value for the aquifer volume surrounding the pumping well. Both transmissivity and storativity parameters are estimated for all the generated fields. In order to understand the relation between the estimated parameters and initial values, the transmissivity estimates are normalized with the geometric mean of the transmissivity field, and the storativity estimates are normalized with the initial storativity used in the pumping tests. As mentioned before,

the geometric mean of the generated transmissivity fields, T_g , is equal to 1, while the storativity, S_0 , is 10^{-4} . Figure 5.5 shows the histogram of normalized transmissivity values estimated for unconditional realizations and Figure 5.6 shows the histogram of normalized storativity values estimated for unconditional realizations. Both parameter estimations are performed at $r/I=0.1$. Here, it is seen that the variation in estimated transmissivity values is much smaller compared to the variation in estimated storativity values. Moreover, the majority of the estimated transmissivities are very close to the geometric mean of transmissivity fields, whereas the estimated storativities can differ a lot from the initial storativity.

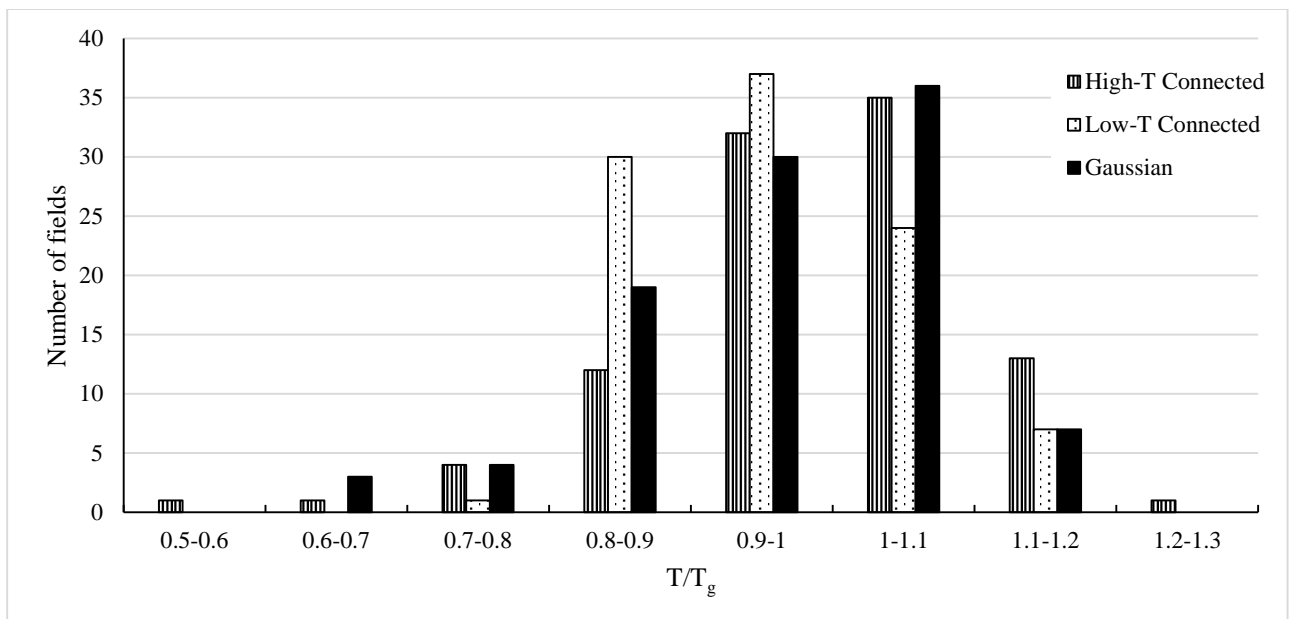


Figure 5.5. Histogram of T/T_g of unconditional realizations where $r/I=0.1$

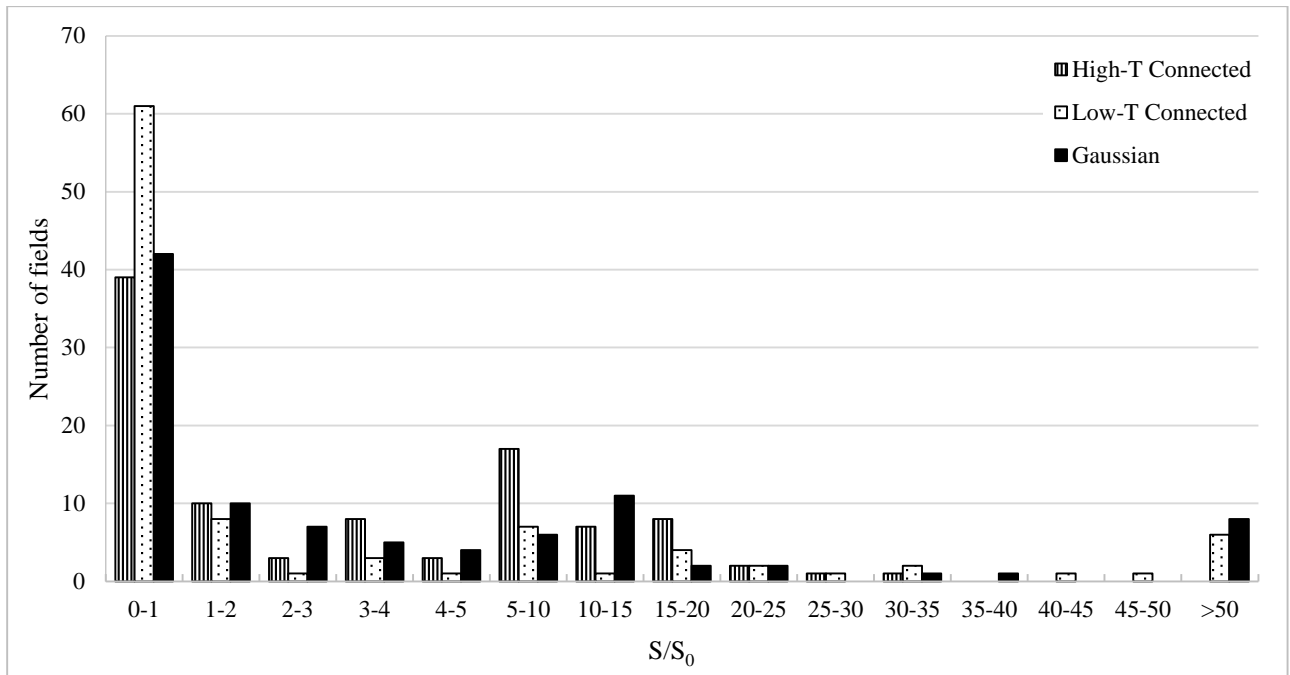
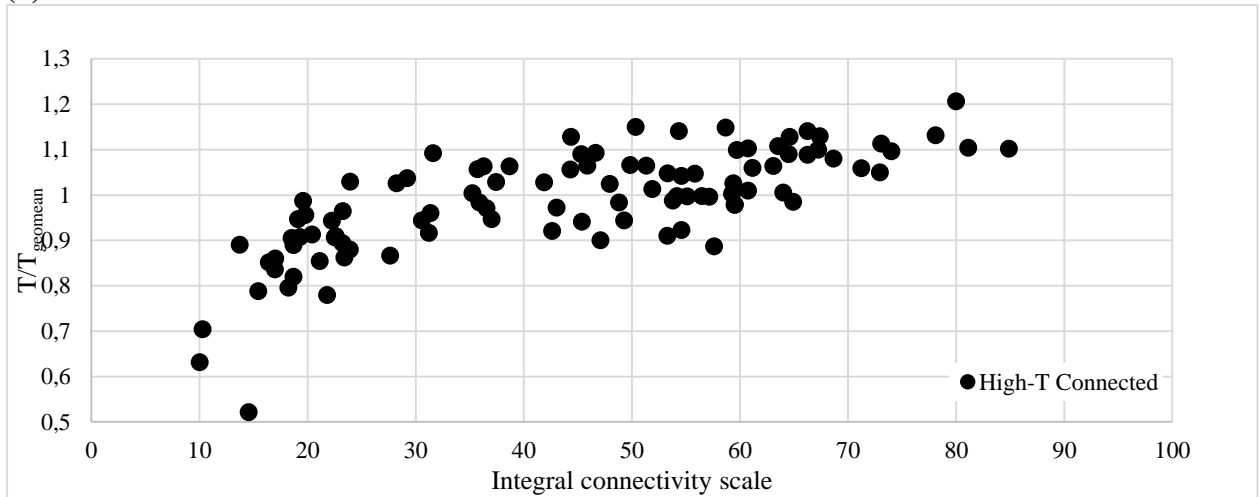


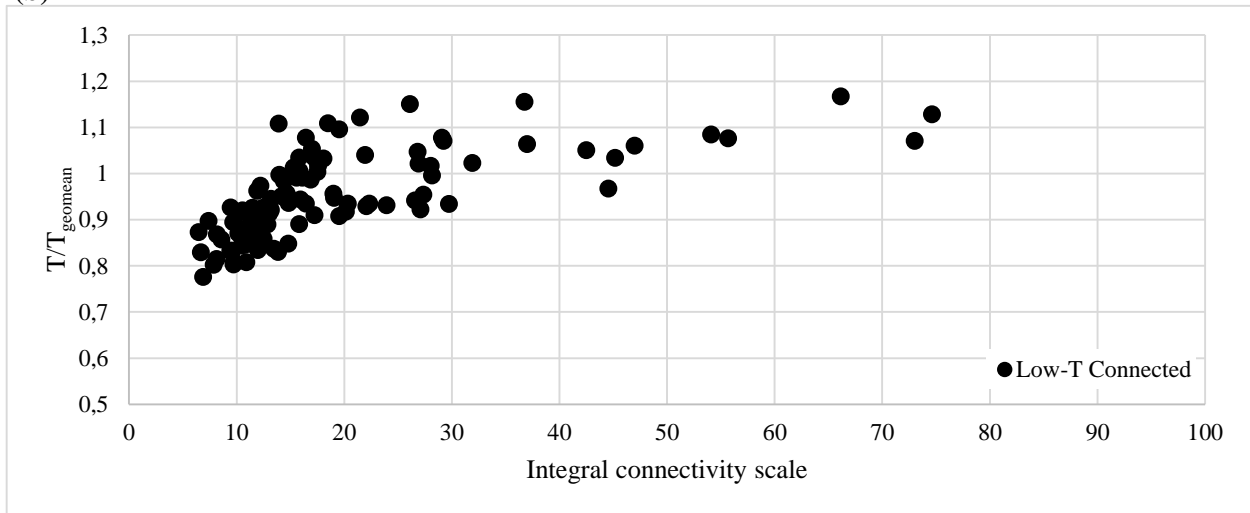
Figure 5.6. Histogram of S/S_0 of unconditional realizations where $r/I=0.1$

Figure 5.7a-c show the transmissivity vs. integral connectivity scale comparison for high-T connected, low-T connected, and Gaussian fields, respectively. Figure 5.7d shows all of them together on one graph to evaluate the parameter estimation more completely. This figure only considers the fields of unconditional realizations as an example, and the estimations are made for the observation well located at $r/I=0.1$. The transmissivity estimations of the remaining fields are not shown graphically because they follow a similar trend. Table 5.2 depicts the corresponding statistics for all types of realizations and observation locations. Here, the average (avg) and the standard deviation (st dev) of transmissivities estimated over different field types are shown. Average transmissivities are all very close to 1, and the standard deviations are considerably small. That can be concluded as that the level of connectivity does not greatly affect the estimation of transmissivity using the Cooper-Jacob method. The estimated transmissivities are also very close to the geometric mean of transmissivity fields. These results are in parallel with the results of previous research that is performed by Meier et al. (1998).

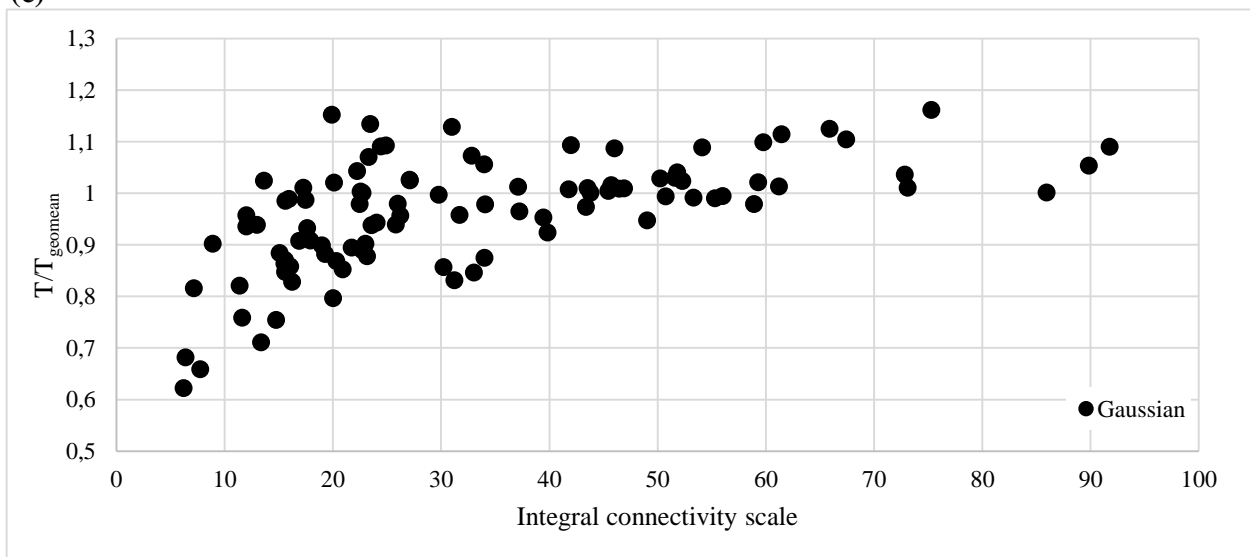
(a)



(b)



(c)



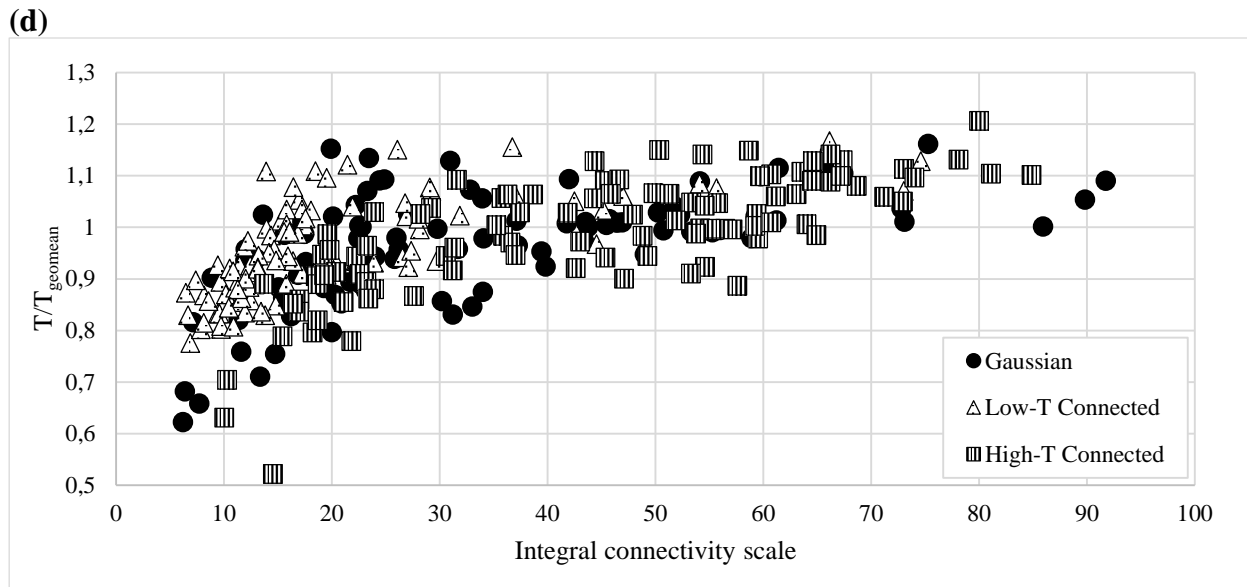


Figure 5.7. Transmissivity vs integral connectivity scale for (a) high-T connected fields, (b) low-T connected fields, (c) Gaussian fields and (d) all fields combined together for unconditional realizations where the observation well is located at $r/I=0.1$

Table 5.2. Average and standard deviation of transmissivities estimated for different types of realizations and fields

Estimated parameter: Transmissivity (T/T_{geomean})	Gaussian		Low-T Connected		High-T Connected		All Combined		
	avg	st dev	avg	st dev	avg	st dev	avg	st dev	
Unconditional realizations	$r/I=0.1$	0.96	0.11	0.95	0.09	0.99	0.11	0.97	0.11
	$r/I=0.5$	0.97	0.09	0.96	0.07	0.99	0.11	0.97	0.09
Conditional realizations	$r/I=0.1$	0.96	0.12	0.95	0.07	1.00	0.08	0.97	0.09
	$r/I=0.5$	0.97	0.09	0.95	0.06	1.00	0.07	0.97	0.08

Figure 5.8a and b show the normalized storativity vs. integral connectivity scales for unconditional fields with the observation well located at $r/I=0.1$ and $r/I=0.5$, respectively. Figure 5.8c and d show the normalized storativity vs. integral connectivity scales for conditional fields with the observation well located at $r/I=0.1$ and $r/I=0.5$, respectively. The logarithmic trendlines numerically show the correlation between the estimated storativity and integral connectivity scales. Figure 5.8 clearly demonstrates the difficulty of estimating the storativity of heterogeneous aquifers from pumping test data. The storativity estimate is directly related to the variation of the transmissivity as some researchers have reported in the literature (Trincherro et al., 2008; Meier et al., 1998) This variability in the transmissivity masks the actual storativity of the aquifer. This observation is true for all Gaussian low-T connected and high-T connected fields. When the transmissivity at the pumping location is fixed, the variability in storativity values decrease significantly.

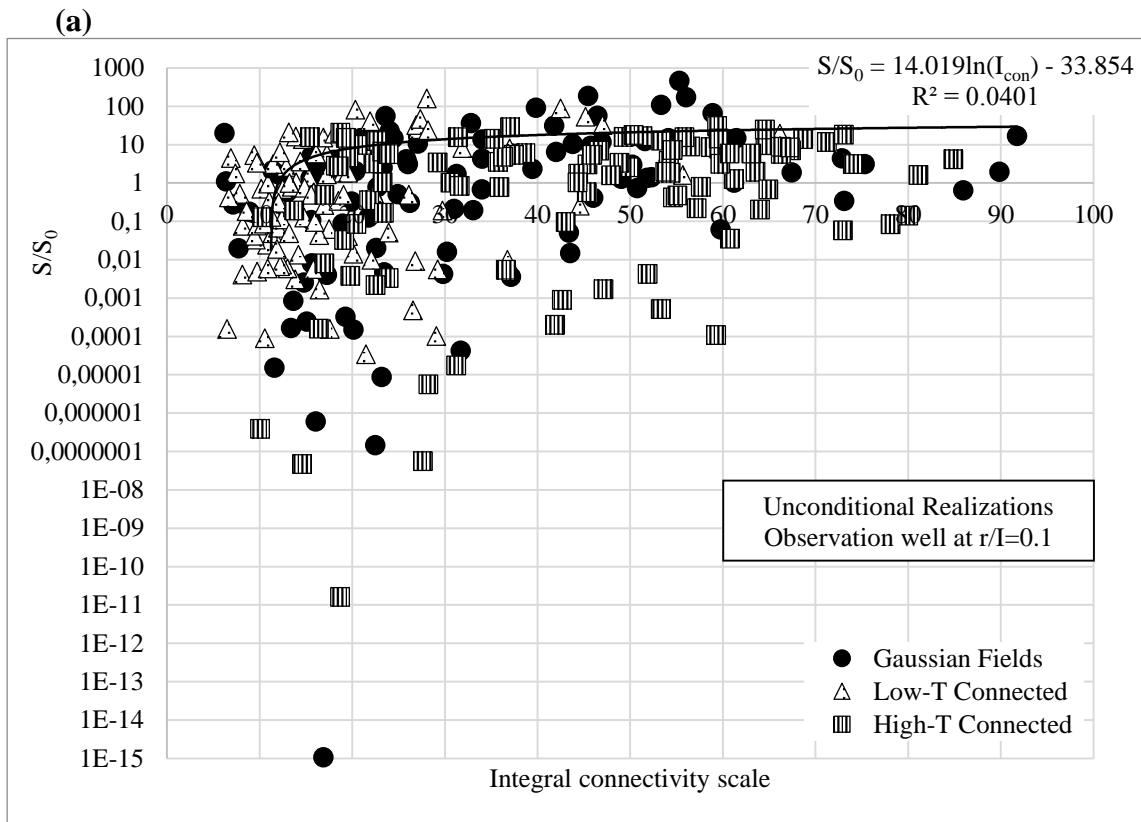
Figure 5.8 also shows that the estimated storativity is influenced by the level of connectivity. For low-T connected fields the estimated storativity is consistently lower than S_0 . On the other hand, the estimated S for the Gaussian and high-T fields over-estimate S_0 . The highest S estimates are for the high-T fields. However, there is significant overlap between these two sets of S estimates. The trendlines show that there is low correlation between the estimated storativity and the integral connectivity scales. As expected, the correlation increases when the transmissivity at the pumping location is fixed. It also increases when the observation well is located at a farther away point because of the averaging of the values.

The variability in integral connectivity scales can also be seen in Figure 5.8. As it was summarized in Table 5.1, on average, low-T connected fields have smaller integral connectivity scales and high-T connected fields have larger integral connectivity scales. However, the integral connectivity scales of individual fields vary widely for all Gaussian, low-T connected and high-T connected fields.

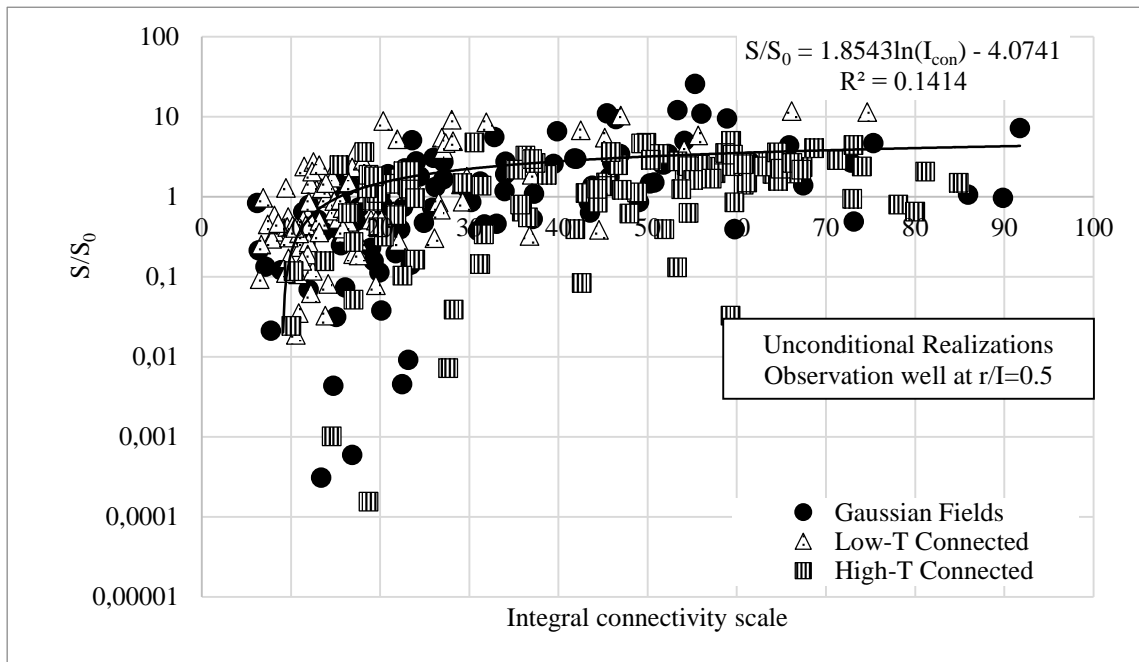
Figure 5.9a-d show the histogram of S/S_0 for unconditional and conditional realizations. Figure 5.9a and b are the histograms of normalized storativities that are estimated at $r/I=0.1$ and $r/I=0.5$, respectively. Figure 5.9c and d show the histograms of S/S_0 that are estimated at $r/I=0.1$ and $r/I=0.5$, respectively. Table 5.3 depicts the related statistics for all types of realizations and observation locations. The average (avg) and the standard deviation (st dev) of normalized storativities estimated over different field types are shown. The standard deviation of the unconditional realizations estimated at $r/I=0.1$ is considerably large for all field types. This wide variety in the distribution can also be seen in both Figure 5.9 and Table 5.3. As the observation location shifts from $r/I=0.1$ to 0.5, the variation decreases for both types of realizations. This observation is consistent with the fact that as the separation distance between the observation and pumping well increases, the estimation averages a larger area, and thus, the variation between different estimations becomes smaller.

When the estimated storativities and the level of connectivities are compared in Table 5.3, it can be seen that there is low correlation between the two. Estimated storativity values vary significantly from realization to realization. This is an important finding as it shows that it is not very likely to reliably quantify the level of connectivity of a field by analyzing its storativity estimation that is determined by the Cooper-Jacob method. This is also the case for the transmissivity estimation as it does not get affected by the level of connectivity of the transmissivity field. In other words, although there is a slight correlation between the estimated storativity and the

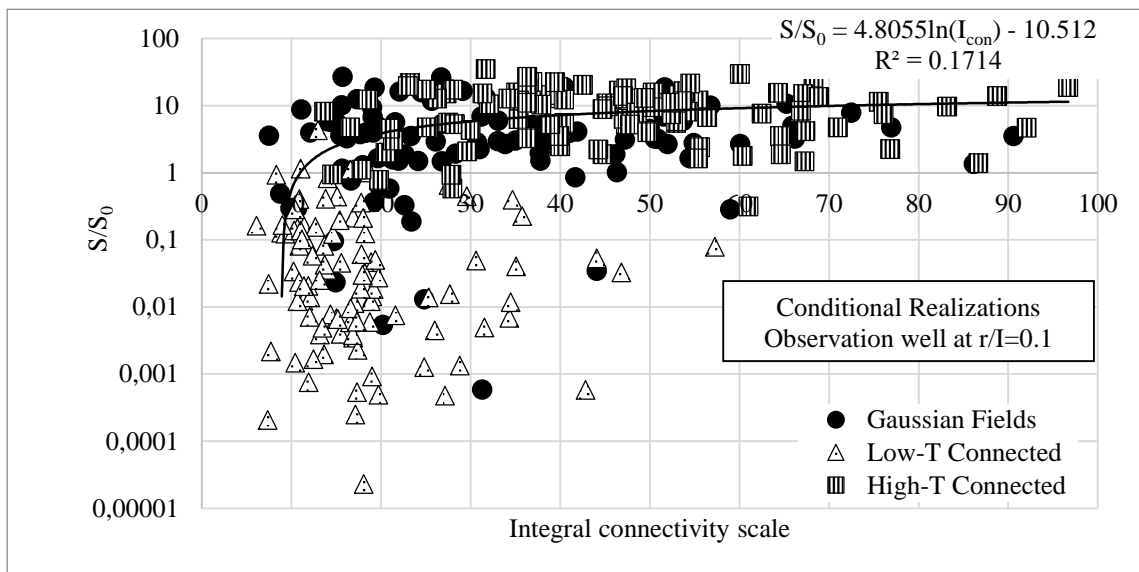
level of connectivity, the flow parameters that are estimated using the Cooper-Jacob method do not uniquely reveal the connectivity structure of the related aquifer.



(b)



(c)



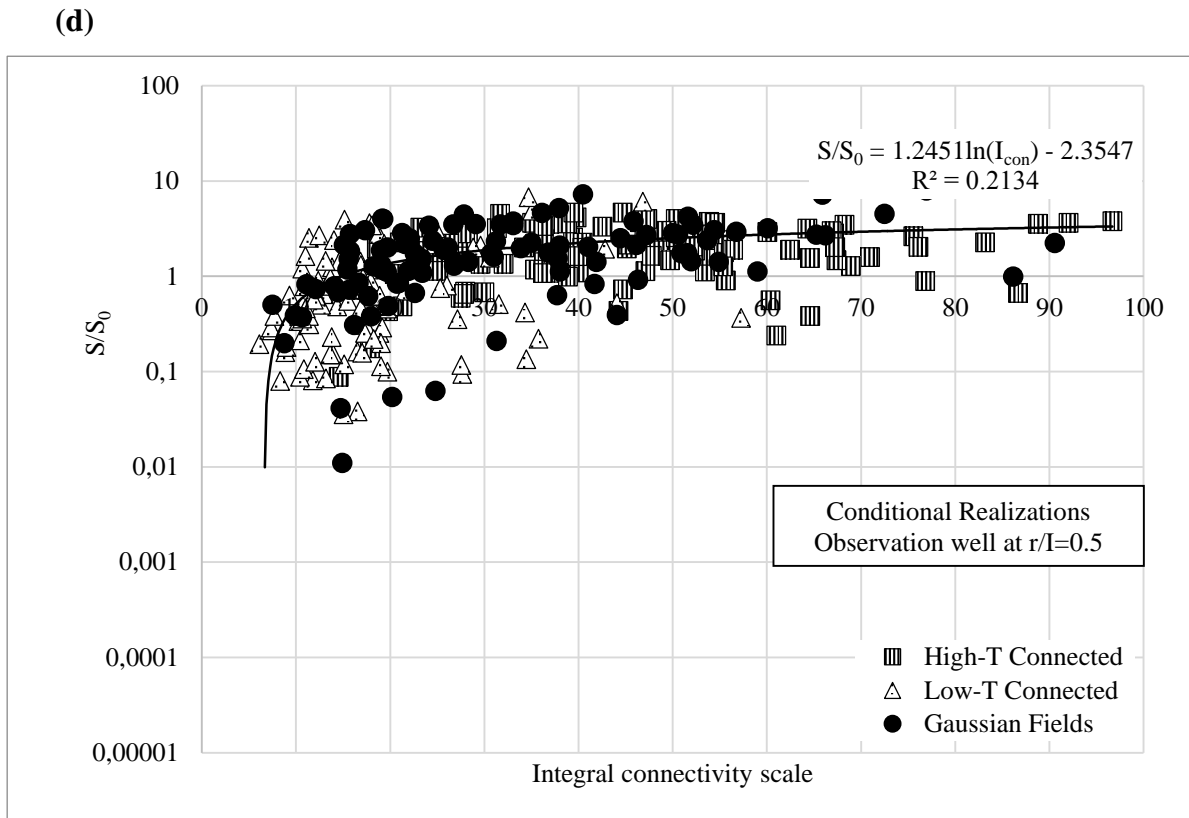
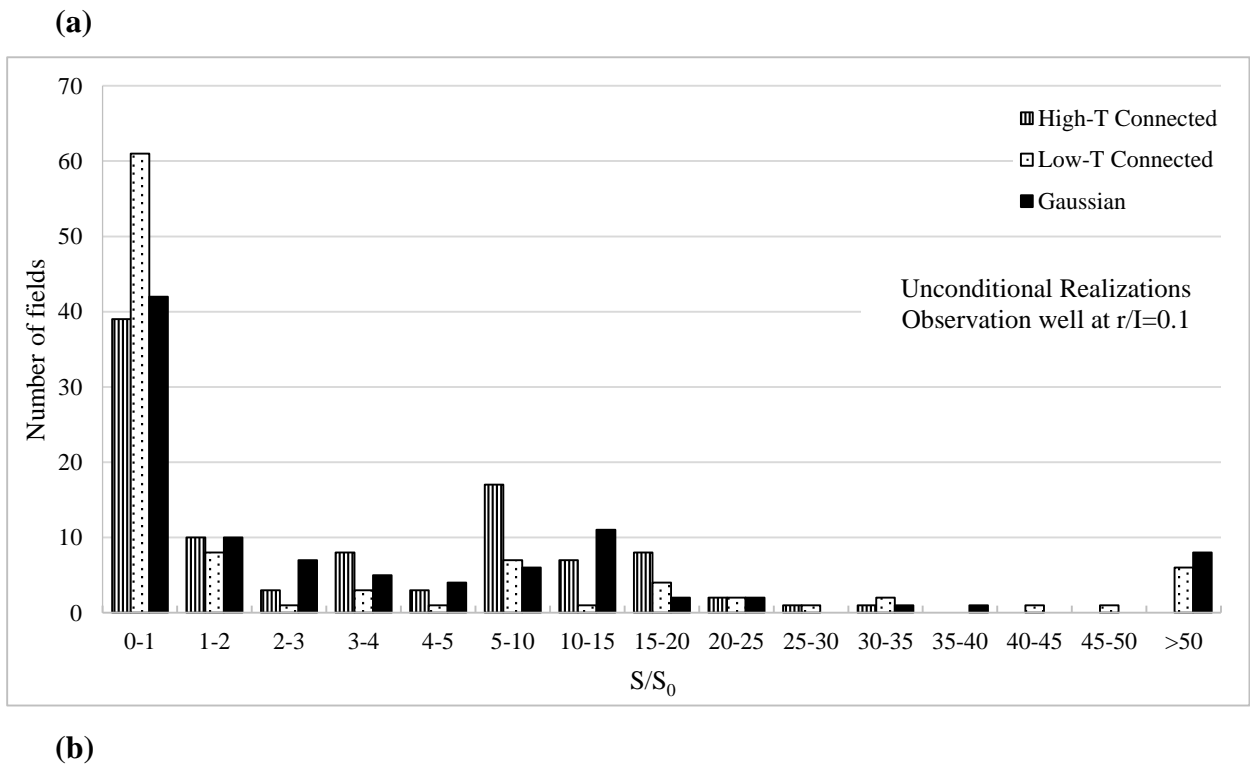
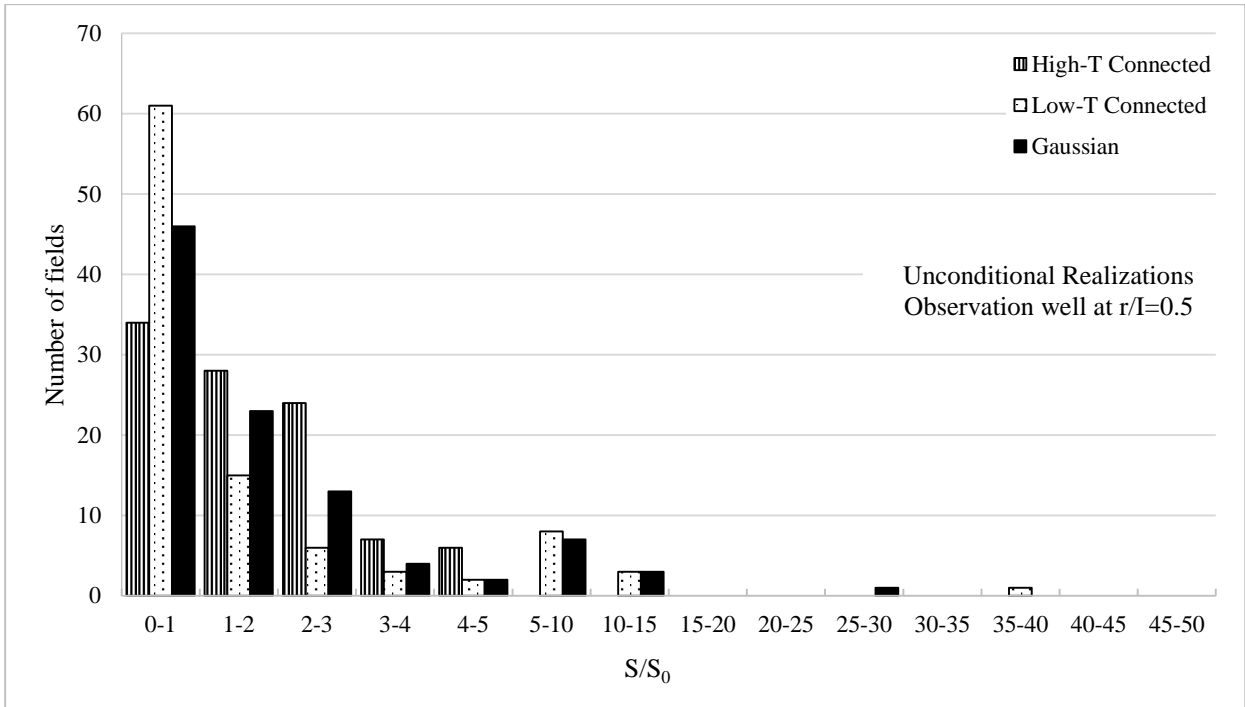


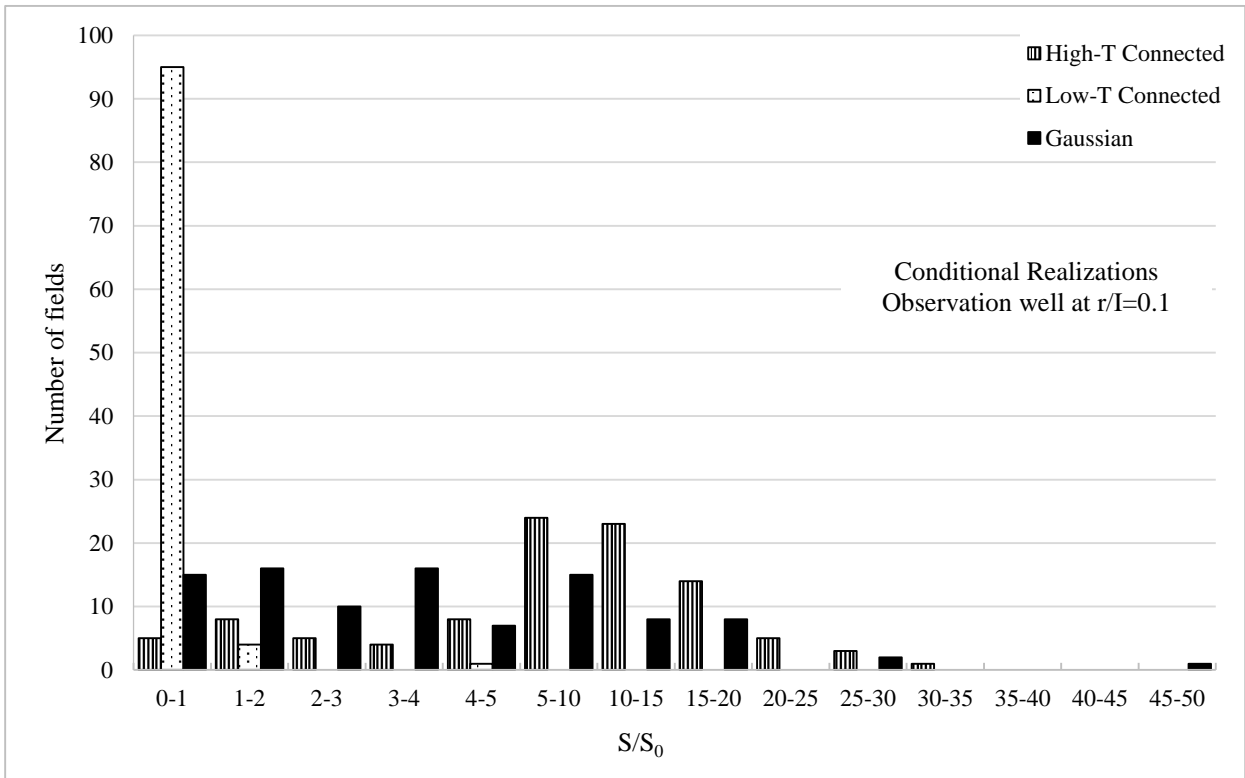
Figure 5.8. Estimated storativity vs integral connectivity scale of combined field sets. (a) and (b) correspond to unconditional realizations with the observation well located at $r/I=0.1$ and $r/I=0.5$, respectively. (c) and (d) show conditional realizations with the observation well located at $r/I=0.1$ and $r/I=0.5$, respectively.



(b)



(c)



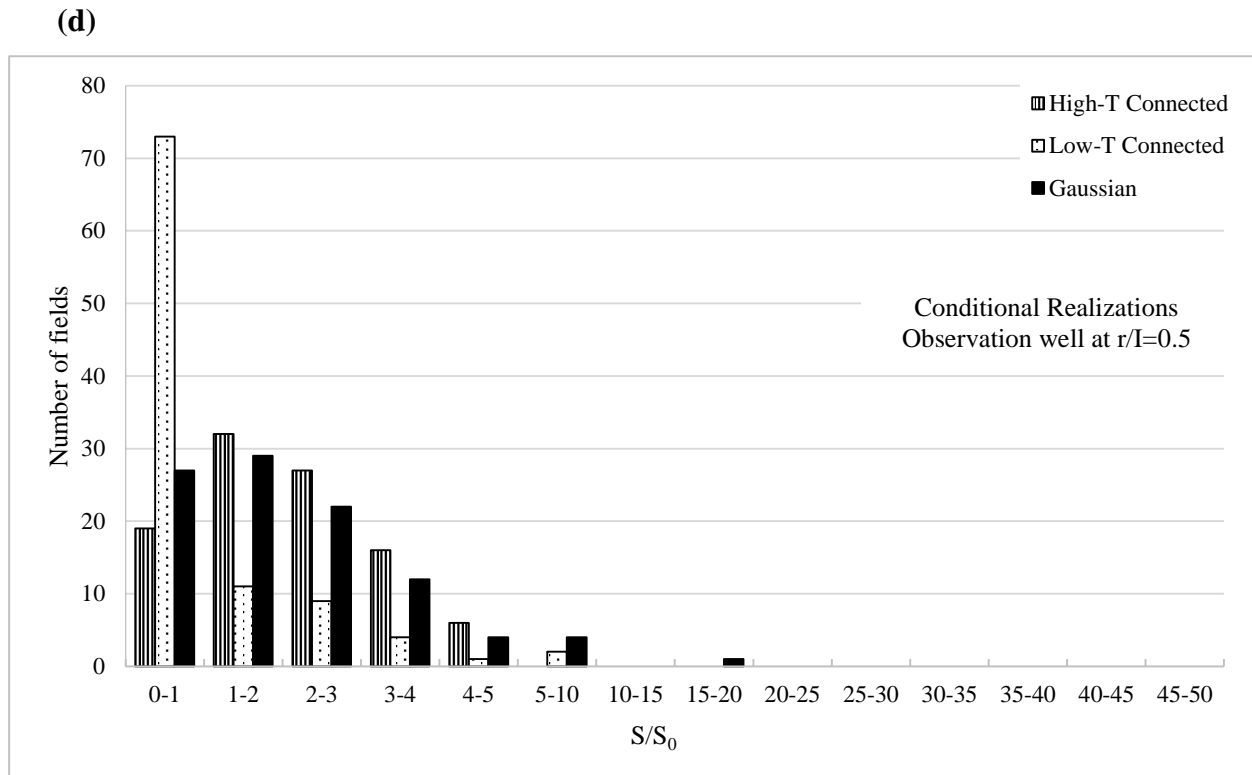


Figure 5.9. Histograms of S/S_0 estimated for unconditional fields where (a) $r/I=0.1$ and (b) $r/I=0.5$ and conditional fields where (c) $r/I=0.1$ and (d) $r/I=0.5$

Table 5.3. Average and standard deviation of normalized storativities estimated for different types of realizations and fields

Estimated parameter: Storativity (S/S_0)		Gaussian		Low-T Connected		High-T Connected		All Combined	
		avg	st dev	avg	st dev	avg	st dev	avg	st dev
Unconditional realizations	$r/I=0.1$	16.22	54.42	14.60	57.83	5.28	6.83	12.03	46.11
	$r/I=0.5$	2.19	3.46	2.11	4.26	1.69	1.25	2.00	3.25
Conditional realizations	$r/I=0.1$	5.78	7.27	0.18	0.49	10.04	7.17	5.33	7.14
	$r/I=0.5$	2.19	2.14	0.98	1.23	2.08	1.13	1.75	1.66

5.5. Application of Continuous Derivation Method

In this section, the Continuous Derivation method (Copty et al., 2001) is used as the second interpretation technique to estimate the flow parameters. Unlike the Cooper-Jacob method, which calculates a single value for parameters, the parameters estimated using the Continuous Derivation method vary in time or, equivalently, with radial distance from the well. The procedure is applied as described in Section 4.3.2 so that transmissivity and storativity are estimated as a function of both groundwater extraction time and then converted to radial distance from the extraction well. The graphs of selected fields are shown and examined. The geometric mean of the transmissivity fields

as a function of radial distance is also calculated and compared with the estimated transmissivity to investigate the correlation between the two. Lastly, storativities estimated at a selected time is shown and the value distribution is investigated.

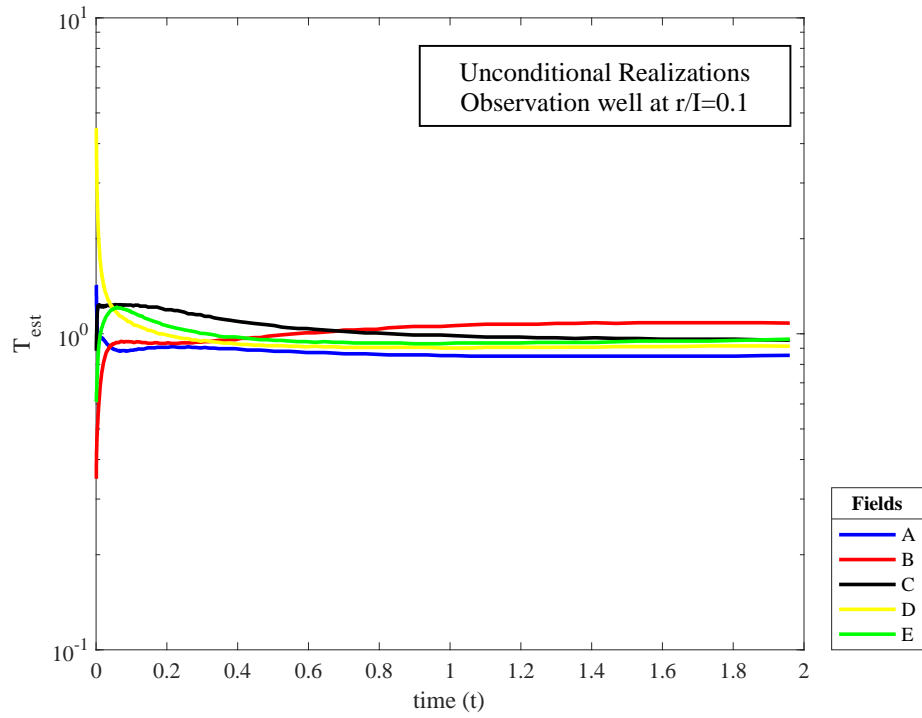
5 fields are randomly selected from all sets of realizations. These fields are chosen for both conditional and unconditional realizations and all three levels of connectivity. The 5 realizations are labelled as A, B, C, D and E. Table 5.4 represents the integral connectivity scales of these selected fields. This table is used for the comparison of the estimated parameters and the integral connectivity scales.

Table 5.4. Integral connectivity scales of selected fields

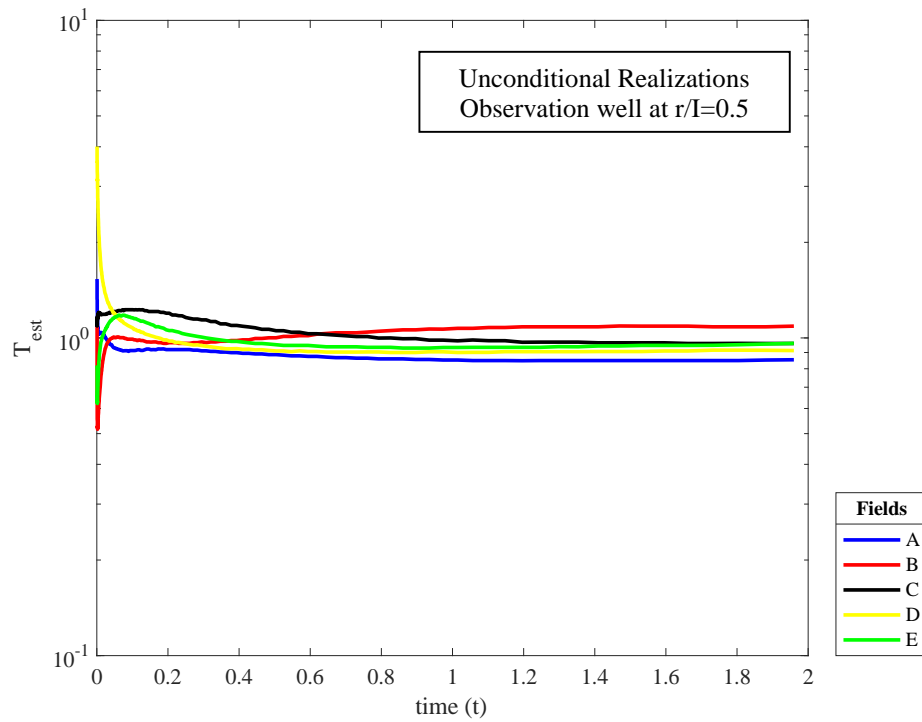
		A	B	C	D	E
Unconditional Realizations	Gaussian	34.01	17.27	51.80	39.83	26.22
	High-T Connected	54.17	78.11	59.39	59.28	67.24
	Low-T Connected	17.50	9.43	10.54	20.34	10.45
Conditional Realizations	Gaussian	21.58	30.73	24.13	54.43	16.64
	High-T Connected	44.73	38.80	45.31	53.64	44.24
	Low-T Connected	27.55	34.47	10.85	12.03	12.37

Estimated transmissivity graphs are grouped as Gaussian, high-T connected, and low-T connected to represent different field types clearly. Figure 5.10-5.12 show the estimated transmissivities as a function of time for Gaussian, high-T connected and low-T connected selected fields, respectively. The non-Gaussian fields are the modified fields corresponding to the Gaussian field (A to E). The first two images show the transmissivity estimations of unconditional fields at $r/I=0.1$ and 0.5 , and the third and the fourth images depict the transmissivities of conditional fields at $r/I=0.1$ and 0.5 , respectively. This ordering of realizations and observation wells are the same for Figure 5.10, 5.11, and 5.12.

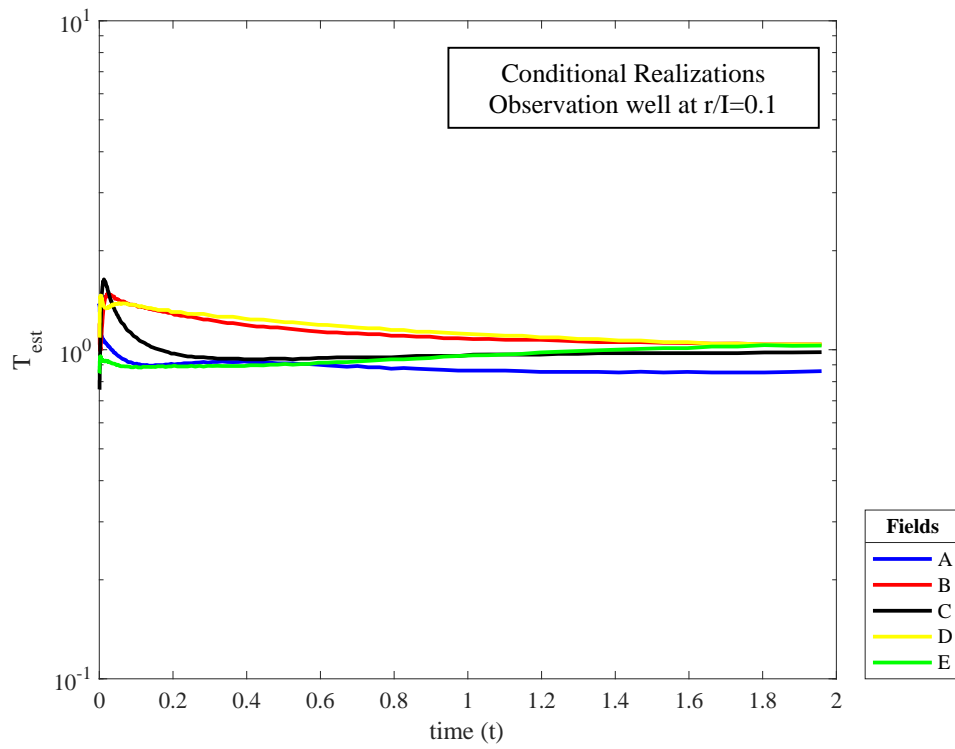
(a)



(b)



(c)



(d)

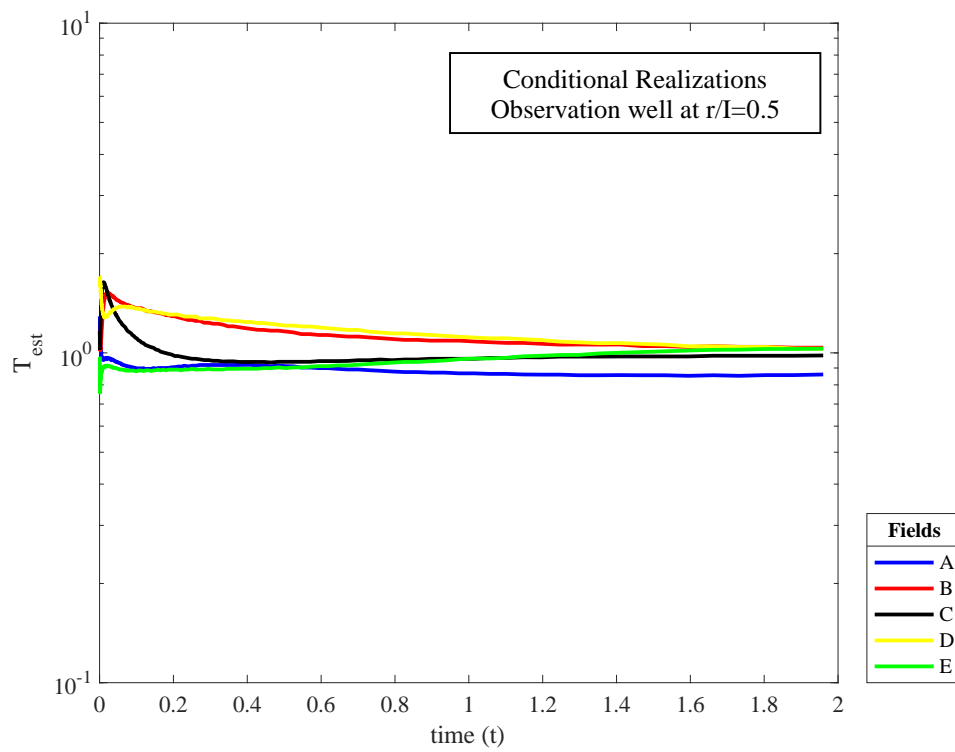
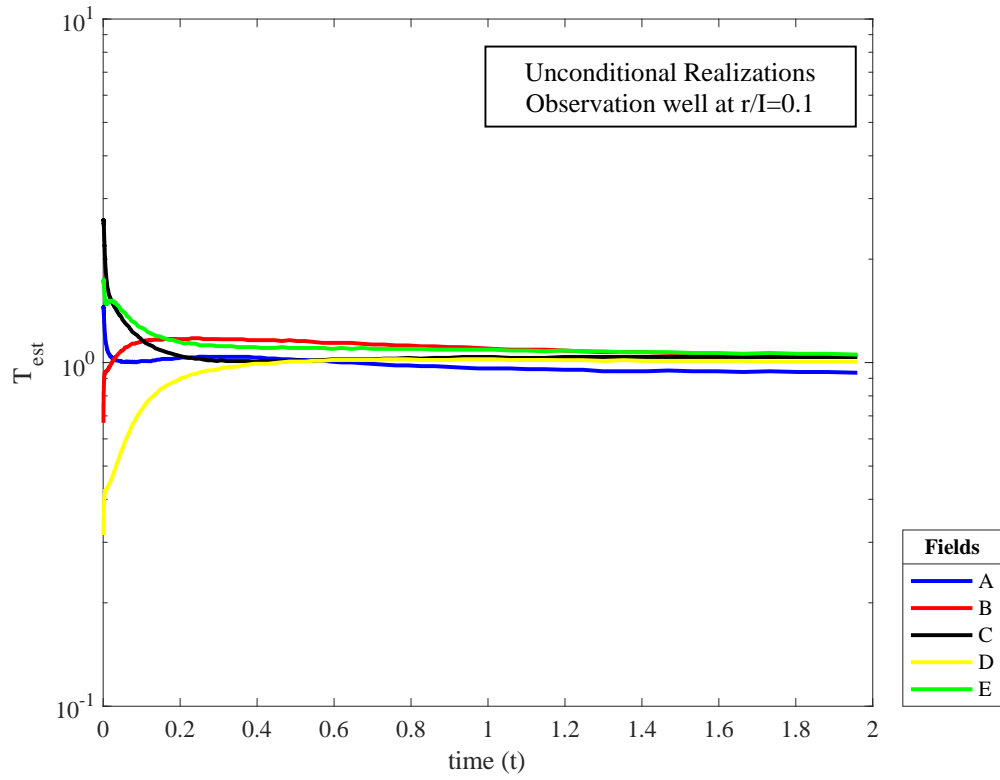
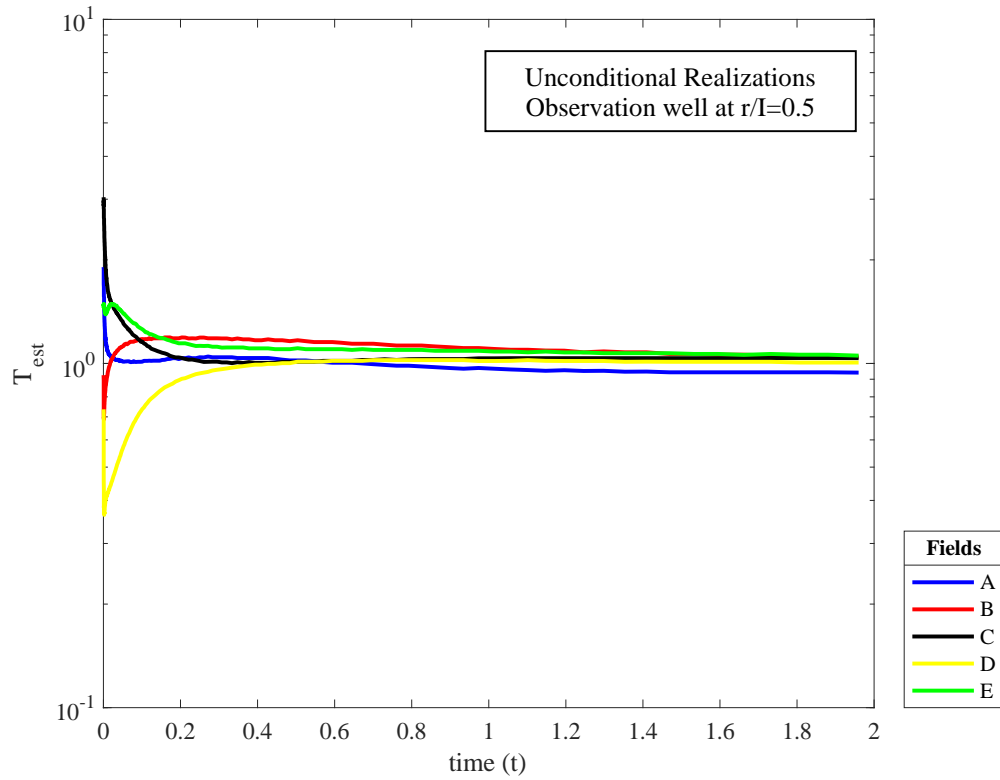


Figure 5.10. Estimated transmissivity as a function of time for randomly selected Gaussian fields. (a) and (b) correspond to unconditional realizations with the observation well located at $r/I=0.1$ and $r/I=0.5$, respectively. (c) and (d) show conditional realizations with the observation well located at $r/I=0.1$ and $r/I=0.5$, respectively

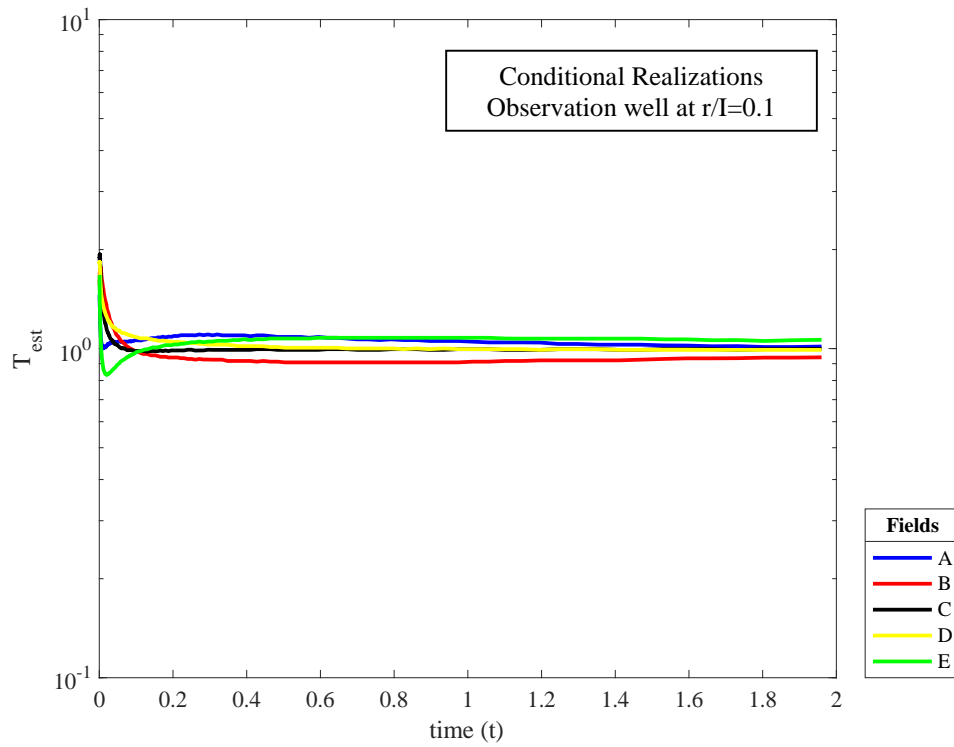
(a)



(b)



(c)



(d)

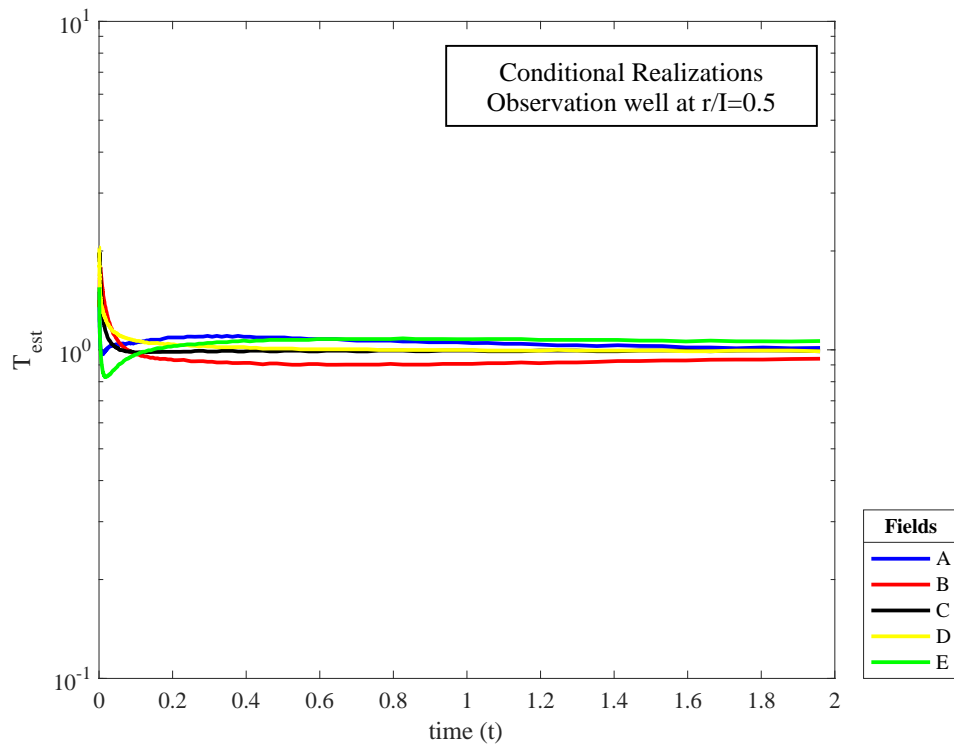
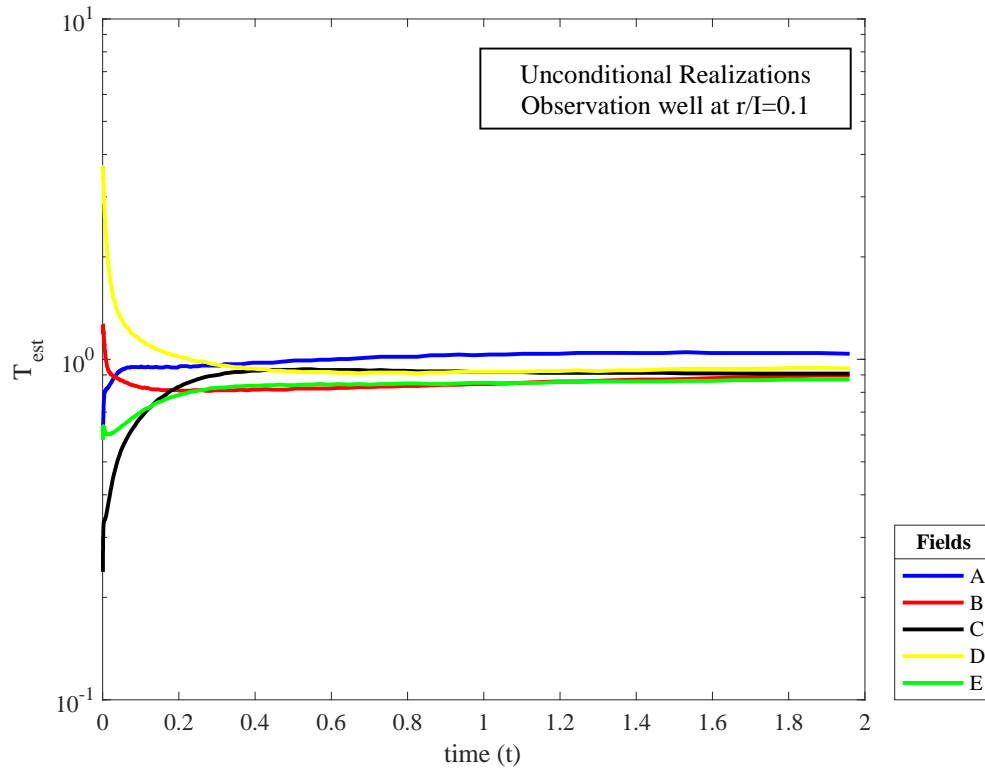
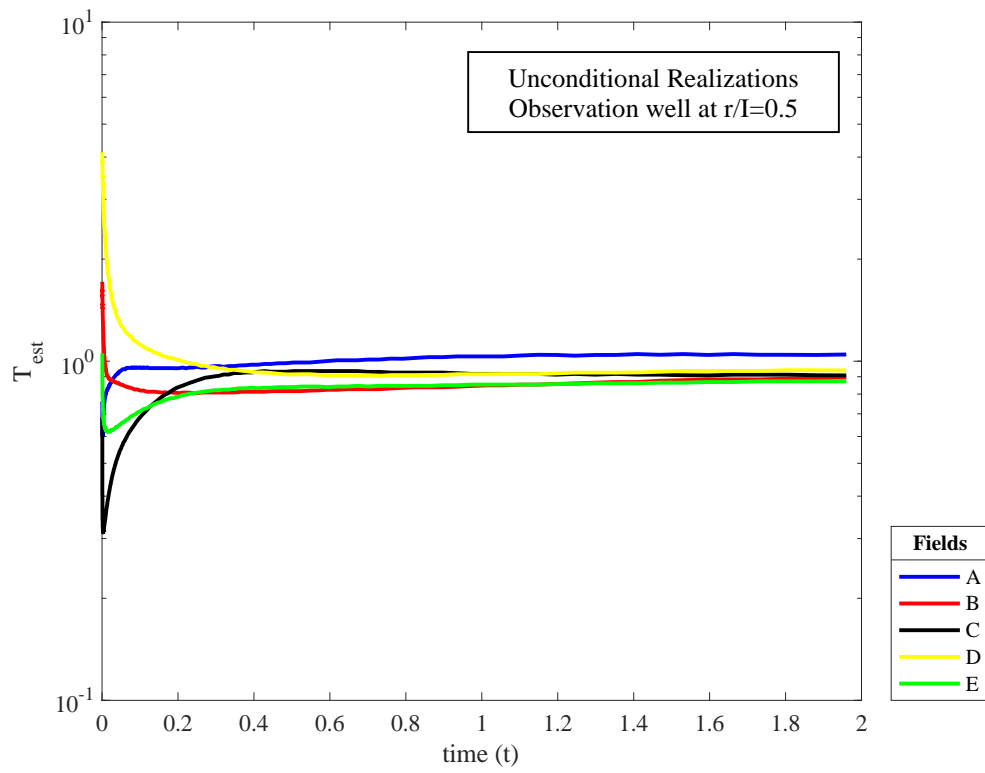


Figure 5.11. Estimated transmissivity as a function of time for randomly selected high-T connected fields. (a) and (b) correspond to unconditional realizations with the observation well located at $r/I=0.1$ and $r/I=0.5$, respectively. (c) and (d) show conditional realizations with the observation well located at $r/I=0.1$ and $r/I=0.5$, respectively

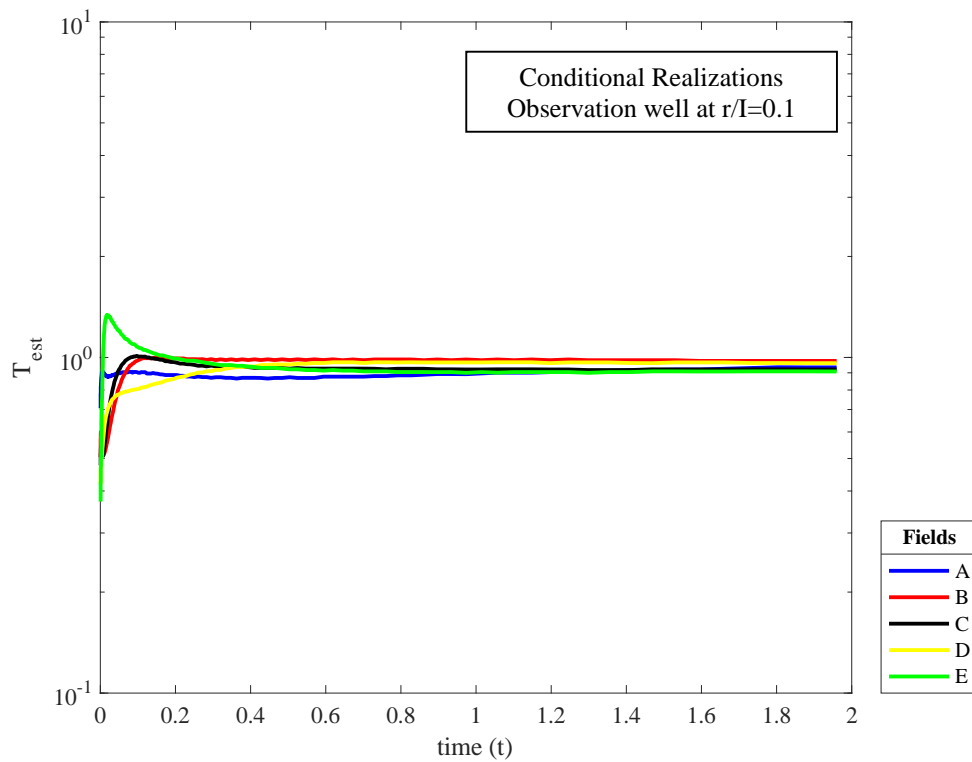
(a)



(b)



(c)



(d)

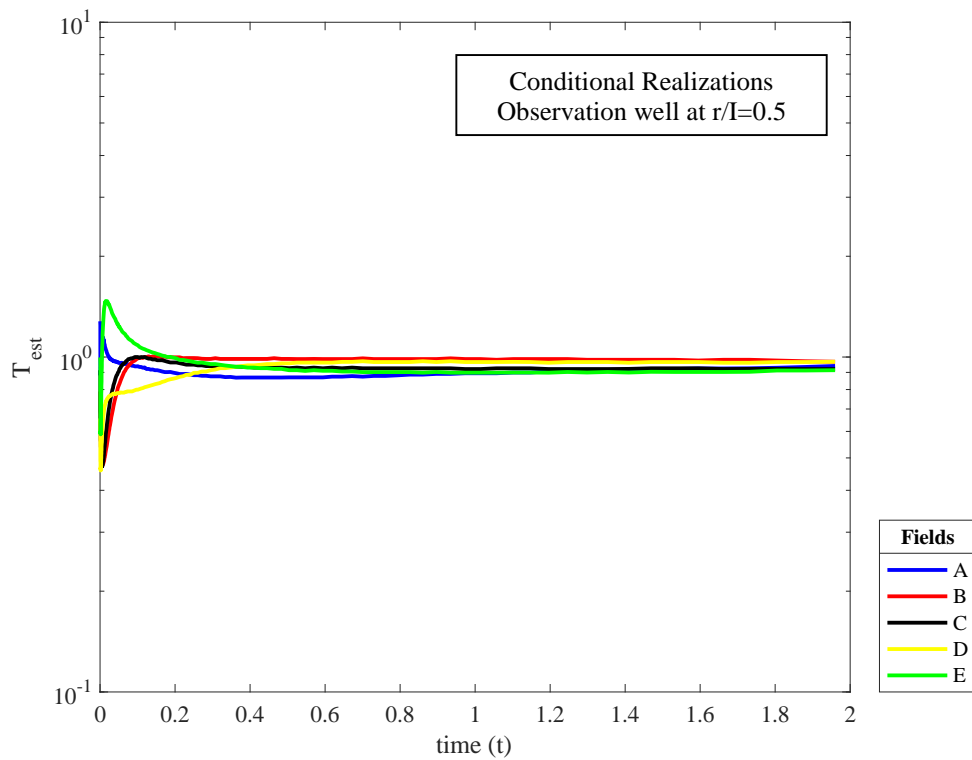


Figure 5.12. Estimated transmissivity as a function of time for randomly selected low- T connected fields. (a) and (b) correspond to unconditional realizations with the observation well located at $r/I=0.1$ and $r/I=0.5$, respectively. (c) and (d) show conditional realizations with the observation well located at $r/I=0.1$ and $r/I=0.5$, respectively

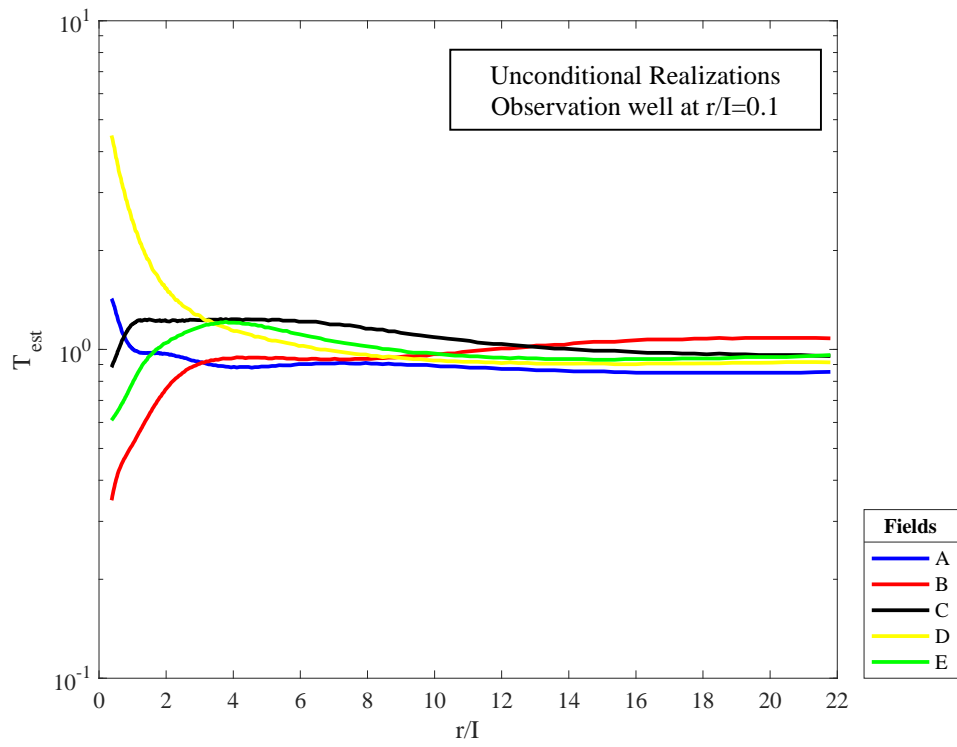
The most compelling similarity between all the transmissivity estimates, independent of their level of connectivities or type of realizations, is that as the groundwater extraction continues, all the curves approach to 1, that is, the estimated transmissivity approaches the geometric mean of the transmissivity fields. This finding is consistent with the previous studies (e.g., Meier et al., 1998; Coptý et al., 2011). This is also in parallel with the estimated parameters using the Cooper-Jacob method which leads to T estimated close to the geometric mean for all cases considered (Table 5.2). At late times, a large volume of the aquifer is perturbed by the pumping well such the well acts like an equivalent homogenous system with transmissivity equal to the geometric mean of the point transmissivities. Moreover, when the Figures 5.10-5.12 are analyzed together, the parameters estimated for the conditional realizations have less variability than the variability of estimated parameters for unconditional realizations. This is because the transmissivity at the well location is constant for the fields of conditional realizations and this constrain limits the range of the estimated transmissivities.

Examination of Figures 5.10-5.12 shows that when the location of the observation point is further away from the pumping well, the early-time variation in the estimated transmissivity is lost. By the time the drawdown signal reaches the observation point, the aquifer has become closer to an equivalent homogeneous system.

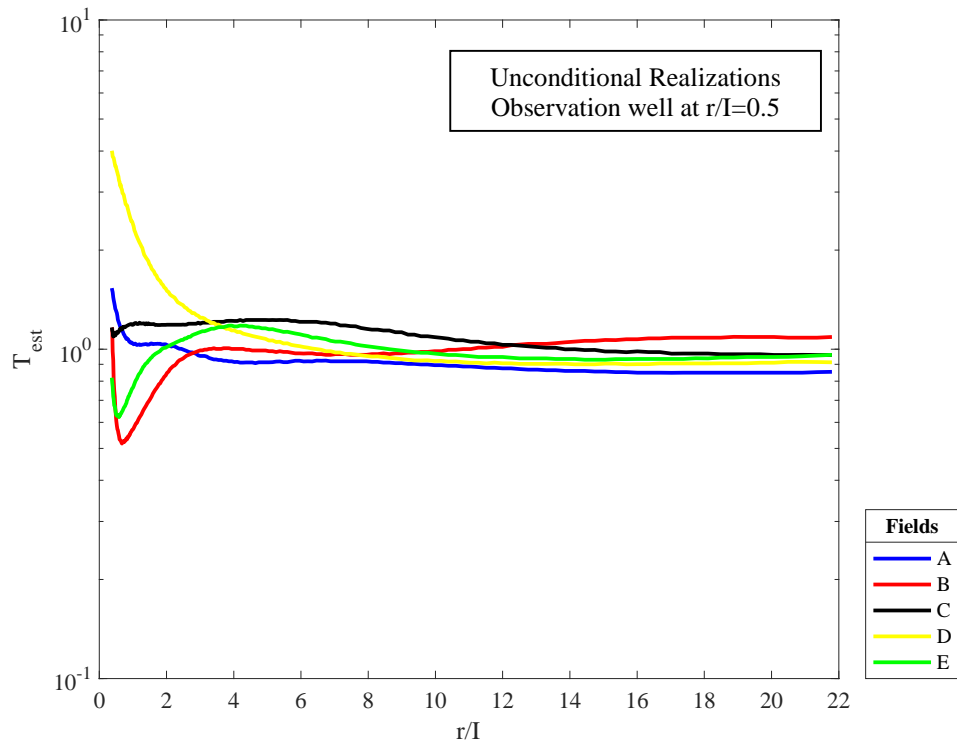
Transmissivity parameter estimation using this method does not appear to be affected by the changes in the level of connectivity. It can also be understood when the figures are compared with the integral connectivity scales shown in Table 5.4. There is no direct correlation between this static measure of connectivity and the estimated transmissivities.

The transient transmissivity curves are transformed to radially dependent curves using Equation 4.15. Figure 5.13 shows the estimated transmissivities as a function of radial distance from the pumping well for the selected Gaussian fields. Again, Figure 5.13 a and b show the unconditional realizations where the observation wells are located at $r/I=0.1$ and 0.5 , respectively, and Figure 5.13 c and d show the estimations of conditional realizations at the same distances, respectively. The time axis of the graphs in Figure 5.8 are transformed to the radial distance to generate the graphs in Figure 5.13. The same procedure is applied to all selected fields.

(a)



(b)



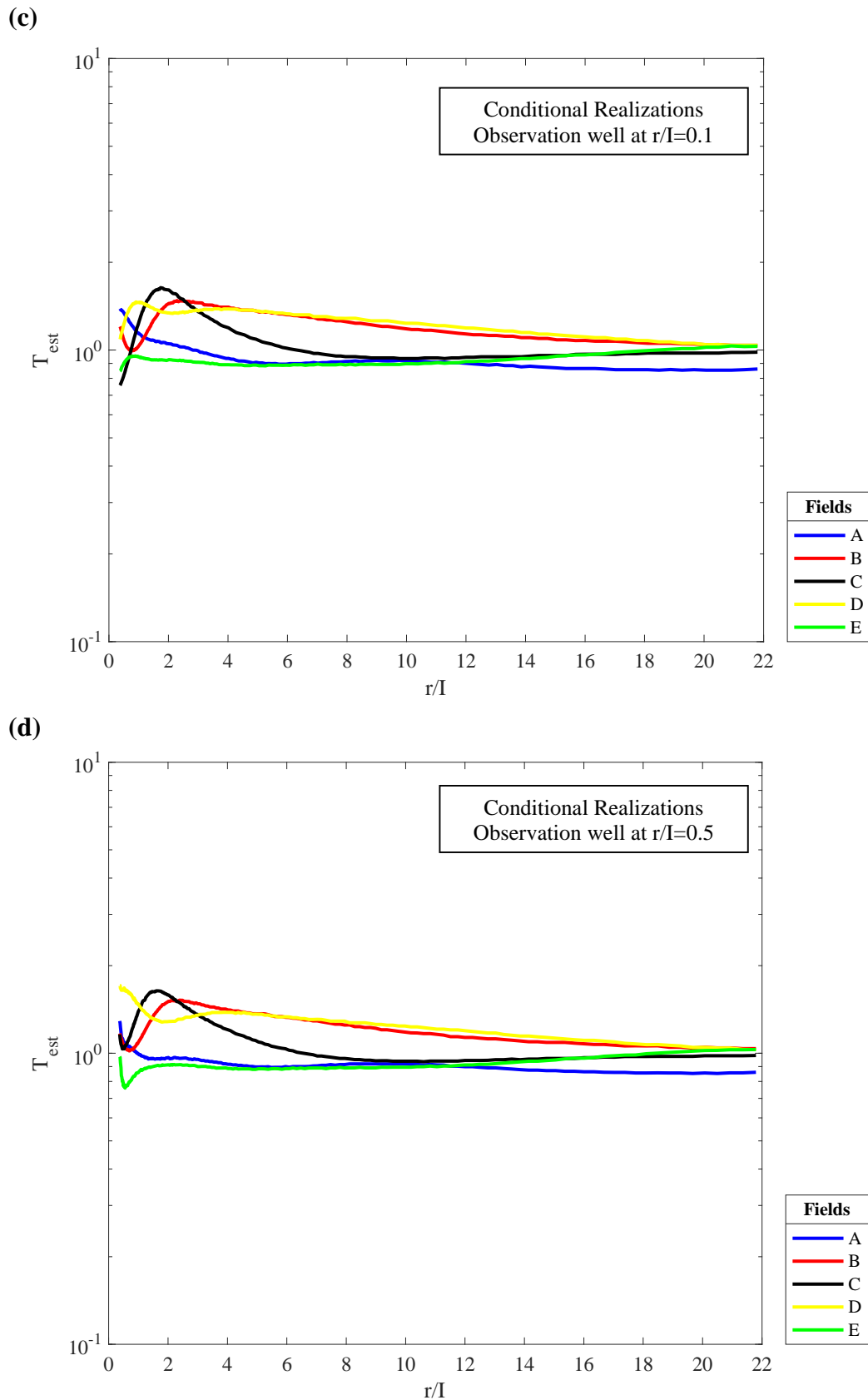
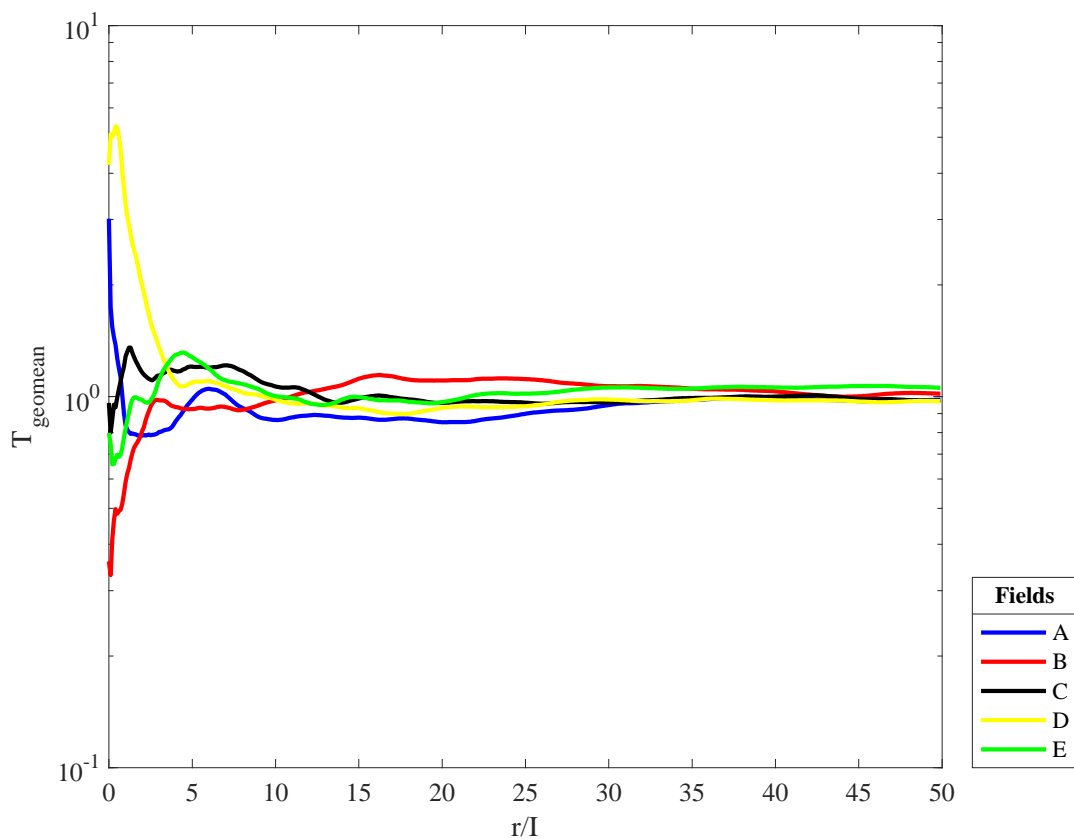


Figure 5.13. Estimated transmissivity as a function of radial distance for randomly selected Gaussian fields. (a) and (b) correspond to unconditional realizations with the observation well located at $r/I=0.1$ and $r/I=0.5$, respectively. (c) and (d) show conditional realizations with the observation well located at $r/I=0.1$ and $r/I=0.5$, respectively

This transformation enables the comparison of the estimated transmissivity curve and the geometric mean curve as a function of the radial distance from the extraction well. In order to actualize this comparison, the geometric mean of transmissivity functions as a function of radial distance are also calculated. The procedure used to calculate them is explained in Section 4.3.2.

Figure 5.14 shows the geometric mean of the selected fields as a function of distance. The unconditional and conditional realizations of Gaussian fields are graphically shown. The same selected fields are used for comparison as they are used in the previous calculations.

(a)



(b)

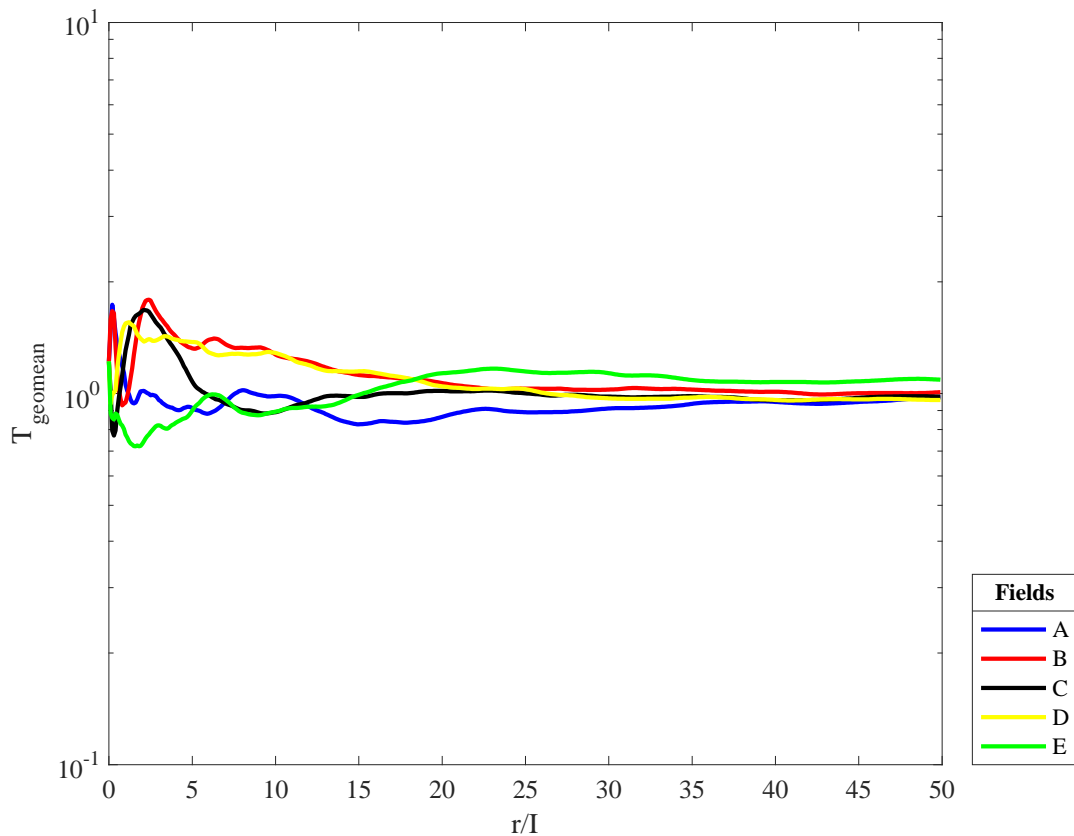
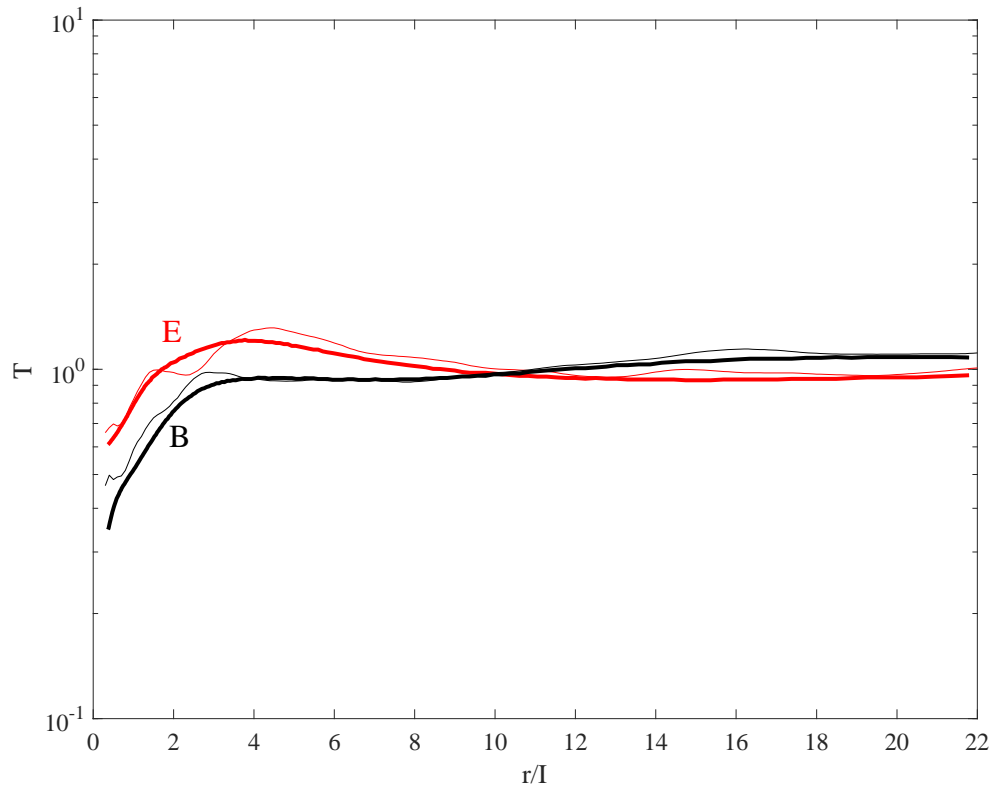
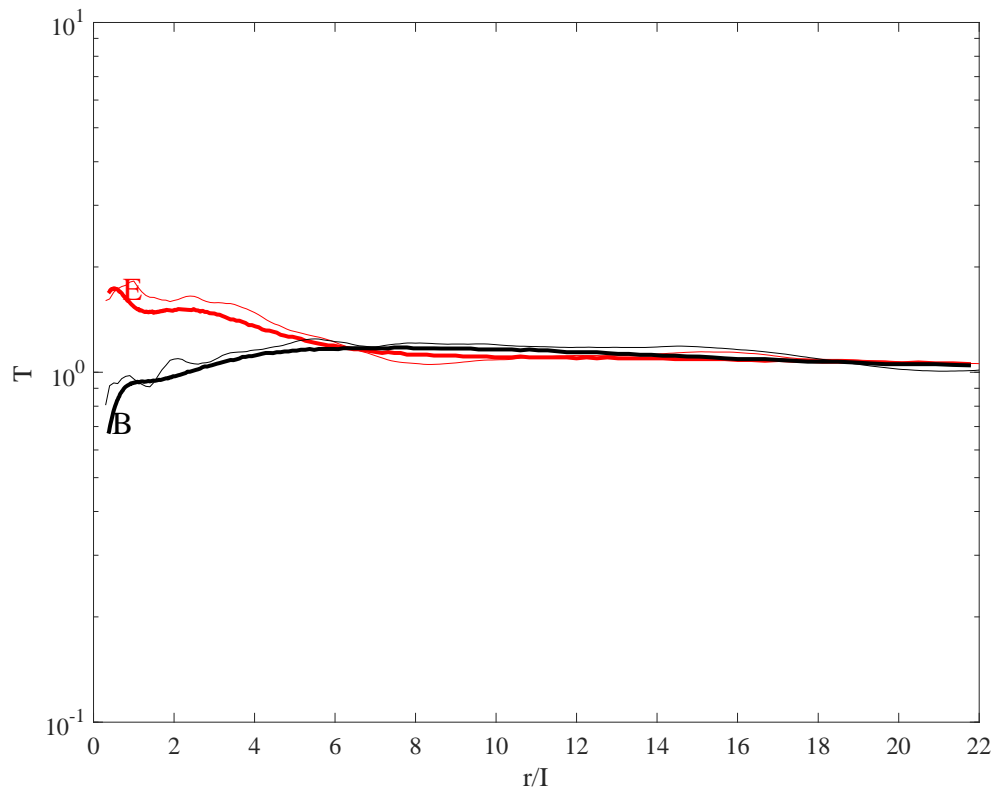


Figure 5.14. Geometric mean of transmissivity as a function of radial distance for randomly selected Gaussian fields of (a) unconditional realizations and (b) conditional realizations

Figure 5.15 superimposes the geometric mean curve (thin lines) and estimated transmissivity curve (bold lines). To better visualize the agreement, the graphs are produced for realizations B and E. However, similar results can also be seen for the other realizations for two realizations only. Figure 5.15a-c are for Gaussian, low-T connected, and high-T connected fields, respectively. For all three types of fields, the estimated transmissivity curves are highly correlated with the field's geometric mean of the transmissivity curve. In other words, the transmissivity curve estimated with the Continuous Derivation method are good estimates of the geometric mean of field transmissivity structure as a function of radial distance. This is true for Gaussian fields as well as non-Gaussian fields. The results are shown only for the unconditional fields but similar results are also obtained for the conditional fields.

(a)**(b)**

(c)

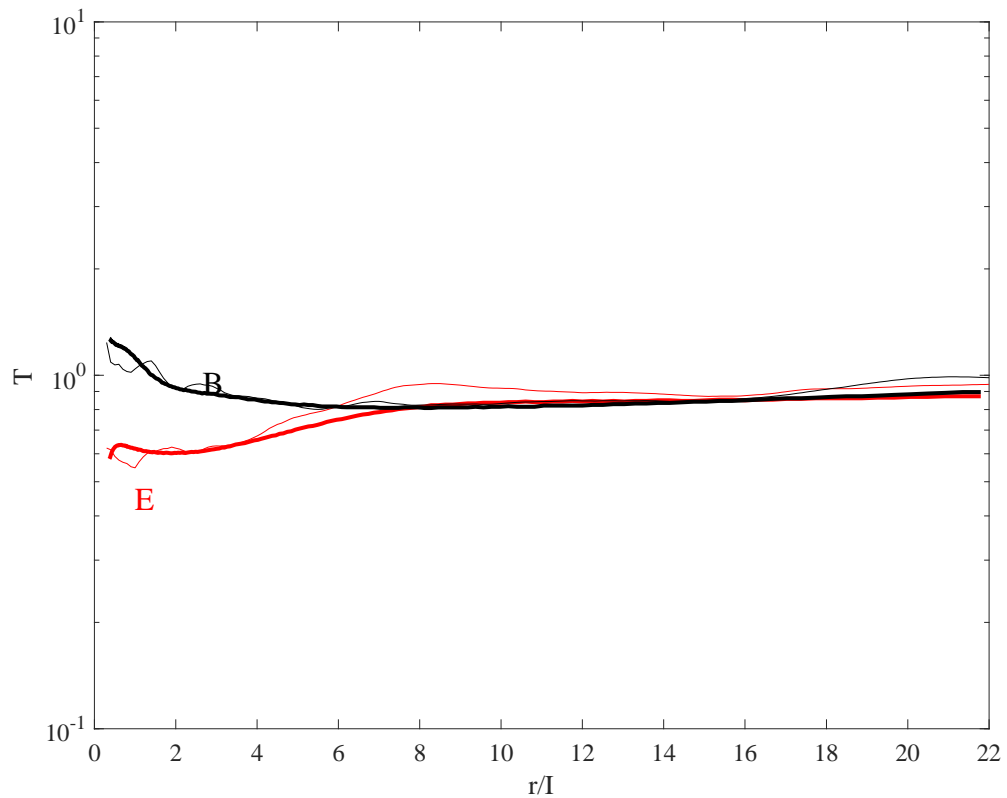
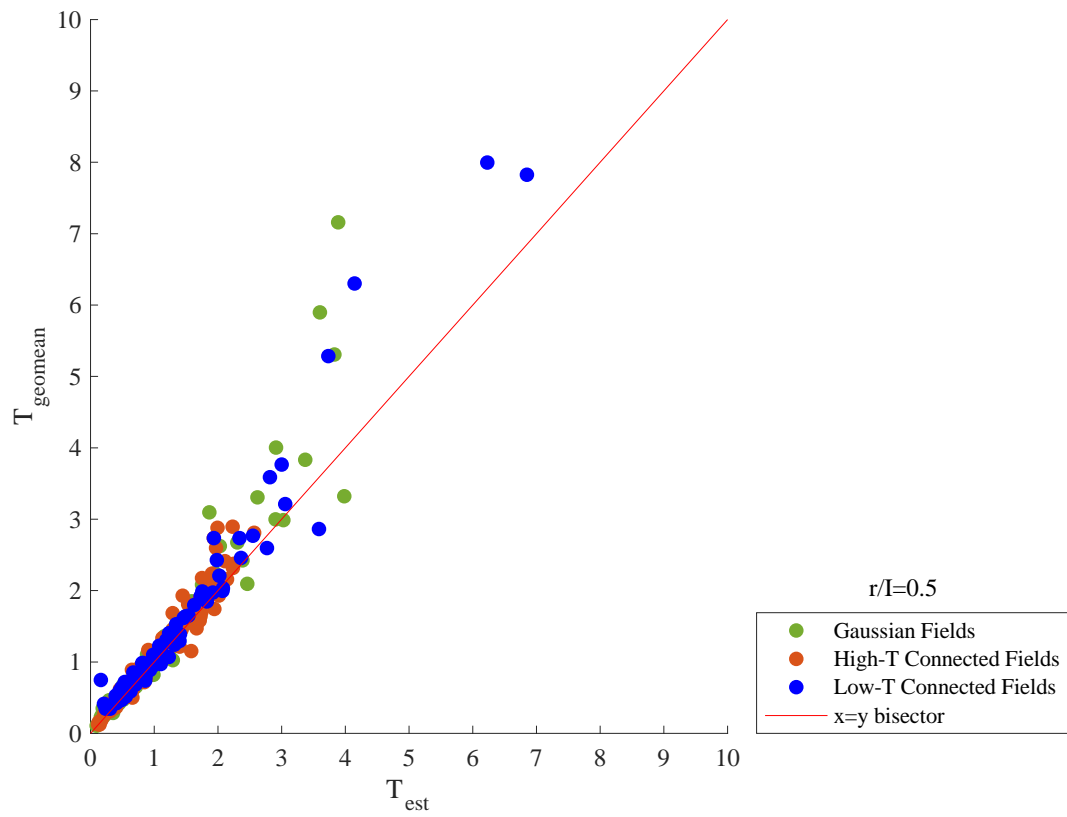


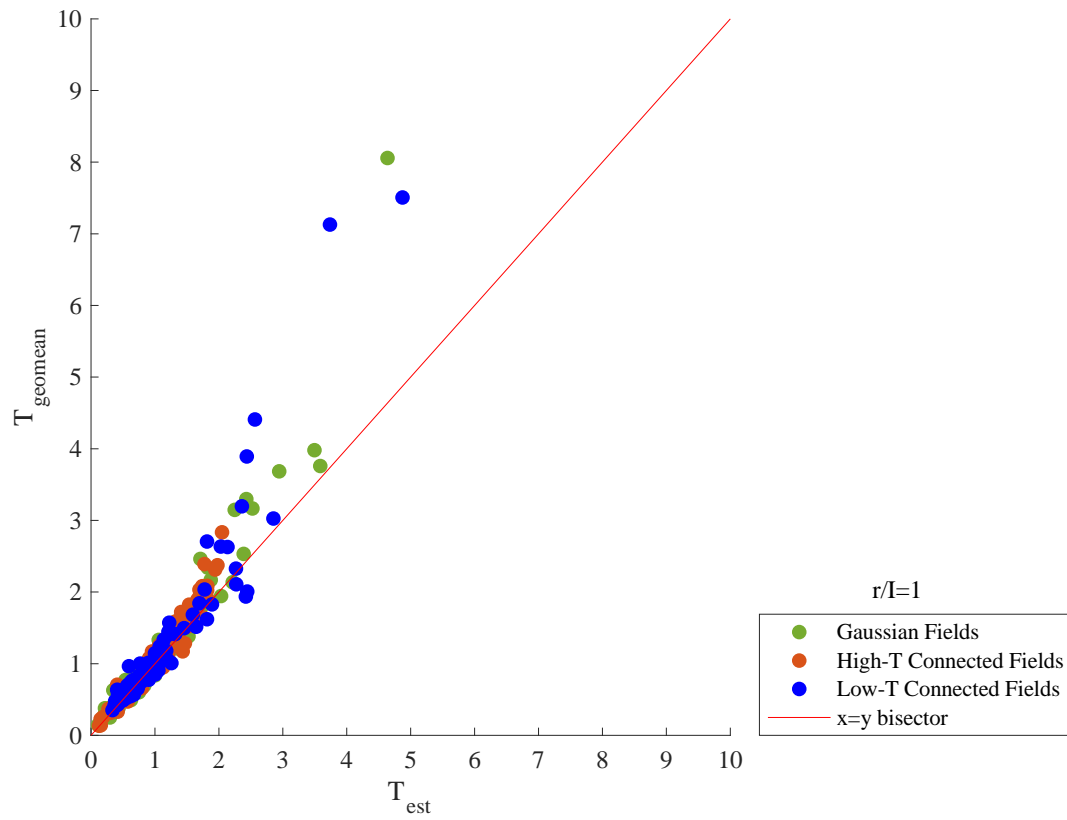
Figure 5.15. Comparison of T_{geomean} (thin lines) and T_{est} (bold lines) as a function of r/I for randomly selected (a) Gaussian, (b) low-T connected, and (c) high-T connected unconditional selected fields. Black lines show field B and red lines show field E realizations. Observation well is located at $r/I=0.1$

In order to investigate the relationship between the transmissivity estimations and the geometric mean calculations of field transmissivities, these two estimates are calculated at various radial distances around the extraction well and compared graphically. Figure 5.16 shows the comparison for unconditional realizations, where the radial distance is taken as $r/I=0.5, 1, 5,$ and $10,$ respectively. For points on the geometric mean of transmissivity vs. the estimated transmissivity curve are close to the $x=y$ bisector, this means that the two values are close to each other. Table 5.5 displays the coefficient of determination, R^2 , of these realizations. All coefficient of determinations are large, showing that the geometric mean values and the estimated transmissivity values are close to each other. However, the coefficient of determination decreases slightly as the radial distance from the well increases. Figure 5.16 also confirms that as the radial distance increases, both the geometric mean values and estimated transmissivity values approach to 1 and this is in parallel with the previous findings of this study.

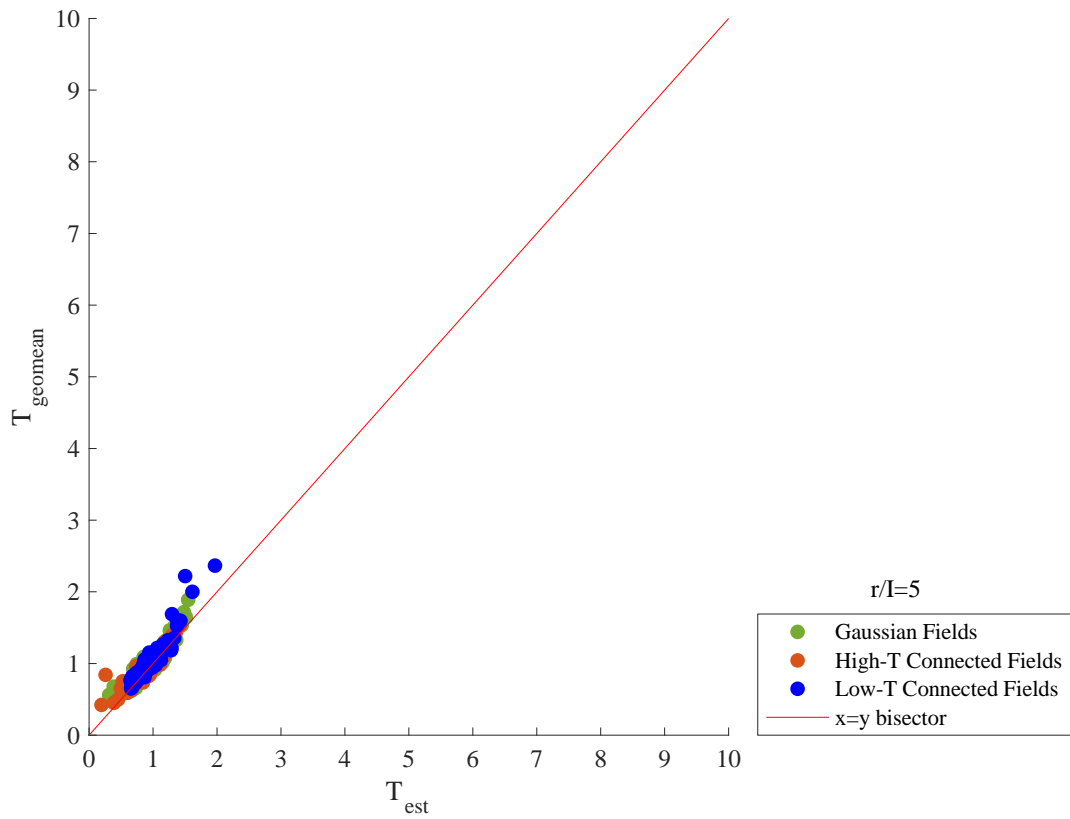
(a)



(b)



(c)



(d)

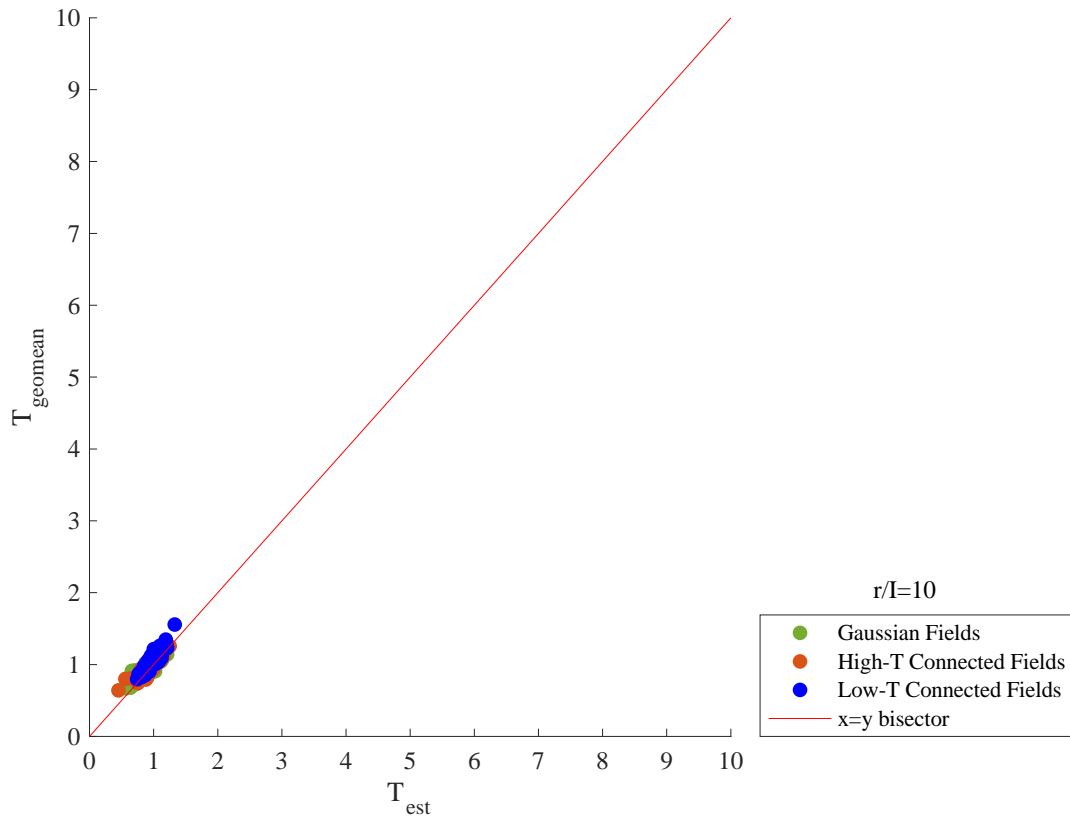


Figure 5.16. T_{geomean} vs. T_{est} at distance (a) $r/I=0.5$, (b) $r/I=1$, (c) $r/I=5$, and (d) $r/I=10$ for all unconditional realizations

Table 5.5. Coefficient of determination for different field types at various distances

r/I	Gaussian	Low-T Connected	High-T Connected
0.5	0.91	0.96	0.94
1	0.91	0.89	0.94
5	0.88	0.89	0.84
10	0.78	0.85	0.84

Figure 5.17-5.19 represents the estimated time-dependent storativity values for selected Gaussian, high-T connected and low-T connected fields, respectively. The first two images in these three figures correspond to unconditional realizations with the observation well located at $r/I=0.1$ and 0.5 , respectively and the third and the fourth images show the conditional realizations with the same observation well positions. Figure 5.20 represents the radially-dependent storativity values for selected Gaussian fields. The transformation from time to radial distance is performed using Equation 4.15. The same procedure is applied to the other selected fields.

Examination of the results shown in Figure 5.17, 5.18 and 5.19 indicate that the estimated storativity values are closer to the initial storativity at early times of extraction, but that the storativity estimate varies significantly as the pumping test evolves. Moreover, according to these figures, the estimated storativities do not vary much after 1 time units of extraction. Figure 5.21 shows the estimated storativities at that time of stabilization plotted against their integral connectivity scales. Figure 5.21a and b show the normalized storativity vs. integral connectivity scales for unconditional fields with the observation well located at $r/I=0.1$ and $r/I=0.5$, respectively. Figure 5.21c and d show the normalized storativity vs. integral connectivity scales for conditional fields with the observation well located at $r/I=0.1$ and $r/I=0.5$, respectively. The logarithmic trendlines numerically show the correlation between the estimated storativity and integral connectivity scales. Again, it is observed that the estimated S generally underestimated S_0 (the value used in the simulation of the pumping tests) for low-T connected fields and overestimated for the Gaussian and high-T connected fields. The trendlines show that there is a low correlation between the estimated storativity and the integral connectivity scales. Table 5.6 shows the average (avg) and the standard deviation (st dev) of estimated storativities at $t=1$ time units for different field types. The standard deviation of the unconditional realizations estimated at $r/I=0.1$ is considerably large for all field types. The standard deviation of the unconditional realizations estimated at $r/I=0.1$ is the largest for all field types. This wide variability is also shown in Figure

5.21a. Moreover, as the observation location shifts from $r/I=0.1$ to 0.5, the variation decreases for both types of realizations as unconditional and conditional. The estimated storativities of conditional fields with the observation well at $r/I=0.1$ captures the correlation between the estimated parameter and the connectivity the most. This can also be seen in Figure 5.21c.

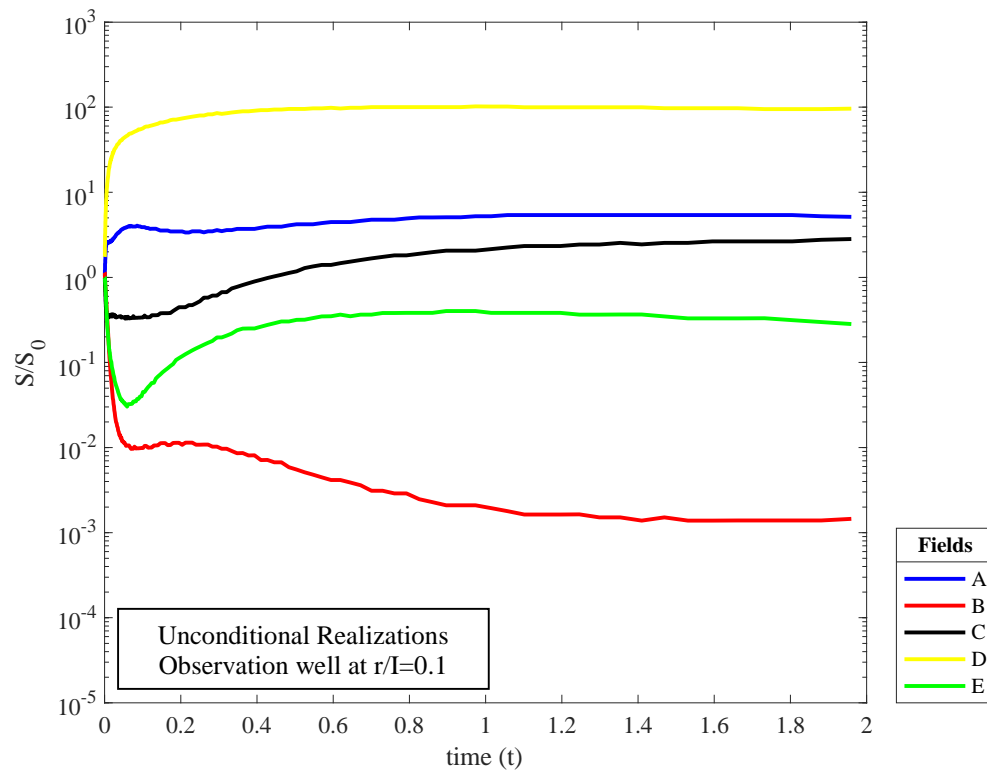
Overall, the variability in the estimated storativities appears to be strongly dependent on the actual transmissivity distribution around the well. This makes it difficult to relate the estimated storativity to the integral connectivity scale, a static connectivity, a binary metric that is based on whether the transmissivity is higher/lower than some threshold. This difficulty is attributed to the difficulty of solving the groundwater inverse problem. In the forward problem, all aquifer parameters are given and used to simulate the head distribution. In the inverse problem, the head distribution is used to estimate the flow problems. Numerous studies have shown that the inverse problem is not unique, meaning that different flow parameters may yield the same head at an observation point. In the context of the current study, the non-uniqueness of the inverse problem means that time drawdown data from a single pumping test may not be adequate to quantify the level of connectivity of the aquifer.

Another finding is that the variability decreases as the observation well is located farther away from the extraction well. This is a reasonable outcome since averaging is more when the observation well is located farther away. The variability is also smaller for the conditional realizations since the initial constraint limits the variation up to a certain degree.

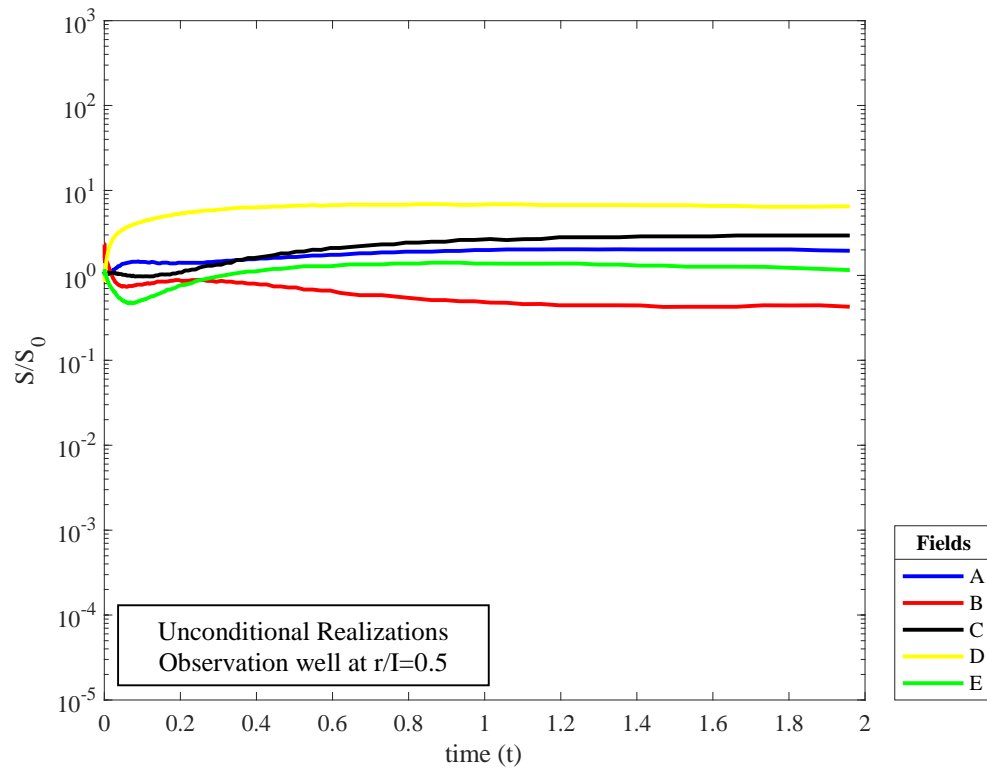
Lastly, when the estimated storativities calculated using the Continuous Derivation method at a particular time is compared with the variability in storativity estimations calculated by the Cooper-Jacob method, clear similarities in the value distribution of storativity can be observed. The widest variability is observed for unconditional fields with the observation well located at $r/I=0.1$. The average estimated storativities and their standard deviations estimated using these two methods are also very close to each other. The variability is slightly smaller for the parameters calculated with the Cooper-Jacob method since it is based on the drawdown data over a range of times (late times) where as the S estimates for the Continuous Derivation method are taken at a single time.

In summary, connectivity is seen as an important parameter that can influence the time-drawdown data due to pumping and that interpreted results. However, because of the complexity of transmissivity spatial distribution and its influence on the estimated flow parameters, reliably estimating the connectivity metric may not be possible from a single pumping test.

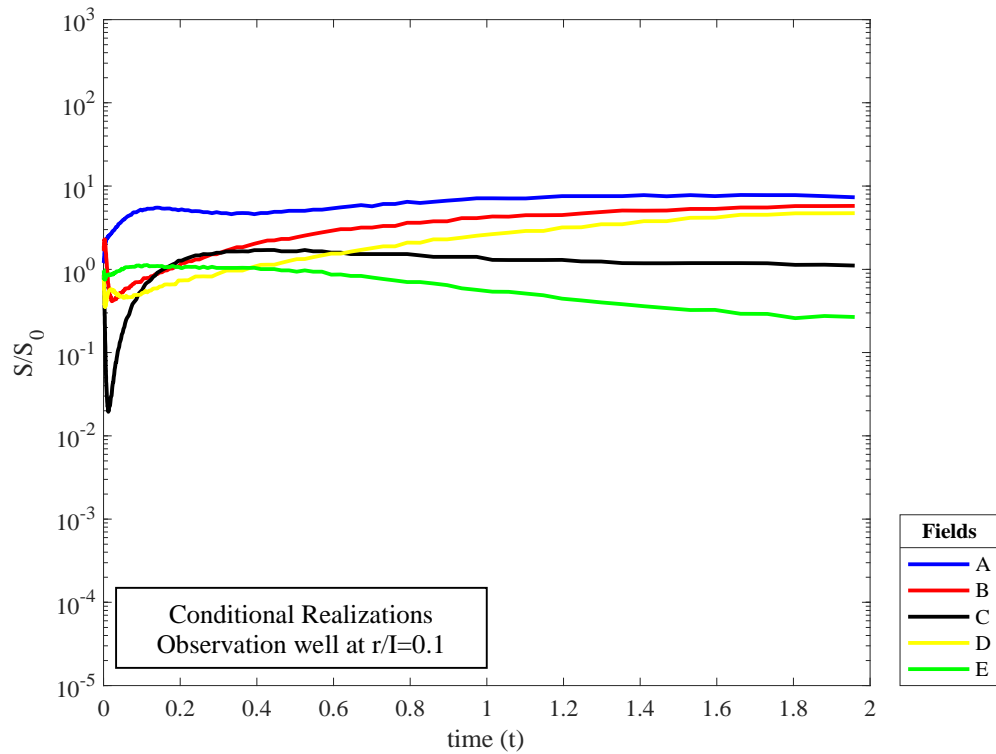
(a)



(b)



(c)



(d)

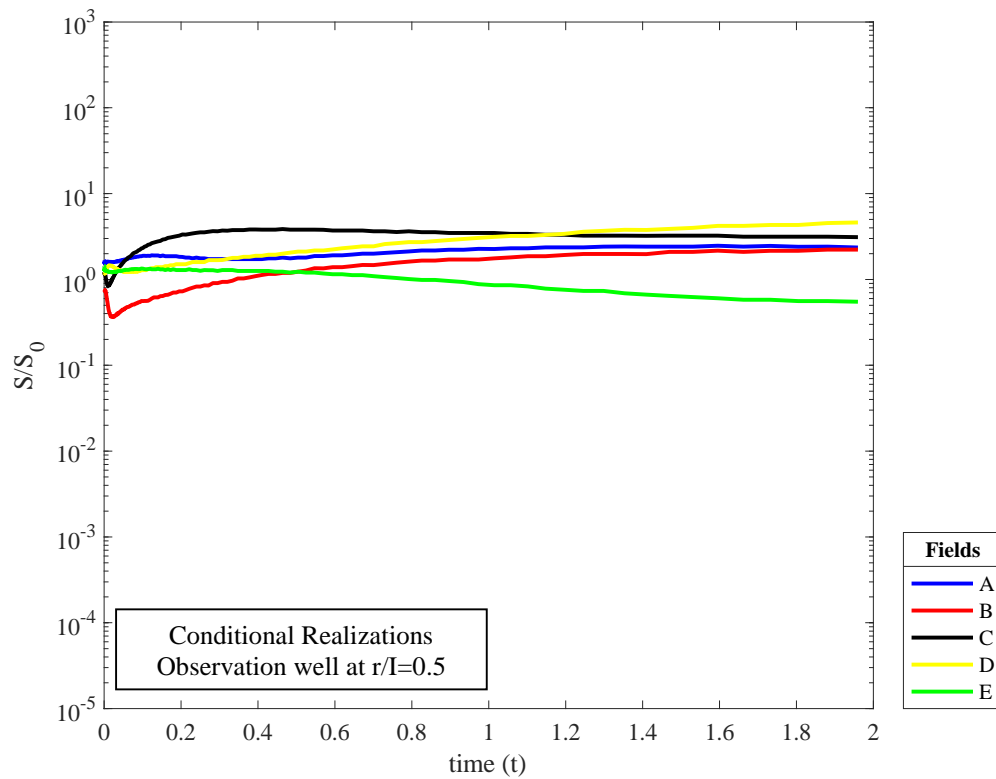
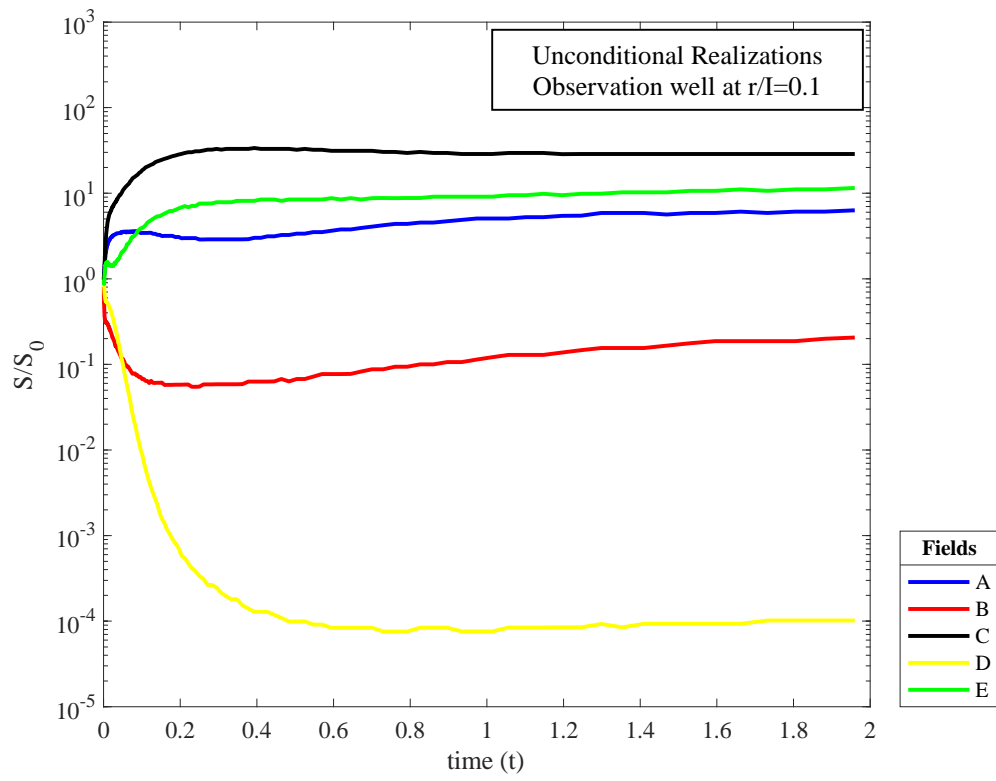
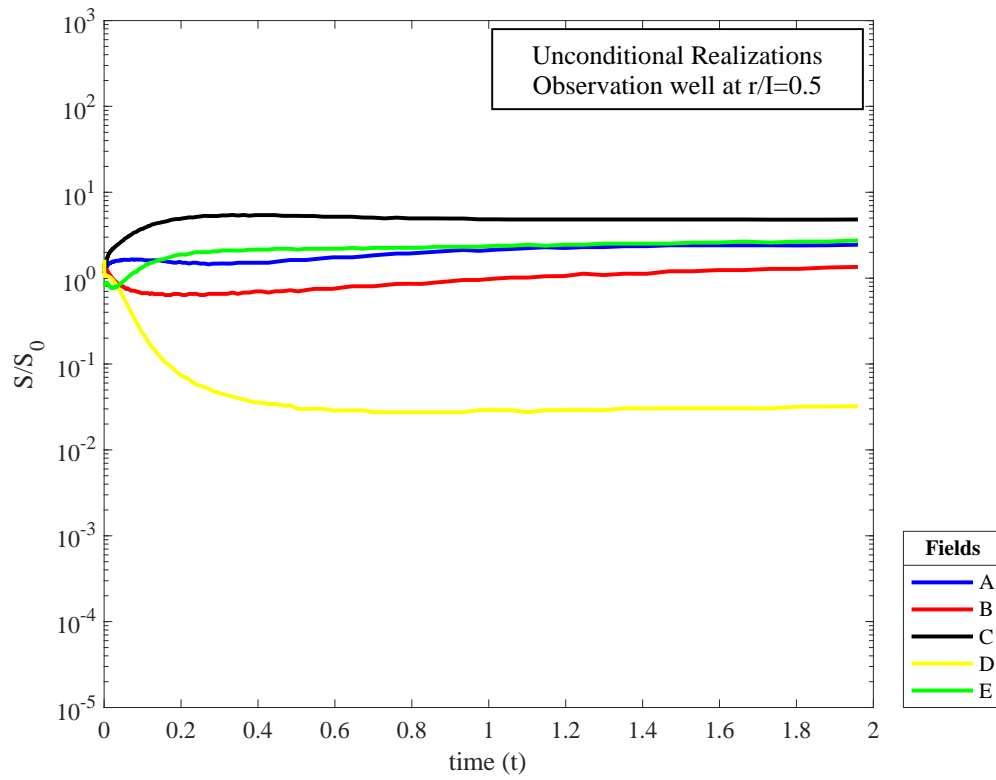


Figure 5.17. Estimated storativity as a function of time for randomly selected Gaussian fields. (a) and (b) shows unconditional realizations where the observation well is located at $r/I=0.1$ and $r/I=0.5$, respectively. (c) and (d) shows conditional realizations where the observation well is located at $r/I=0.1$ and $r/I=0.5$, respectively

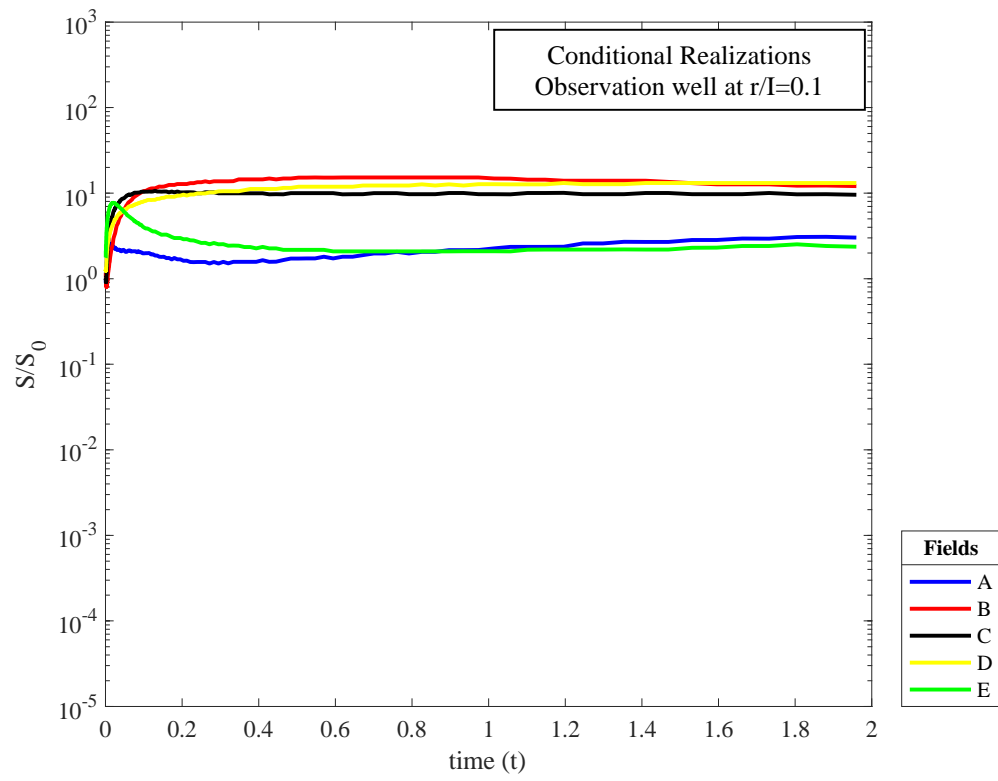
(a)



(b)



(c)



(d)

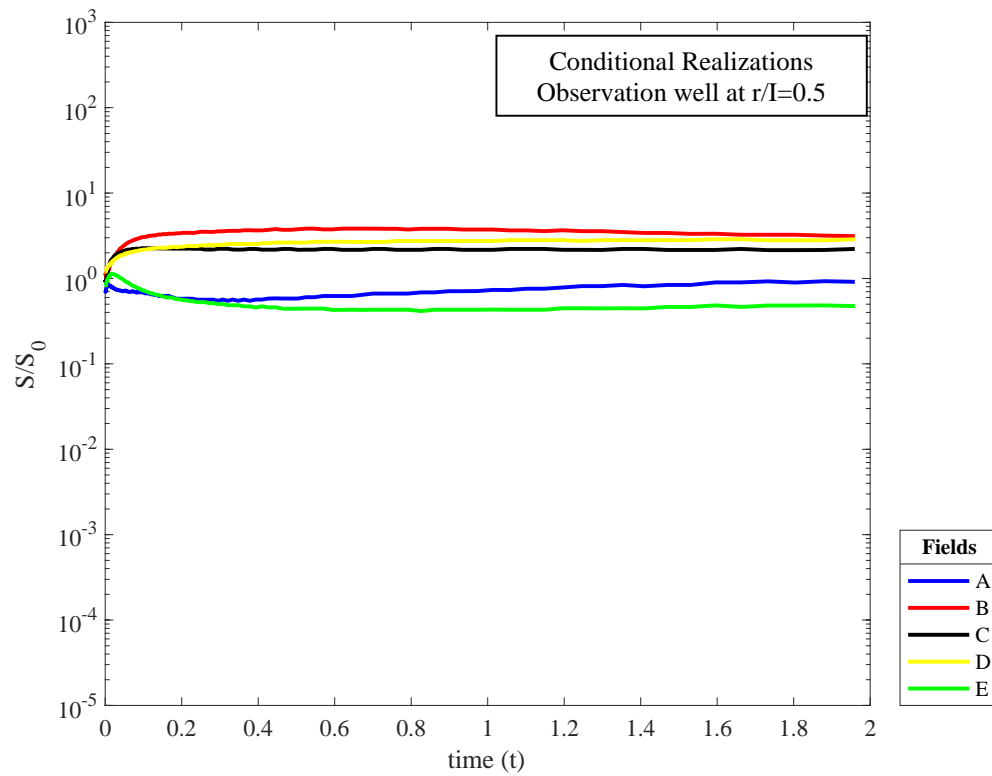
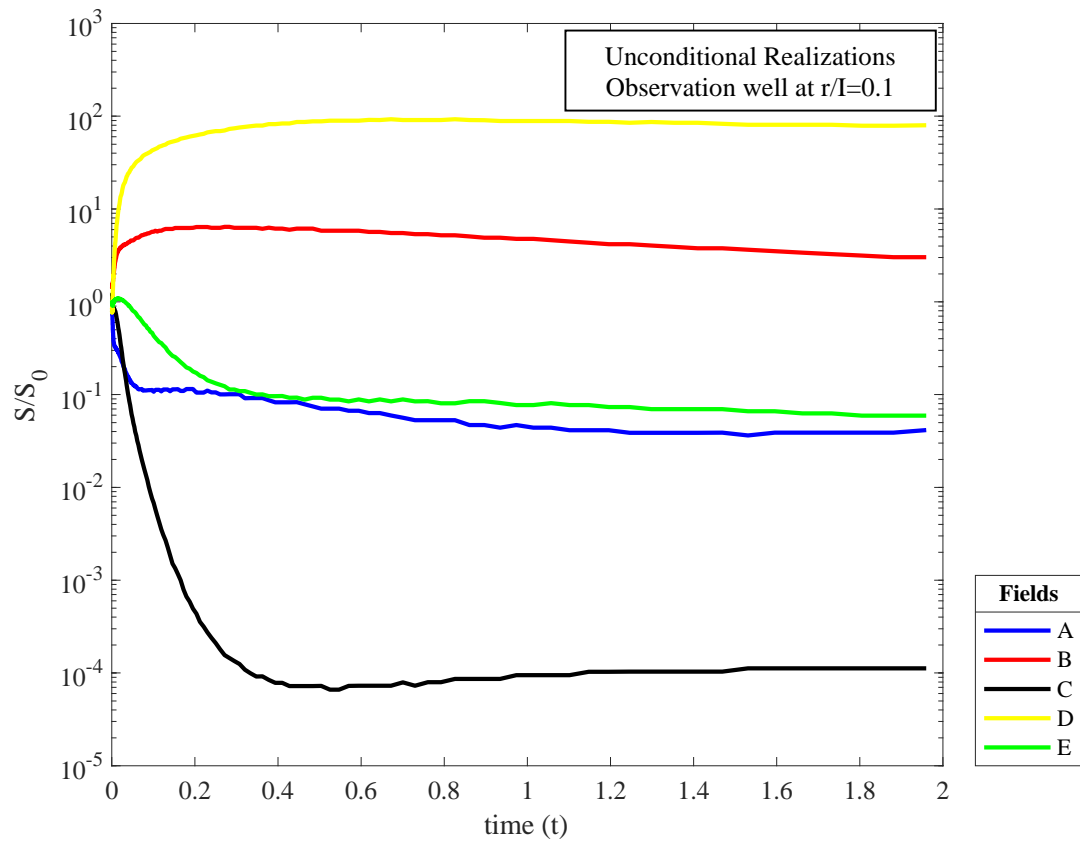
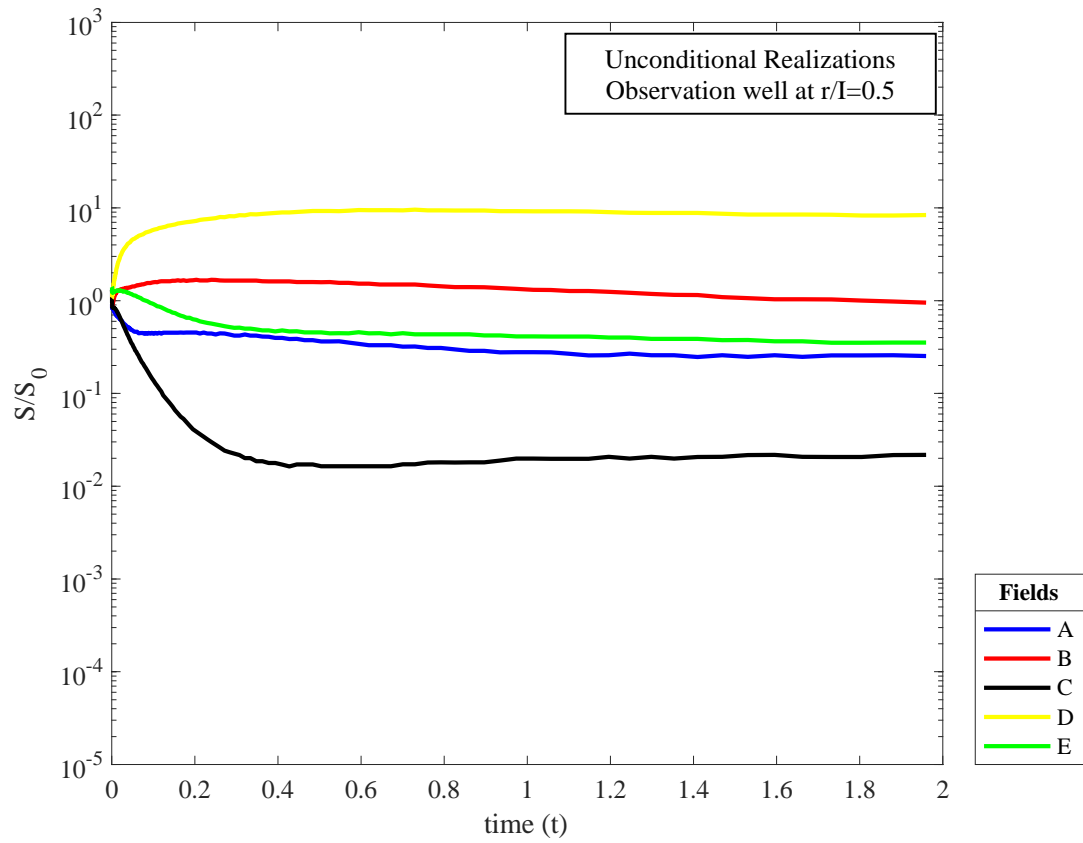


Figure 5.18. Estimated storativity as a function of time for randomly selected high-T connected fields. (a) and (b) shows unconditional realizations where the observation well is located at $r/I=0.1$ and $r/I=0.5$, respectively. (c) and (d) shows conditional realizations where the observation well is located at $r/I=0.1$ and $r/I=0.5$, respectively

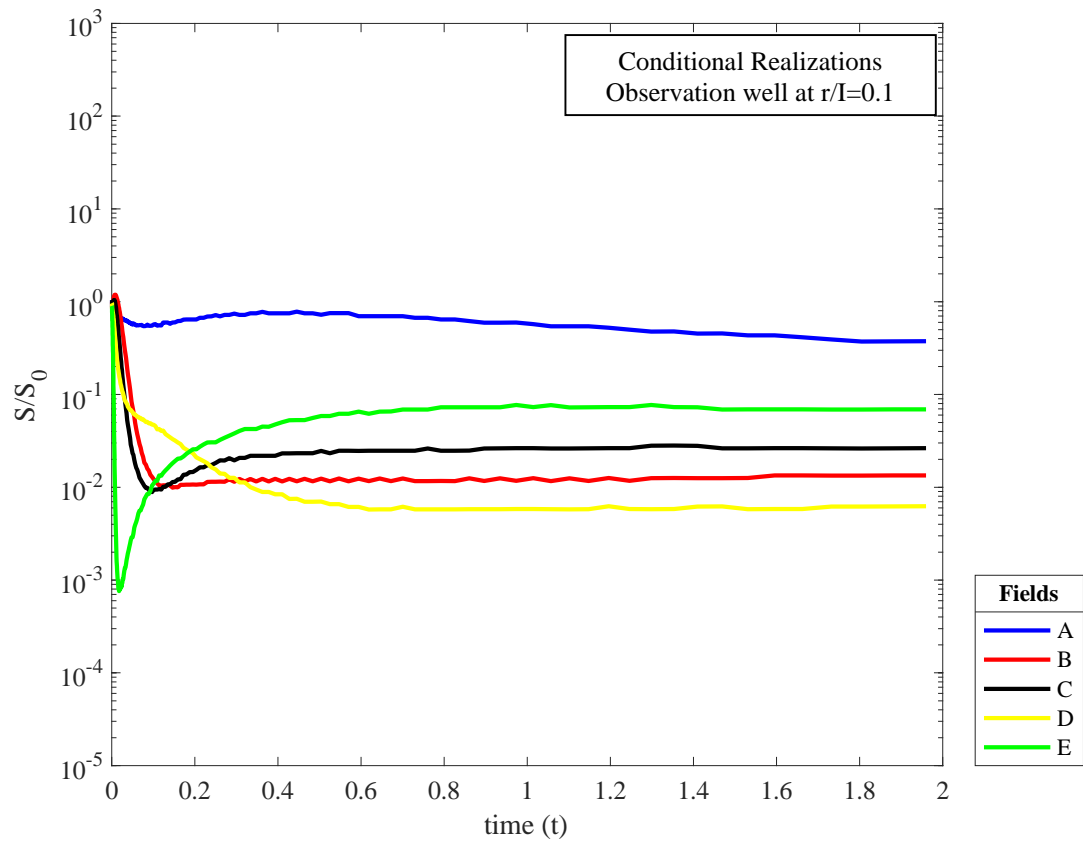
(a)



(b)



(c)



(d)

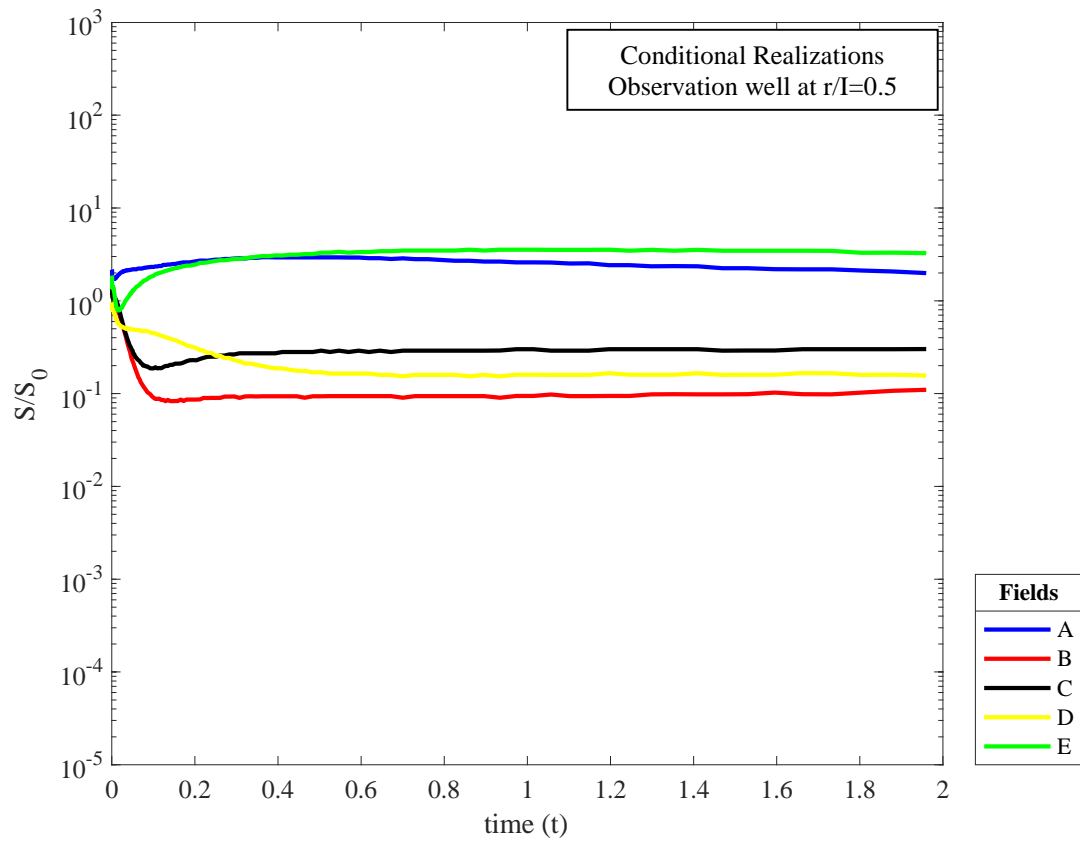
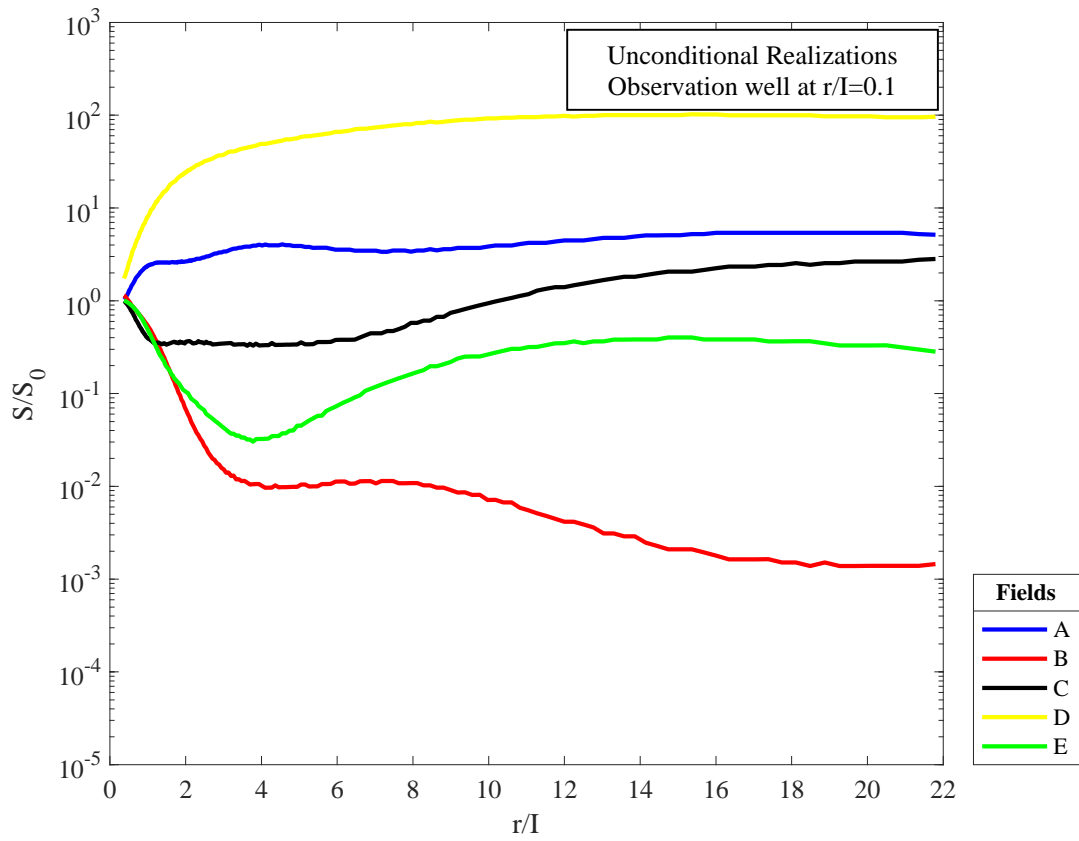
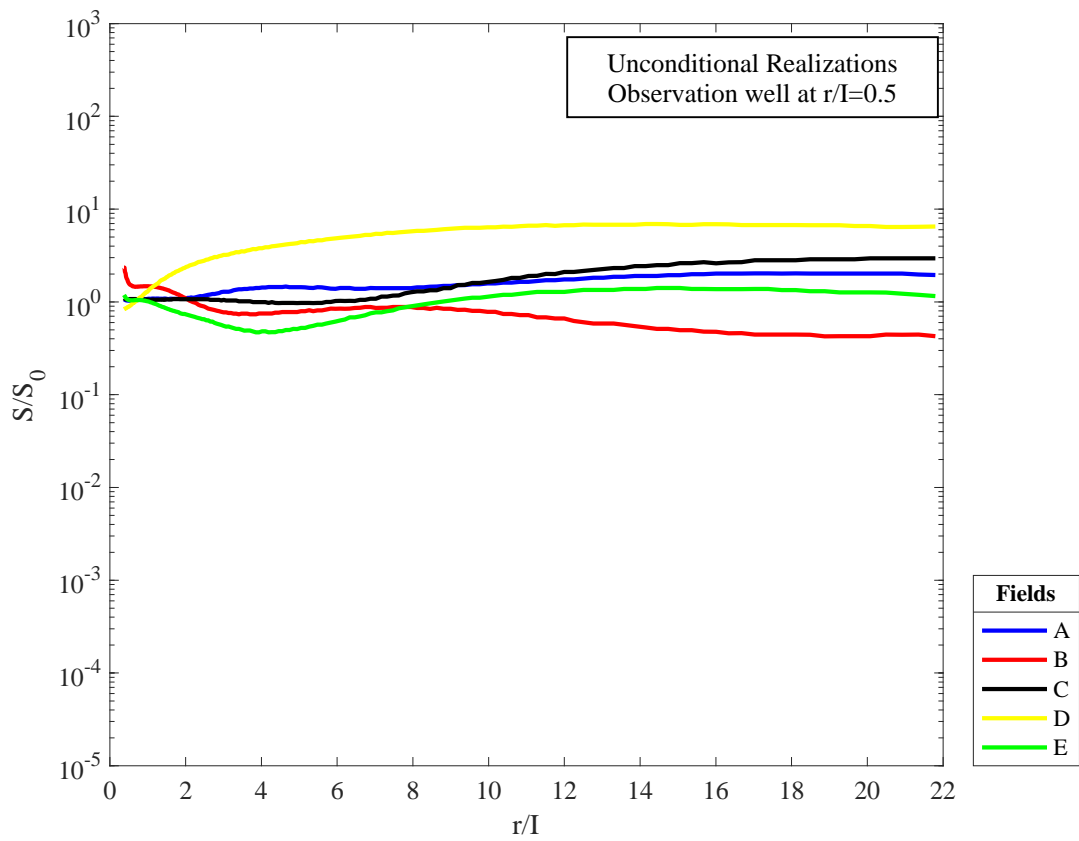


Figure 5.19. Estimated storativity as a function of time for randomly selected low-T connected fields. (a) and (b) shows unconditional realizations where the observation well is located at $r/I=0.1$ and $r/I=0.5$, respectively. (c) and (d) shows conditional realizations where the observation well is located at $r/I=0.1$ and $r/I=0.5$, respectively.

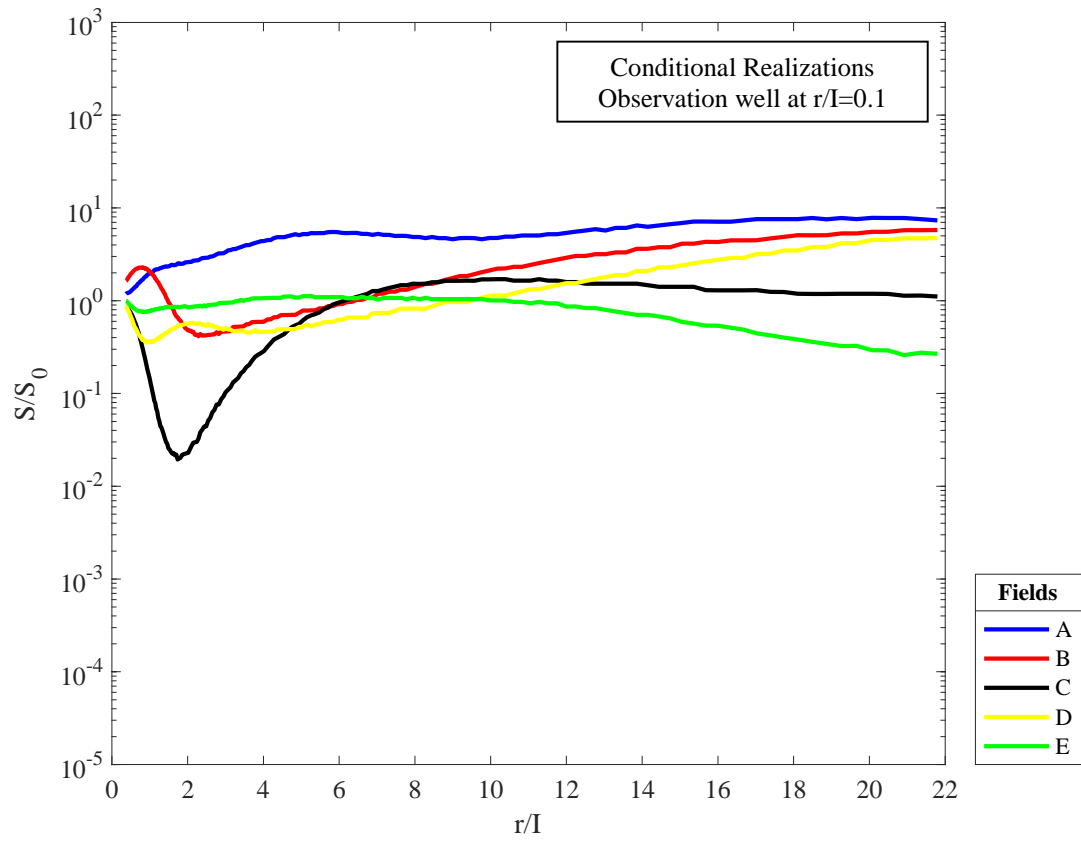
(a)



(b)



(c)



(d)

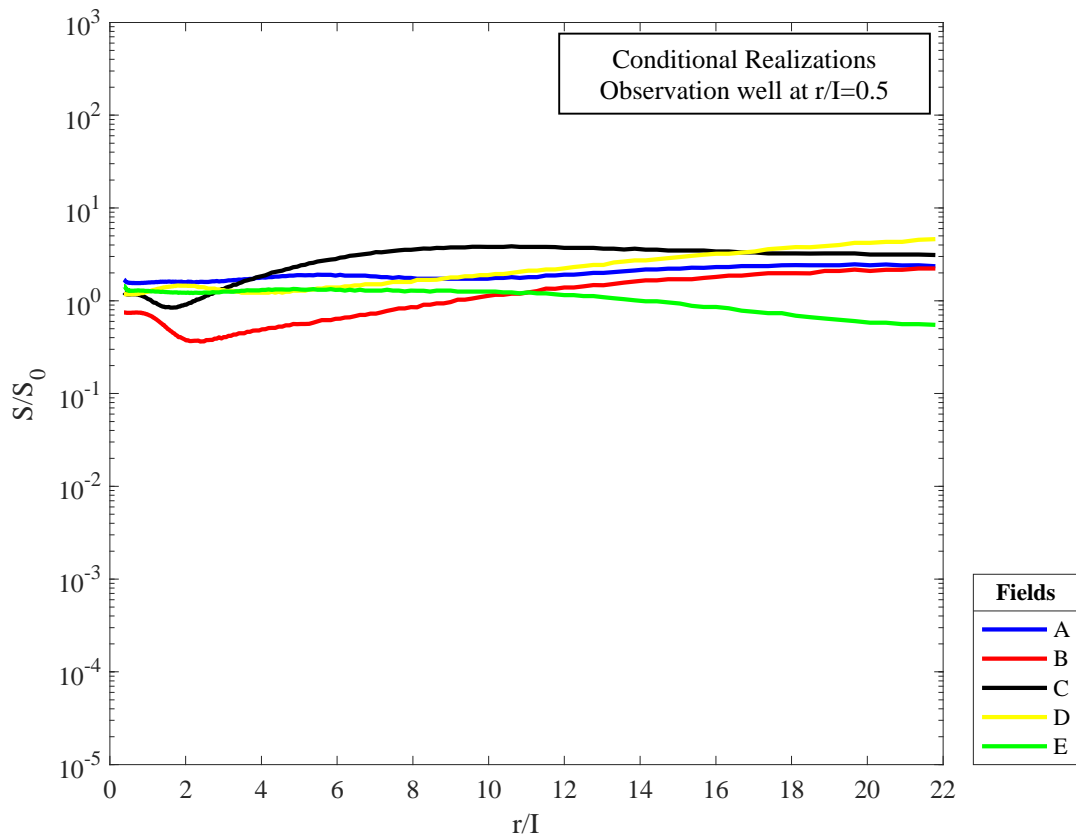
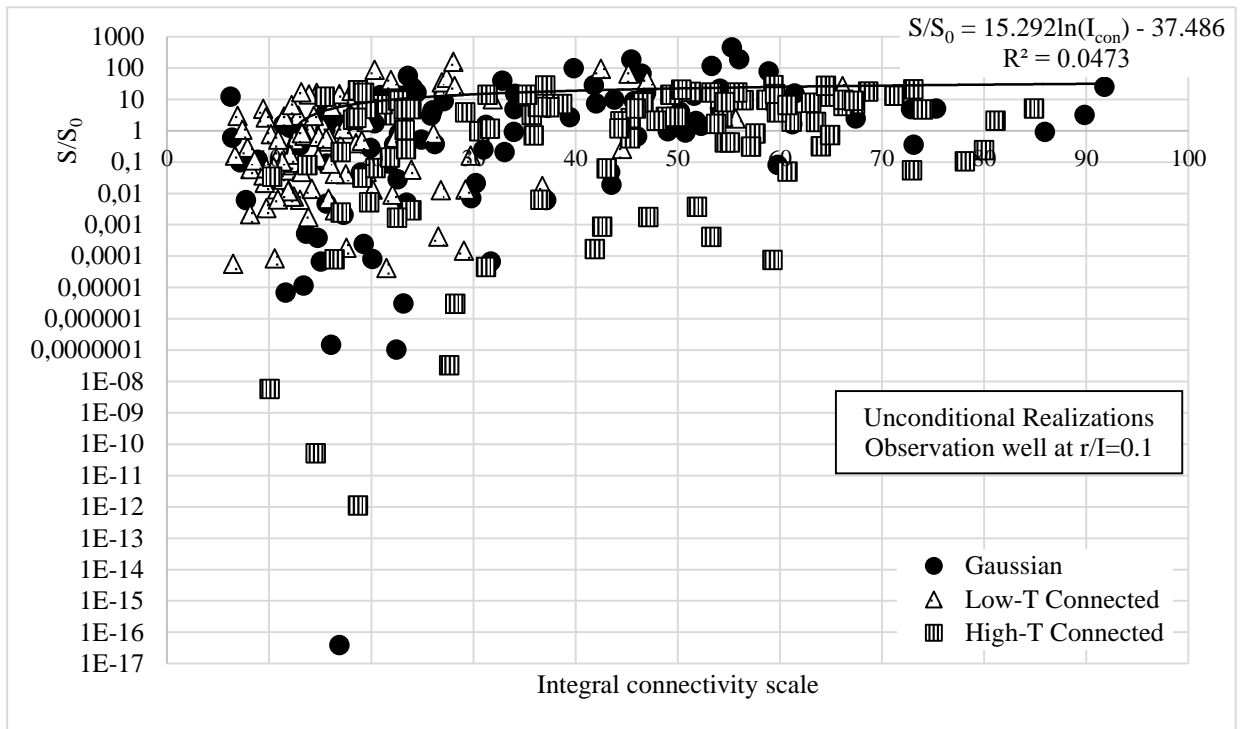
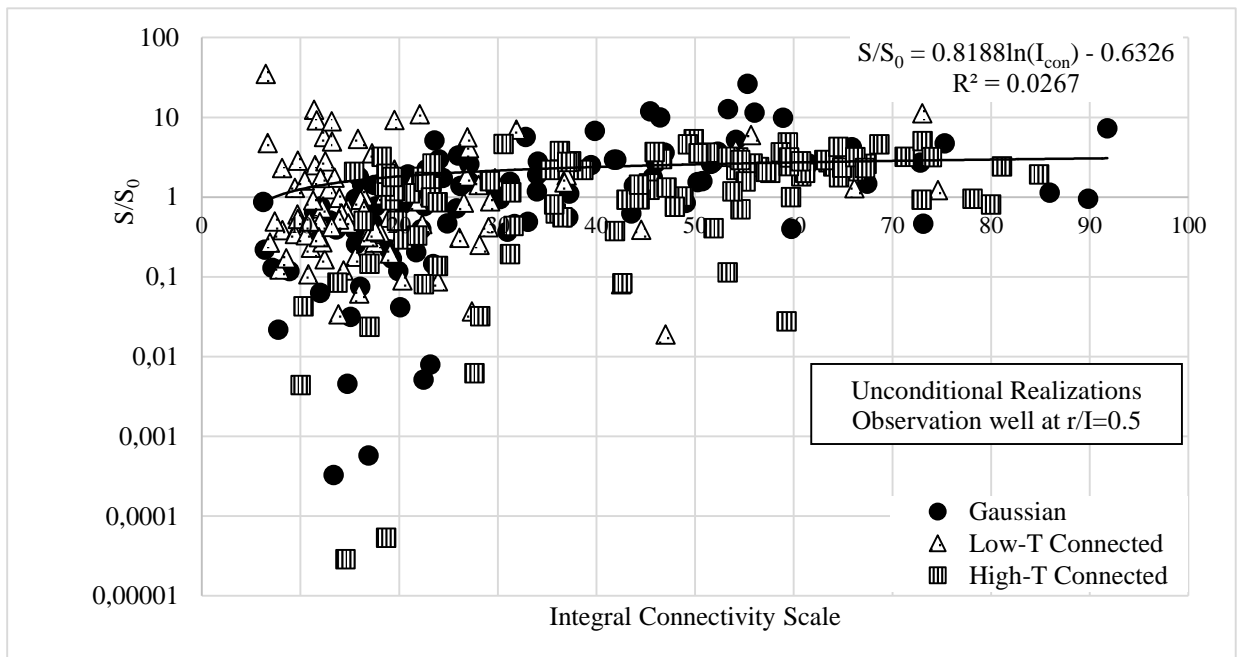


Figure 5.20. Estimated storativity as a function of radial distance from the extraction well for randomly selected Gaussian fields. (a) and (b) shows unconditional realizations where the observation well is located at $r/I=0.1$ and $r/I=0.5$, respectively. (c) and (d) shows conditional realizations where the observation well is located at $r/I=0.1$ and $r/I=0.5$, respectively

(a)



(b)



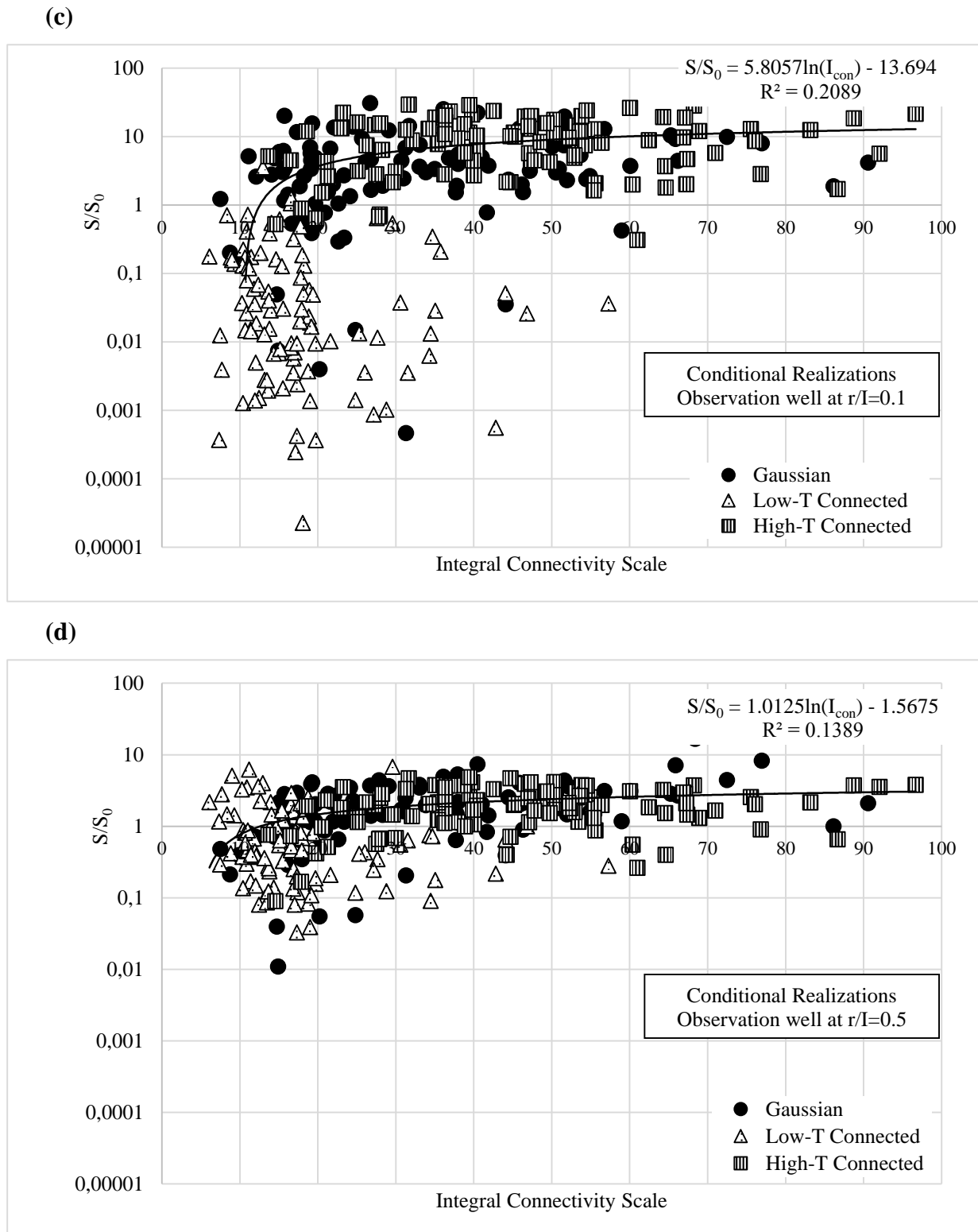


Figure 5.21. Estimated storativity at $t=1$ vs integral connectivity scale of combined field sets. (a) and (b) correspond to unconditional realizations with the observation well located at $r/I=0.1$ and $r/I=0.5$, respectively. (c) and (d) show conditional realizations with the observation well located at $r/I=0.1$ and $r/I=0.5$, respectively

Table 5.6. Average and standard deviation of normalized storativities estimated at $t=1$ time units for different types of realizations and fields

Estimated parameter: Storativity (S/S_0)		Gaussian		Low-T Connected		High-T Connected		All Combined	
		avg	st dev	avg	st dev	avg	st dev	avg	st dev
Unconditional realizations	$r/I=0.1$	17.00	55.58	15.21	57.11	5.49	7.00	12.57	46.31
	$r/I=0.5$	2.23	3.57	2.12	4.26	1.79	1.35	2.05	3.30
Conditional realizations	$r/I=0.1$	5.97	8.85	0.16	0.42	10.21	7.38	5.45	7.81
	$r/I=0.5$	2.21	2.14	1.00	1.25	2.11	1.16	1.77	1.67

6. CONCLUSIONS AND FUTURE RESEARCH

The modeling of groundwater flow and contaminant transport depends on accurate definition of the flow parameters over the entire domain of interest. In order to model groundwater flow and contaminant transport behavior of an aquifer realistically, the necessary flow parameters transmissivity and storativity should be estimated properly. Pumping tests are traditionally used for the estimation of flow parameters. Traditional interpretation methods of pumping tests are based on the assumption of the homogeneous distribution of flow parameters. However, these parameters vary greatly in space and their complex heterogeneous structure complicates the parameter estimation. This complexity in the spatial variability of subsurface formations has led researchers to use geostatistics to advance the accuracy of estimations (Gelhar, 1993).

Commonly used geostatistical approaches are based on two-point statistics, where the correlation between two points is taken into consideration. However, this two-point statistical approach may not be sufficient to fully represent complex patterns of flow and transport in heterogeneous subsurface systems. Two aquifers may have the same two-point statistical parameters, variance, and integral scale, but may end up showing very different water flow or solute transport behaviors (Zinn and Harvey, 2003). As a novel approach to address this issue, the concept of flow connectivity has been introduced in recent years to describe how different regions of the aquifer relate to each other. Flow connectivity refers to the presence of preferential flow channels where the groundwater flow and contaminant transport can occur faster than the other regions of the aquifer. Although the concept itself is clear and easy to comprehend, the unique quantitative measure of connectivity has not yet been defined (Renard and Allard, 2011). Moreover, the impact of connectivity on the interpretation of pumping tests is still not well understood.

The first objective of this study was to numerically investigate the effect of flow connectivity on pumping test data and on the estimated groundwater flow parameters, transmissivity and storativity. The analysis considered 2D transient flow in a confined aquifer. Synthetic transmissivity fields were generated using the sequential Gaussian simulation, GSLIB geostatistical library (Deutsch and Journel, 1998). The conditioning technique proposed by Zinn and Harvey (2003) was applied to these Gaussian fields to generate low-transmissivity (low-T) connected and high-transmissivity (high-T) connected fields.

In order to investigate the impact of transmissivity on the location of extraction, a second set of realizations were generated. The transmissivity at the extraction well is fixed at a constant value for this set and they are referred to as the conditional realizations. This way, the effect of the local transmissivity on flow parameter estimation is investigated by comparing these two sets of realizations.

Because the variability of the storativity is much less than that of the transmissivity, the storativity is assumed to be uniform. The storativity value is assumed to be 10^{-4} which is typical for confined aquifers (Freeze and Cherry, 1979). Then, pumping tests were conducted using the MODFLOW groundwater flow simulation program for each generated field (Harbough et al., 2000). The decrease in the groundwater level as a function of time was recorded at two different observation wells located at $r/I=0.1$ and $r/I=0.5$, where r represents the radial distance from the extraction well, and I represents the integral scale of the transmissivity field. These output data were used for the estimation of the groundwater flow parameters transmissivity and storativity using two different interpretation techniques, namely the Cooper-Jacob Method (1946) and the Continuous Derivation Method (Copty et al., 2011). The correlation between the transmissivity estimate and the geometric mean of the transmissivity field as a function of radial distance was also examined.

When the flow parameters estimated using the Cooper-Jacob Method were investigated, it was seen that the type of field and their connectivity structure did not have a big impact on the transmissivity estimations. Overall, the estimated transmissivities were close to the geometric mean of the transmissivity fields. This finding is in parallel with previous research (Meier et al., 1998; Sanchez-Vila et al., 1999). Estimated storativities, on the other hand, had much larger variability. In general, low-T connected fields had smaller storativities and high-T connected fields had larger estimated storativities. The Gaussian fields had estimated storativity values between the two, but they had the largest variability. These trends were particularly explicit for conditional fields. It showed the transmissivity at the location of extraction affects the storativity estimation greatly.

The outputs of the Continuous Derivation method also showed that as the extraction proceeds, the estimated transmissivity approaches to the geometric mean of the transmissivity field. The variabilities between different realizations with different levels of connectivity were considerably small. Again, the connectivity structure did not have a big effect on the transmissivity estimation. The geometric mean of the transmissivity field as a function of radial distance from the extraction well was also compared with the transmissivity estimation curve. The two curves were very similar

to each other showing that the Continuous Derivation method provides an accurate estimation of transmissivity.

Estimated storativities calculated using the Continuous Derivation started from a value close to the storativity value used in pumping simulations and varied as the pumping test progressed in time. Specifically, the estimated storativity was seen to be highly dependent on the spatial variability of the transmissivity field. The variability was less for the conditional realizations, demonstrating the heavy impact of transmissivity at the point of extraction. It was also less for the observation well at $r/I=0.5$ because the effective area of extraction is larger for this point. As the effective area increases, the estimation averages a larger volume of the aquifer volume, and thus, the variation between different estimations becomes smaller. It was observed that with time the variability of the storativity decreased indicating that the aquifer system starts to behave as an equivalent homogeneous system. However, the apparent storativity estimate at these late times can be orders of magnitude different than the storativity value used in the simulation of the pumping tests. As it was the case for the storativity estimations performed using the Cooper-Jacob method, the low-T connected fields mostly had the smallest estimated storativities, followed by the Gaussian fields and high-T connected fields, respectively. At late times, the estimated storativity values over different field types and their standard deviations were very similar to that of calculated by Cooper-Jacob. This finding showed that after a certain time of extraction, the values calculated with the Continuous Derivation method were close to the values estimated with the Cooper-Jacob method. As the latter method averages the late time data of the head drawdown curve, this finding was also expected. This is in contrast to the storativity estimated at intermediate times which tend to be strongly dependent on time. This also proved that the drawdown derivative curve could give more detailed information about the flow parameters than the drawdown curve itself.

The second objective of this study was to quantify a static measure of connectivity and examine its relationship with the estimated parameters and to investigate whether estimated flow parameters could give some information about the level of field connectivity. The connectivity measure proposed by Western et al. (2001) was chosen as the static connectivity indicator and the connectivity scale of each synthetically generated field was calculated. The relationship between the connectivity scale and estimated parameters was analyzed as well.

It was observed that, on average, low-T connected fields had the lowest integral connectivity scale, followed by the Gaussian fields and high-T connected fields, respectively. This behavior was observed both for conditional and unconditional realizations. However, although the average

integral connectivity scales followed this trend, this is not always the case for individual realizations, indicating the complex relation between the drawdown and the spatial variability of the transmissivity field.

The relationship between the integral connectivity scales and the transmissivity values estimated with the Cooper-Jacob Method are examined, and no correlation between the two is detected. Most fields had a transmissivity value near the geometric mean of the transmissivity field, independent of the field's integral connectivity scale. The estimated storativities showed a low correlation with the integral connectivity scales. The correlation was larger for the conditional realizations, showing that the integral connectivity scale had an impact on storativity estimation, but not as dominant as the impact of local transmissivity. The late time estimations of storativities using the Continuous Derivation method had the same features as the ones estimated with the Cooper-Jacob method. There is a slight correlation between the estimated storativities and the integral connectivity scales and the correlation is larger for conditional realizations. In other words, the transmissivity around the well has a larger impact on flow parameter estimation than the impact of this static connectivity measure.

Overall, this study is performed to investigate the impact of connectivity on the analysis of pumping tests and to assess whether connectivity metrics can be estimated from pumping tests. An improved estimation of the flow parameters will ultimately lead to more accurate groundwater flow models that can more reliably simulate the effects of heterogeneity and flow connectivity. The results of this study demonstrate the difficulty of interpreting the meaning of the estimated flow parameters conducted in heterogeneous aquifer systems. In particular, the storativity estimate is seen to vary strongly with the spatial variability of the transmissivity field casting some doubt on the meaning of the estimated flow parameters and how they relate to actual aquifer systems. There is clear evidence that the storativity is influenced by the connectivity of the transmissivity field but the time-drawdown data obtained from single pumping tests is not adequate to reliably estimate aquifer connectivity.

Future research related to this study should focus on:

- Considering different levels of soil heterogeneity by changing the variance and the integral scale of the generated fields.

- Testing the estimation of the integral connectivity scale by changing the threshold value differentiating between high/low transmissivity values.. Increasing the threshold might be helpful to differentiate highly connected fields. The estimation of the correlation between the integral connectivity scale and the estimated flow parameters for different threshold values can shed additional light on the aquifer's level of connectivity.
- Improving the quantitative measure of the flow connectivity and developing novel approaches to measure the static connectivity. Here only one method is examined (proposed by Western et al., 2001) but there is still a need for research on accurate measures of connectivity.
- Developing three-dimensional models of the aquifer instead of two-dimensional models. The flow through the well in the vertical direction is assumed negligible in this research. Taking the heterogeneity in the third direction into consideration would obviously complicate the flow system but may also provide additional information about the connectivity of an aquifer. Although it would increase the computer memory requirement of the study tremendously, recent advancement in the technology would make it possible to work on a number of 3D realizations easily.

REFERENCES

- Allard, D., Heresim Group, 1993. On the connectivity of two random set models: the truncated Gaussian and the Boolean. In: Soares A. (Eds.), *Geostatistics Tróia*, 467-478, Springer, Dordrecht, the Netherlands.
- Avcı, C.B., Şahin, A.U., Çiftçi, E., 2011. Aquifer parameter estimation using an incremental area method. *Hydrological Processes*, 25, 2584-2596.
- Avcı, C.B., Şahin, A.U., Çiftçi, E., 2013. A new method for aquifer system identification and parameter estimation. *Hydrological Processes*, 27, 2485-2497.
- Butler, J.J., 1990. The role of pumping tests in site characterization: some theoretical considerations. *Ground Water*, 28, 3, 394-402.
- Cooper, H.H., Jacob, C.E., 1946. A generalized graphical method for evaluating formation constants and summarizing well-field history. *Transactions, American Geophysical Union*, 27, 4, 526-534.
- Coptý, N.K., Findikakis, A.N., 2004a. Stochastic analysis of pumping test drawdown data in heterogeneous geologic formations. *Journal of Hydraulic Research*, 42, 59-67.
- Coptý, N.K., Findikakis, A.N., 2004b. Bayesian identification of the local transmissivity using time-drawdown data from pumping tests. *Water Resources Research*, 40, 12, W12408.
- Coptý, N.K., Trincheró, P., Sanchez-Vila, X., 2011. Inferring spatial distribution of the radially integrated transmissivity from pumping tests in heterogeneous confined aquifers. *Water Resources Research*, 47, 5, W05526.
- Dagan, G., 1986. Statistical theory of groundwater flow and transport: pore to laboratory, laboratory to formation, and formation to regional scale. *Water Resources Research*, 22, 9, 120-134.
- Dagan, G., Neuman, S.P. (Eds), 1997. *Subsurface Flow and Transport: A Stochastic Approach*. Cambridge University Press, U.S.A.

Di Dato, M., Bellin, A., Fiori, 2019. Convergent radial transport in three-dimensional heterogeneous aquifers: the impact of the hydraulic conductivity structure. *Advances in Water Resources*, 131, 103381.

Delleur, J.W. (Ed), 1999. *The Handbook of Groundwater Engineering*. CRC Press, U.S.A.

de Marsily, G., Delay, F., Gonçalves, J., Renard, P., Teles, V., Violette, S., 2005. Dealing with spatial heterogeneity. *Hydrogeology Journal*, 13, 161-183.

Demir, M.T., Coptý, N.K., Trinchero, P., Sanchez-Vila, X., 2017. Bayesian estimation of the transmissivity spatial structure from pumping test data. *Advances in Water Resources*, 104, 1, 174-182.

Feitosa, G.S., Chu, L., Thompson, L.G., Reynolds, A.C., 1994. Determination of permeability distribution from well test pressure data. *Society of Petroleum Engineers*, 46, 7, 607-615.

Fernandez-Garcia, D., Trinchero, P., Sanchez-Vila, X., 2010. Conditional stochastic mapping of transport connectivity. *Water Resources Research*, 46(109, W10515.

Fogg, G.E., Noyes, C.D., Carle, S.F., 1992. Geologically based model of heterogeneous hydraulic conductivity in an alluvial setting. *Hydrogeology Journal*, 6, 131-143.

Foster, S.S.D., Chilton, P.J., 2003. Groundwater: the processes and global significance of aquifer degradation. *Philosophical Transactions of the Royal Society B: Biological Sciences*, 358, 1957-1972.

Freeze, R.A., 1975. A stochastic-conceptual analysis of one-dimensional groundwater flow in nonuniform homogeneous media. *Water Resources Research*, 11, 5, 725-741.

Freeze, R.A., Cherry, J.A., 1979. *Groundwater*. Prentice-Hall, New Jersey, U.S.A.

Gelhar, L.W., 1984. Stochastic analysis of flow in heterogeneous porous media. *Fundamentals of Transport Phenomena in Heterogeneous Porous Media*, 82, 673-717.

Gelhar, L.W., 1993. Stochastic Subsurface Hydrology. Prentice-Hall, New Jersey, U.S.A.

Gomez-Hernandez, J.J., Wen, X.H., 1998. To be or not to be multi-Gaussian? A reflection on stochastic hydrogeology. *Advances in Water Resources*, 21, 47-61.

Harbough, A. W., Banta, E. R., Hill, M. C and McDonald, M. G., 2000. Modflow-2000, The U.S. geological survey modular groundwater model user guide to modularization concepts and the groundwater flow process. U.S. Geological Survey Open-File Report 00-92, Virginia, U.S.A.

Hovadik, J.M., Larue, D.K., 2007. Static characterizations of reservoirs: refining the concepts of connectivity and continuity. *Petroleum Geoscience*, 13, 195-211.

Journel A.G., Deutsch, C.V., 1993. Entropy and spatial disorder. *Mathematical Geology*, 25, 329-355.

Kitanidis, P.K., 1997. Introduction to Geostatistics: Applications to Hydrogeology, Cambridge University Press, U.S.A.

Knudby, C., Carrera, J., 2005. On the relationship between indicators of geostatistical, flow and transport connectivity. *Advances in Water Resources*, 28, 4, 405-421.

Knudby, C., Carrera, J., 2006. On the use of apparent hydraulic diffusivity as an indicator of connectivity. *Journal of Hydrogeology*, 329, 3-4, 377-390.

Kresic, N., 2007. Hydrogeology and Groundwater Modeling, Second Ed., CRC Press, U.S.A.

Kuang, X., Jiao, J.J., Zheng, C., Cherry, J.A., Li, H., 2020. A review of specific storage in aquifers. *Journal of Hydrology*, 581, 124383.

Meier, P.M., Carrera, J., Sanchez-Vila, X., 1998. An evaluation of Jacob's Method for the interpretation of pumping tests in heterogeneous formations. *Water Resources Research*, 34, 5, 1011-1025.

Neuman, S.P., Guadagnini, A., Riva, M., 2004. Type-curve estimation of statistical heterogeneity. *Water Resources Research*, 40, W04201.

Neuman, S.P., Blattstein A., Riva, M., Tartakovsky, D.M., Guadagnini A., Ptak, T., 2007. Type curve interpretation of late-time pumping test data in randomly heterogeneous aquifers. *Water Resources Research*, 43, W10421.

Renard, P., Allard, D., 2013. Connectivity metrics for subsurface flow and transport. *Advances in Water Resources*, 51, 168-196.

Riva, M., Guadagnini A., Bodin, J., Delay, F., 2009. Characterization of the hydrological experimental site of Poitiers (France) by stochastic well testing analysis. *Journal of Hydrogeology*, 369, 1-2, 154-164.

Rubin, Y., 2003. *Applied Stochastic Hydrogeology*, Oxford University Press, New York, U.S.A.

Sanchez-Vila, X., Carrera, J., Girardi, J.P., 1996. Scale effects in transmissivity. *Journal of Hydrology*, 183, 1-2), 1-22.

Sanchez-Vila, X., Meier, P.M., Carrera, J., 1999, Pumping tests in heterogeneous aquifers: an analytical study of what can be obtained from their interpretation using Jacob's Method. *Water Resources Research*, 35, 4, 943-952.

Sanchez-Vila, X., Guadagnini, A., Carrera, J., 2006. Representative hydraulic conductivities in saturated groundwater flow. *Reviews of Geophysics*, 44, 3, RG3002.

Schwartz, F.W., Zhang, H., 2002. *Fundamentals of Ground Water*, John Wiley and Sons, Inc., U.S.A.

Serra, J., 1984. *Image Analysis and Mathematical Morphology*. Academic Press, London, UK.

Seyfried, M.S., Wilcox, B.P., 1995. Scale and the nature of spatial variability: field examples having implications for hydrologic modeling. *Water Resources Research*, 31, 173-184.

Theis, C.V., 1935. The relation between the lowering of the piezometric surface and the rate and duration of discharge of a well using ground-water storage. *Transactions, American Geophysical Union*, 16, 519-524.

Trincherro, P., Sanchez-Vila, X., Fernandez-Garcia, D., 2008. Point-to-point connectivity, an abstract concept or a key issue for risk assessment studies?. *Advances in Water Resources*, 31, 12, 1742-1753.

Western, A.W., Blöschl, G., Grayson, R.G., 2001. Toward capturing hydrologically significant connectivity in spatial patterns. *Water Resources Research*, 37, 83-97.

Zheng, L., Silliman, S.E., 2000. Estimating the variance and integral scale of the transmissivity field using head residual increments. *Water Resources Research*, 36, 5, 1353-1358.

Ziegel, E.R., Deutsch, C.V., Journel, A.G (Eds), 1998. *Geostatistical Software Library and User's Guide*. Oxford University Press, New York, U.S.A.

Zinn, B., Harvey, C.F., 2003. When good statistical models of aquifer heterogeneity go bad: A comparison of flow, dispersion, and mass transfer in connected and multivariate Gaussian hydraulic conductivity fields. *Water Resources Research*, 39, 3, 1051.